Comparison of Thermal Infrared and Multispectral UAV Imagery for Detecting Pine Trees (*Pinus Brutia*) Health Status in Lefka Ori National Park in West Crete, Greece

AZEB GIDEY KAHSAY
July, 2022

SUPERVISORS:
Dr. E. Neinavaz
Dr. P. Nyktas

Comparison of Thermal Infrared and Multispectral UAV Imagery for Detecting Pine Trees (*Pinus Brutia)* Health Status in Lefka Ori National Park in West Crete, Greece

AZEB GIDEY KAHSAY
Enschede, The Netherlands, Month, 2022

Thesis submitted to the Faculty of Geo-Information Science and Earth Observation of the University of Twente in partial fulfilment of the requirements for the degree of Master of Science in Geo-information Science and Earth Observation.
Specialization: Geoinformatics

SUPERVISORS:
Dr. E. Neinavaz
Dr. P. Nyktas

THESIS ASSESSMENT BOARD:
Dr. ir. T.A. Groen (Chair)
Dr. Dimitris Zianis (External Examiner, Agricultural University of Athens)

ABSTRACT

Natural and anthropogenic stressors such as drought, pests, and diseases exert increasing pressure on the forests' condition. Forest health assessment, mapping, and monitoring are crucial for targeted management interventions and conservation. Direct forest health assessment in the field, despite considers as accurate, is a labour-intensive approach. Remote sensing (RS) is widely used in forest health assessment to create standardized methods that reduce subjectiveness, extrapolate observations in unvisited, inaccessible areas, and reduce labour and costs. Unmanned aerial systems (UAS) have gained popularity in many forest-related management activities and research. Stress in trees causes a change in their physiological process, resulting in a change in the reflectance of multispectral bands (visible; 0.55 - 0.735 μm and near-infrared (NIR) 0.79μm bands) and a temperature rise in the canopy. Thermal infrared (TIR, 7.5 -13.5 μm) remote sensing data can detect such canopy temperature changes. Previous research has confirmed the ability of UAS imagery to detect plants' health status. This study aims to investigate whether UAS-TIR imagery can be used to accurately map the health and infestation status of Pine trees (*Pinus brutia*) and compare the prediction accuracy with results obtained using multispectral remote sensing (MS) data. The usefulness of UAS-acquired TIR and multispectral data were examined in an open Mediterranean Pine forest in west Crete, Greece. The UAS campaign was conducted between 30 August and 1 September 2021, covering 0.4 km^2. During fieldwork, the defoliation as an indicator of the health assessment and discoloration for *Marchalina hellenica* infestation assessment of individual trees were recorded, and preliminary analysis was done using 105 observation data. Canopy temperature and vegetation indices were computed and further, extracted for the delineated tree crowns, and used to classify trees' health and infestation status; RGB image output was also used to improve the segmentation accuracy. In line with past research in other ecosystems, the results from present study indicate that canopy temperature was able to show the separability between health classes using defoliation as an indicator; however, the difference in discoloration-based infestation class was not significant. Alongside, vegetation indices find it difficult to show a defined relation with defoliation-based health class, although the separability between infestation classes was significantly demonstrated. Among the calculated vegetation indices, SAVI obtained the highest separability in the discoloration-based infestation classes. A weak negative correlation was observed between canopy temperature and vegetation indices. Further investigation is needed to assess the performance of TIR data hyperspectral.

Keywords: Forest health, UAS, UAV, Thermal infrared, Canopy temperature, Infestation.

ACKNOWLEDGEMENTS

First and foremost, I would like to praise and thank God, the almighty, who has granted me countless blessings, knowledge, and opportunity.

I would like to express my deepest thanks of gratitude to my supervisor Dr. Elnaz for the immense support of my research and for her patience, motivation, and enormous knowledge. Please accept my deepest thanks Elnaz, for the courage you gave me on my weak days. I would also like to thank my supervisor Dr. Panagiotis for making your office open on the weekends and after regular office hours. I am grateful for making our fieldwork possible and for all the valuable comments on my paper.

I am grateful to the student affairs, who were like a family during Tigrian's fellow students toughest time. Your doors were open 24/7, and you were there when needed for consultancy, appreciate your utmost understanding of the situation on Tigray. I want to show my deep gratitude to the OKP without your contribution, this would not be possible.

I would like to pay my special regards to my family and my husband Yonas.

Last but not least, I'd also like to acknowledge the help of Lello and Musku for being by my side during the hardest time I could ever be, Haftom, Yechale, and Haftamu for the courage and worthwhile comments on my thesis and throughout my two-year course lectures.

Eternal glory to martyrs who paid the ultimate price for our freedom. My deepest honor to the bravery of the TDF (Tigray defense force), who risk their lives on behalf of our country and citizens.

TABLE OF CONTENTS

LIST OF FIGURES

LIST OF TABLES

1. INTRODUCTION

1.1. Why Forest health monitoring

Forest ecosystems are among the most critical natural resources providing numerous ecosystem services. Healthy forests are used to generate energy (Hall, 2002), construction material (Eriksson et al., 2007), and are considered as a source of food (Rowland et al., 2017) as well as the primary source of oxygen (Trumbore et al., 2015), and can also increase the amount and quality of water (Neary et al., 2009). Forests are also known for creating stabilized local weather conditions, accumulating carbon emissions, and providing shelter for biodiversity; Since the well-being of humans relies on the forest, forest condition highly influences human activity (Trumbore et al., 2015).

The well-being of the forests can be affected by various factors such as disturbances. Forest disturbance can be natural or anthropogenic (Sebald et al., 2021). Each disturbance has a variety of effects on forests; some cause large-scale tree mortality, whereas others affect ecosystem structure and/or function without resulting in massive mortality. Forest stress can be caused due to biotic and abiotic factors (Dash et al., 2018). A change in climate might influence the temperature and moisture (e.g., soil), resulting in rapidly multiplying introduced viruses and bacteria, such as pathogens, that cause disease and stress in the forest (Smigaj et al., 2015). In this respect, pests are considered as one of the primary factors that affect forest health. They can damage the forest by consuming the foliage and later spreading to the woody parts, posing a threat to species and biodiversity (Spanos et al., 2021). There can also be other types of insects that destroy the trees, starting from the root and spreading to the leaves. Pests around the forest ecosystem could also destroy or shorten the growth of trees and contribute to an increase in the amount of CO_2 in the atmosphere (Tubby and Webber, 2010). A change might occur in plants' photosynthesis and respiration rate due to insect attacks (Moore et al., 2013). Trees under insect attack can have different symptoms, e.g. stress in water content, loss of leaf/needle, and change in color (Wulder and Franklin, 2003). Visual observation of tree defoliation and discoloration status can be used as indicators for a tree health assessment (Lakatos et al., 2014). Previous studies have used visual observation to record tree defoliation and discoloration percentages in assessing tree health and also to validate defoliation and discoloration observation from other sources (e.g. UAV and satellite) (Otsu et al., 2018; Cardil et al., 2019; Oerke et al., 2006).

Calabrian Pine (*Pinus brutia*) is classified as a species of Mediterranean flora due to their adaptability to arid ecosystems (Boydak, 2004). It can be found from sea level to 1300 m, with few occurrences reaching up to 1500 m where the limit can be different from one region to another region (Yesil et al., 2005). Pines are discussed concerning environmental protection as they help stabilizing the climate, reduce soil erosion, and provide habitat for wildlife (Kukarskih et al., 2020).

Marchalina hellenica is one of the pests that attack and infest pine trees in the Mediterranean region, which led to infecting some parts of the trees that can be used as a food source for honeybees (Mita et al., 2002). This insect can be found all over the eastern Mediterranean region, like Turkey, Greece, and Italy (Gallis, 2007). In many regions of Greece and Turkey *M. hellenica* was introduced by humans to support honey production from pine in the various areas of Greece and Turkey (Oğuzoğlu et al., 2021). In the 1990s, expansion of the distribution of *Marchalina hellenica* was promoted by the Greek ministry of agriculture to support the pine honey economy (Tsiaras et al., 2016). Santas (1983) revealed that among five types of insects that can be considered as important in the production of forest honeydew *Marchalina hellenica* takes the lead in Greece. It can have a significant influence on the production of honeydew, where the honeybee is dependent on the insect substance and have a contribution to the honey economy (Turhan et al., 2008).

Infestation of Pine trees decreases the tree's water and affects photosynthesis, considerably affecting the pines' health status (Gallis, 2007).

In circumstances where the forest is under threat, forest monitoring plays a vital role in controlling the disturbance and mitigating forest stress, which requires a well-defined monitoring system. Analysis should be conducted to begin implementing a management plan. Adopting management interventions to help diminish the spread of contamination in the forest; can be managed by discovering and observing affected forests as early as possible (Smigaj et al., 2015). However, the main challenge relies on how to sustainably monitor trees' health, come up with promising follow-up approaches, and how quickly identification may be completed in order to decide, implement and adjust forest health-related decisions. In this respect, remote sensing is one of the most vital approaches to forest health assessment (Huete, 2012). This technology is combined with computer-aided signal and image analysis; such a method helps identify the stage and extent of natural and manmade attacked trees to provide mitigation plans if needed (Lange and Solberg, 2008).

1.2. Unmanned Aerial Vehicle for assessing tree health

Researchers apply diverse approaches to identify trees' infestation, such as field assessment and remote sensing data. Visual inspection in the field is an example of a traditional approach that has widely been used in detecting an infestation on trees (Ahmed et al., 2019). For monitoring and assessing of tree's health different variables are retrieved using various remote sensing platforms. Among the platforms used by researchers are applying canopy temperature using TIR remote sensing data (Kaukoranta et al., 2005), using different spectral signatures through multispectral (Lenk et al., 2007), hyperspectral, and LiDAR data (Degerickx et al., 2018).

Syifa et al. (2020) identified Pine trees that are indicated as infested by Pine wilt disease (PWD) based on the land cover map produced from a consumer-grade Unmanned Aerial Vehicle (UAV) images (DJI Phantom 4). Generally, UAVs have an ultra-high spatial resolution but a lower spatial coverage; therefore, individual trees and tree stress status can be easily identified and detected using UAV data (Iizuka et al., 2018). The UAV (with multispectral sensor) helps alleviate the stress associated with acquisition time and also is considered less expensive compared to the acquisition of hyperspectral images using an airborne platform (Nisio et al., 2020); however, it needs technical attention, mainly when thermal infrared sensors are mounted (Pineda et al., 2020).

1.3. Thermal infrared remote sensing

TIR remote sensing data includes acquiring the interpretation of remotely sensed images in the TIR domain (Neinavaz, 2017). TIR remote sensing measures the emitted radiation, whereas visible remote sensing mostly considers the reflected radiation (Prakash, 2000).

Land surface temperature (LST) retrieved from TIR data plays a vital role in observing the radiation energy coming from the Earth's surface (e.g., vegetation and bare soil) (Hulley et al., 2019). The reduction of green vegetation leads to an increase in the LST that also introduces a change in the ecosystem environment (Kafy et al., 2021). Relatively LST is higher in defoliated trees than in healthy trees, where stem volume and canopy height model (CHM) strongly correlate with LST (Junttila et al., 2016).

A reduction of water content and stomatal closure in vegetation occurs as a result of stress in the tree, which leads to an increase in the canopy temperature (Lin and Lv, 2010). Assessing the temperature on the canopy using TIR data can be used as an indicator of water stress in trees which helps the tree health monitor and management process (Giménez-Gallego et al., 2021). The TIR emissivity in a green canopy tree with sufficient available water content is high (Gupta et al., 1997). Not only does defoliation increase the temperature in the canopy, but maturity, canopy structure, and age also contribute to the variation in canopy temperature (Junttila et al., 2016).

A recent study revealed that plant stress has a relationship with changes in leaf temperature, which can be determined using TIR data (Pineda et al., 2020). Another study also revealed that TIR remote sensing data enable to detection of the variation in the leaf and canopy temperature at the early stage of foliar pathogens infection (Lindenthal et al., 2005); additionally, it may provide a promising result for identifying changes in tree infestation status (Ahmed et al., 2019).

Some studies have been conducted on the potential application using TIR remote sensing in infested plants (Ahmed et al., 2019; Pineda et al., 2020; Vidal and Pitarma, 2019). It was demonstrated that TIR data could be used to detect the thermal change occurring as a result of insect pest infestation on the tree (Vidal and Pitarma, 2019). Literature review showed that TIR remote sensing data had successfully detected stress in the plants infested by *Conophthorus coniperda*, *Anoplophora chinenis*, *Anobium punctatum*, and *Rhynchophorus ferrugineus* (Al-doski et al., 2016). Additionally, it can indicate the health of trees when there is no visible change on the trees' exterior (Meola and Carlomagno, 2004).

1.4. Multispectral remote sensing

Multispectral (MS) remote sensing is useful in assessing and mapping tree health, where the reflectance and absorption in green, red, and NIR bands are used as indicators (Fletcher et al., 2001). Also, a relationship can be defined between the spectral reflectance and the health status of a tree (Masaitis et al., 2013). A healthy tree contains chlorophyll that absorbs the green and red bands. The reflectance in red-edge and NIR is also higher for trees with higher chlorophyll content (Marx and Kleinschmit, 2017; Baynes, 2007). Vegetation indices can be calculated from the MS reflectance band, which helps to fill the gap of information from broadband data and helps to produce a tree health status map of a given area (Gupta and Pandey, 2021).

MS data contains multiple bands, including RGB gives an option to generate different indices suitable for forest health assessment. Red-edge and near-infrared are among the multispectral bands often applied in detecting tree stress (Dash et al., 2017). MS data over visible-shortwave infrared (0.45 – 0.88µm) has been previously used for the detection of forest stress or health by generating vegetation indices such as Normalized Difference Vegetation Index (NDVI) and Red Edge Normalized Vegetation Index (NDRE) (Dash et al., 2018). NDVI and NDRE have been commonly used in assessing tree health (Marx and Kleinschmit, 2017; Chávez and Clevers, 2012). Other vegetation indices are also introduced based on the previously observed gap in vegetation indices. For instance, soil brightness highly affects the NDVI value; to minimize the effect of soil background, Soil Adjusted Vegetation Index (SAVI) was developed with adjustment factors that depend on the density of trees (Huete, 1988). However, SAVI has low greenness sensitivity for higher biomass areas, consequently linearity-adjustment factor was added to SAVI and a new vegetation index was developed called two-band Enhanced Vegetation Index (EVI2) (Jiang et al., 2008).

The green and NIR band-based indices also give a promising result by adding leaf area index (LAI) and chlorophyll content at the leaf level. The green chlorophyll index (GCI) was developed to include the LAI sensitivity where NDVI and SAVI are less sensitive, i.e. LAI is used in estimating canopy structure (Gitelson et al., 2003). Also, the green normalized difference vegetation index **(**GNDVI) involves the chlorophyll content at the leaf level in the canopy (Gitelson et al., 1996).

Various researchers explore both TIR and MS remote sensing data to understand their potential as indicators of tree health. Previous studies showed that TIR and MS-based vegetation indices have a negative correlation with vegetation health (Lin and Lv, 2010; Ferreira and Duarte, 2019; Ramakrishna, 1989). In this regard, the slope in the correlation between surface temperature and vegetation index can be used as an indicator of change in canopy resistance (Ramakrishna, 1989) where the steepness of the slope increases in mature vegetation than in the early stage (Gupta et al., 1997). One of the examples from MS-based vegetation indices is NDVI, where the opposite trend with LST is highly seen in sparse than dense vegetation coverage (Lambin and Ehrlich, 1995).

Recent observation revealed that *Marchalina hellenica* could be a cause of stress for Calabria Pine trees (Tsiaras et al., 2016). In order to detect these threats, remote sensing techniques can be relied upon. To our knowledge, research relating to applying TIR remote sensing for monitoring tree health is limited and has not been addressed widely in the open forest environment. In this regard, this research attempts to fill the knowledge gap by applying TIR data to detect an infestation. It also aims to compare the detection accuracy of Pine trees' health status obtained from TIR and multispectral remote sensing data.

1.5. Research Objective, research question, and hypothesis

General Objective

This thesis aims to evaluate the classification accuracy of MS UAV imagery and TIR data in detecting forest health status and *M. hellenica* infestation in an open Mediterranean Pine forest. The area under investigation is located in Anopoli forest, within the Samaria-Lefka Ori National Park in west Crete, Greece.

Research objective 1: Assess the classification accuracy of the MS and TIR UAV data in detecting the health status of Mediterranean Pine trees.

Research Question 1.1: Can UAV-based TIR temperature data map the health status of Mediterranean Pine trees?

Research Question 1.2: What is the difference in classification accuracy of the MS and TIR UAV images for detecting the health status of Mediterranean Pine trees?

Hypothesis 1: UAV-based TIR data can achieve higher accuracy than multispectral UAV-based data in detecting the health status of Mediterranean Pine trees.

Research objective 2: Assess the ability of TIR UAV data to detect Mediterranean Pine trees infested by *Marchalina hellenica.*

Research Question 2: Can TIR UAV data detect the variability in infestation by *Marchalina hellenica* in Pine trees?

Hypothesis 2: TIR can successfully detect Mediterranean Pine trees infested by *Marchalina hellenica.*

2. METHODOLOGY

2.1. Study area

Crete is the largest Greece island with an area of 8336 km^2. Lefka Ori is a National Park (NP, geographically situated at 35.29^{o}N, 24.03^{o}E), located in the west part of Crete, including the famous and longest Gorge found in Greece called Samaria Gorge. Lefka Ori NP contains a mountain with white limestone rocks, resulting in the name "The white mountains". The Lefka Ori NP is also registered under the Natura 2000 network. Of the total plant species found in Lefka Ori, 26.6% are endemic to the island (Pediaditi et al., 2008). This national park beside the Samaria Gorge also has different vegetation types such as maquis, phrygana, conifer woodland, and alpine (Catsadorakis, 1994).

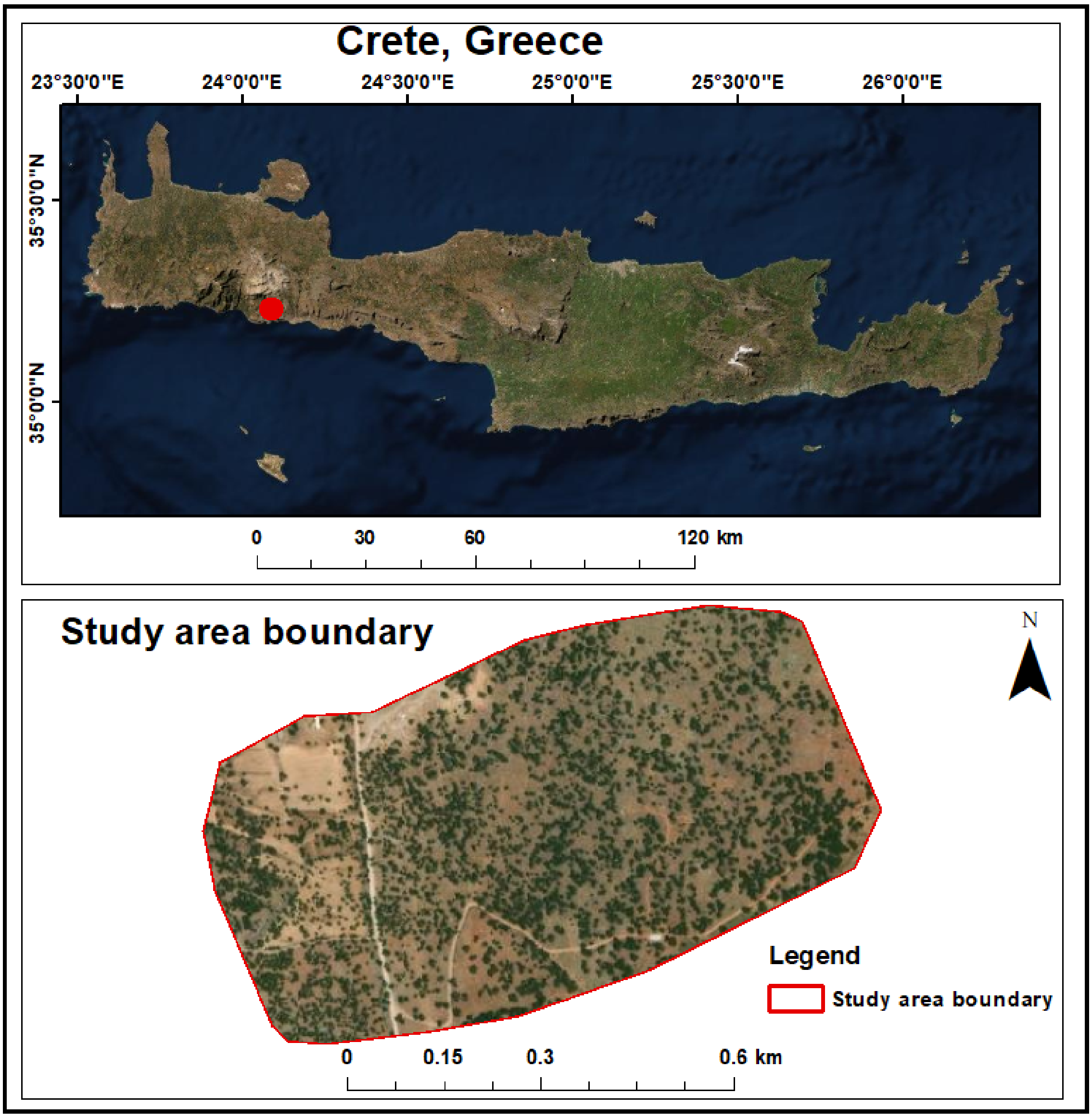

Figure 1: Study area Lefka Ori National Park.

The Lefka Ori NP forest coverage is degrading as the result of tree death caused by pests (e.g., *Marchalina hellenica*, *Matsucoccus josephi,* and *Thaumetopoea pityocampa*) and drought. *Marchalina hellenica* is one of the insects that is contributing to forest degradation in this NP. In the Lefka Ori NP, honey production activities were observed as a common practice (Figure 2). Honey production is boosted greatly due to the presence of *Marchalina hellenica* pest. This pest is a monophagous species that is predominantly found in Pine trees; the white substance in the branch and trunk helps to produce honeydew, later used by the bees to produce honey (Tsagkarakis et al., 2016).


Figure 2: *Marchalina hellenica* and infested branch.

Matsucoccus josephi is the other pest type that can be found in the Lefka Ori NP. The damage can range from creating spots in the Pine needles to killing the whole tree; it also damages the water transport of trees (Tsiaras et al., 2016). Like other pests, it is not easy to identify *Matsucoccus josephi* visually (Figure 3).


Figure 3: Adult female *Matsucoccus josephi* and highly infested trunk.

Another pest that is seen to widely affect the Mediterranean region, as well as the study area, is *Thaumetopoea pityocampa* (Figure 4). Pine trees are the main tree species affected by this pest; it affects the needle, which could later affect growth and reduce the photosynthesis rate (Tsiaras et al., 2016). They have a chemical that helps them protect themselves from external factors through their hair; close contact with the caterpillars can result in severe skin irritation, allergic reaction, and other health problems. The nest-looking shelter of these pests can be easily identified in the tree's different locations. In addition to the three listed pests, drought is another factor that causes tree mortality.

Figure 4: *Thaumetopoea pityocampa* and nest created on the pine trees.

Below are the methodology used in this study to observe the link between MS or TIR data with defoliation-based health assessment and assess the relation of both data (i.e., MS and TIR) with discoloration-based *Marchalina hellenica* infestation class on Pine trees (Figure 5). In addition, the link between discoloration from infestation and defoliation was examined.

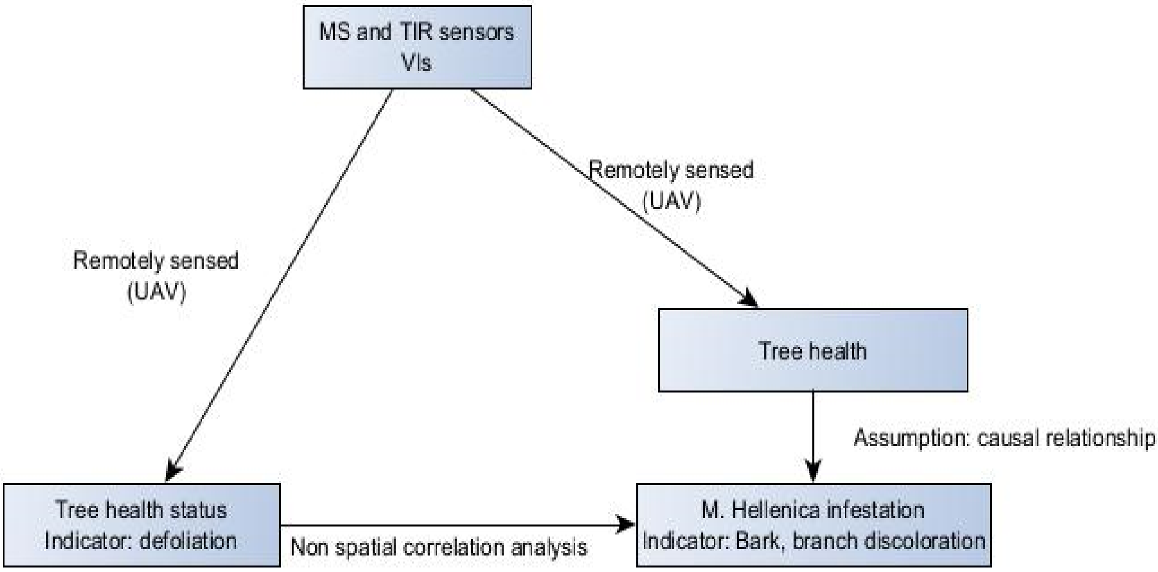

Figure 5: Overview of the study.

The flow chart in Figure 6 shows the overall workflow and methods of the research study to answer the raised research questions, including data collection, processing, and analysis.

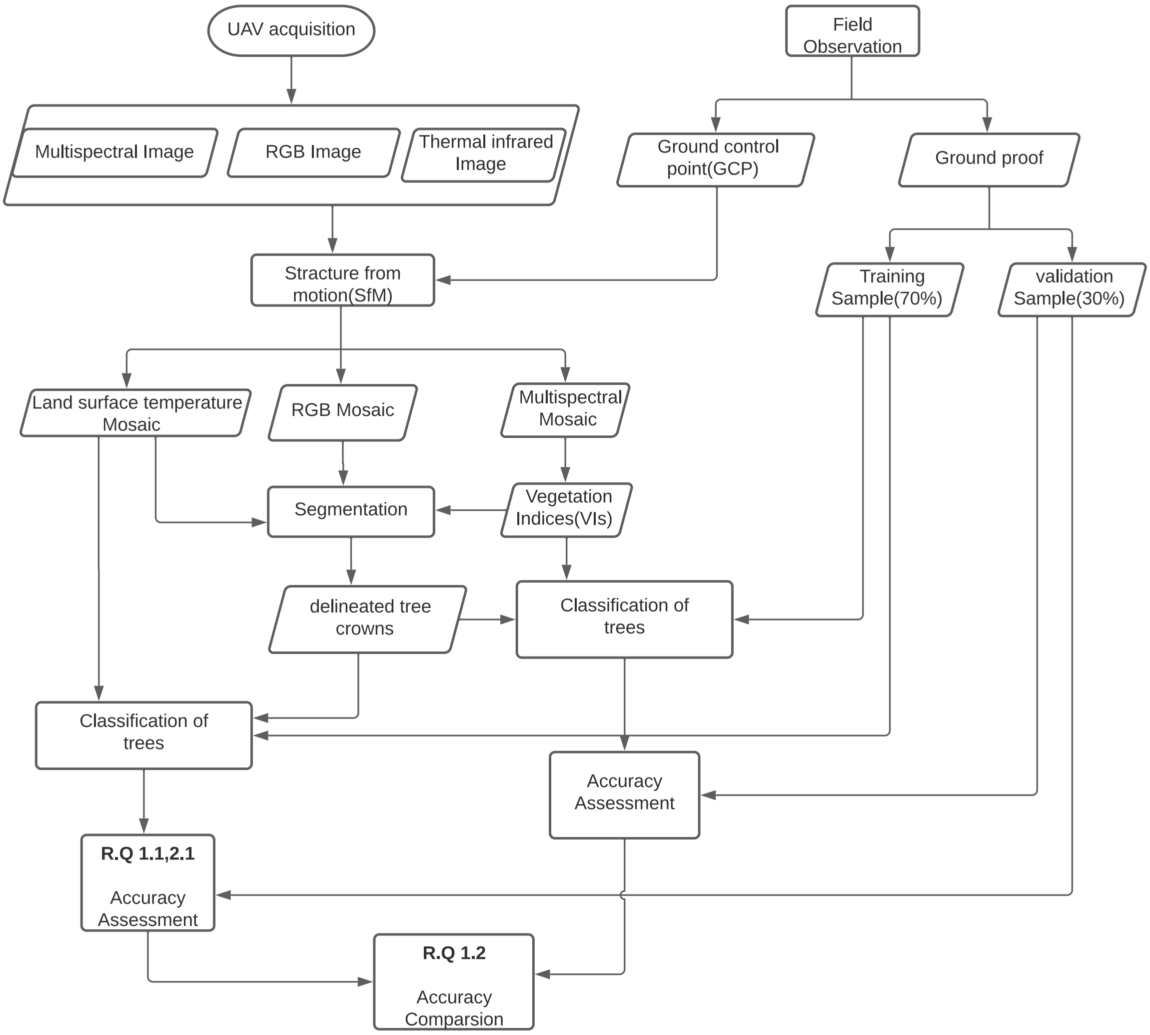

Figure 6: Flow chart for a methodology of the study area.

2.2. Data collection

In this study, primary data was collected to address the research objectives and questions. Based on the accessibility and representativeness, a study area was selected in Lefka Ori NP. The area coverage for the study area is approximately 0.5 km^2, where it is fully covered with Pine trees. DJ Phantom 4 UAV was used with mounting FLIR Vue Pro R and Parrot Sequoia cameras to capture TIR and MS images in addition to the RGB camera. The UAS campaign was conducted between 30 August and 1 September 2021. LEICA differential Global Navigation Satellite Systems (GNSS) was also used to record the location of the Ground Control Points (GCPs) as well as individual sample trees (Table 1). For processing and analysis purposes, different software was used that, are listed in Table 2.

Table 1: Dataset used for the study

Data	Source
Thermal Infrared image	FLIR Vue Pro R TIR sensor
MS image	Parrot sequoia MSS sensor
RGB image	DJ Phantom 4 with RGB Sensor mounted
Ground control point	LEICA Global Navigation Satellite (GNSS)
Tree location and health indicators	LEICA Global Navigation Satellite (GNSS), visual inspection in fieldwork
Google earth image	Google earth pro
A supportive picture with coordinate	SW Maps, Avenza Maps in fieldwork

Table 2: Software used in the study

Software	Function
Pix4D mapper	Photogrammetry process
eCognition Developer 10.0	Image segmentation and classification
Arc GIS 10.8.1	Produce map and Data analysis
IBM SPSS Statistics	Comparison between classes
RStudio	Data analysis
Microsoft excel	Data analysis

2.2.1. Field Observation

During the fieldwork, Pine trees' health and infestation status was observed and recorded within the study area. The random sampling strategy was applied because the study site consisted of Pine trees only. In total, observations were made from 109 sample trees. From the total samples, four observations are out of the area captured by the UAV and therefore were excluded from analysis.

According to Lakatos et al., (2014) "*Defoliation is defined as needle/leaf loss in the assessable crown when compared to a reference tree*". Defoliation can be used to indicate health status by recording the loss of leaves in the canopy. Causes of the defoliation in the study area can be associated with the three pests (i.e., *Marchalina hellenica*, *Matsucoccus josephi,* and *Thaumetopoea pityocampa)* or/and drought. UNECE and EU-based classification approaches (Table 3) were applied to assess the defoliation percentage and health status of the Pine trees (Figure 7).

(a) No Defoliation (b) Slightly Defoliation (c) Moderately Defoliation (d) Severely Defoliation

Figure 7: Field observation considering defoliation level.

To observe the infestation level caused by *Marchalina hellenica,* information related to the discoloration was also collected. In this case, discoloration implies the color change in the bark and branches of Pine trees as a result of infestation (Figure 9). Based on the visually observed discoloration, percentage infestation classes were defined (Table 4). Additional information is documented about white substance coverage caused by *Marchalina hellenica* and distinguishes which part of the tree's color was changed (Figure 8). To differentiate among the stages of the infestation, the Pine tree was grouped into three classes, namely lower, middle, and upper part, which later was used to investigate the degree of the infestation using remote sensing images. Field observations were recorded in a form that can be found in Appendix 1. Remarks were added for further clarification or additional information.

Figure 8: Discoloration of Pine trees infested by *Marchalina hellenica*.

(a) No Discoloration (b) Slightly Discoloration (c) Moderately Discoloration (d) Severe Discoloration

Figure 9: Field observed concerning discoloration level.

Table 3: Tree health classification based on UNECE and EU classification (Lakatos et al., 2014).

Class	**Defoliation Status (%)**	**Class**
None/Healthy	Up to 10%	0
Slightly unhealthy	>10-25%	1
Moderately unhealthy	>25-60%	2
Severely unhealthy	>60-<100%	3
Dead	100%	4

Table 4: Infestation classification based on the discoloration in bark and branches of Pine trees

Class	Discoloration status (%)	Class
None infested	Up to 10%	0
Slightly infested	>10-25%	1
Moderately infested	>25-60%	2
Severely infested	>60-<100%	3

It should be highlighted that in this study, defoliation was considered as an indicator of Pine tree health, whereas discoloration was used as an indicator of the infestation from *Marchalina hellenica*.

2.2.2. Ground Control Points

Ground Control Points (GCPs) are marked points in the ground used to measure geographic coordinates with high accuracy. GCPs are used to rectify images with geometric distortion and were possibly caused by flight altitude, camera, and curvature of the earth (Liew et al., 2012). GCPs were collected to be used in photogrammetry block adjustment, to obtain georeferenced TIR and multispectral ortho-mosaic. In planning GCP distribution and number, the area extent and accessibility were taken into consideration. In order to have fully identified GCP, it is recommended to have them in an open field (e.g., side roads or open area) and avoid confusing features. GCPs can be marked before the acquisition, so-called pre-marking, or find a visible object which can be seen in the acquired image (i.e., postmarking) (Figure 10). For this research study, visible objects that could be seen clearly from the UAV were selected as GCPs. A total of eight GCPs were collected during the fieldwork and used to process the RGB, MS and TIR photogrammetry projects; however, the GCPs were not well distributed in the study area. LEICA differential GNSS GS14 is also used to record the coordinate system of selected GCPs in Real Time Kinematic (RTK) mode.

(a)

(b)

Figure 10: Type of ground control points (a) premark (b) postmark.

2.2.3. Unmanned Aerial Systems

Unmanned Aerial Systems (UAS) include the UAV, the sensor, a person in charge of remotely controlling the flight, and a system that connects both. For image acquisition for the selected study area, DJI Phantom 4 UAV was used (Figure 11). The DJI Phantom 4 Pro, with a weight of 1375 gr, and approximately 30-minute maximum flight duration, use a gimbal camera to stabilize the image during acquisition. It has amounted RGB camera with 20Mpixels, and an image size of 4000 x 3000 pixels. The UAV was modified to mount other additional cameras so that the payload of the cameras would not affect the UAV.

Figure 11: DJI Phantom 4 UAV (Source: ITC Geoscience-laboratory).

2.2.3.1. Multispectral image

Parrot Sequoia camera was used to acquire MS images (Figure 12). This camera has four 1.2-megapixel monochrome sensors where the single band resolution is 1,280x960 pixels with bands of green (0.55 µm), red (0.66µm), red-edge (0.735 µm), and near-infrared (0.79 µm); It also has a 16-megapixel RGB sensor (not used in this study). It is small and lightweight, making it easy to mount in the UAV as an additional device. Parrot Sequoia camera has its GPS antenna to estimate the accurate location of the receiver, whereas it uses a UAV battery to charge its battery. The camera comes with its own irradiance sensor (i.e., right item in Figure 12) and a calibration plate, both used to deliver reflectance data.

Figure 12: Parrot Sequoia camera.

2.2.3.2. Thermal infrared image

FLIR Vue Pro R camera with a bandwidth of 7.5 – 13. 5 μm was used to capture TIR images (Figure 13). FLIR Vue Pro R is a radiometric camera where the individual pixels represent temperature. The sensor resolution for the captured images was 640x512 pixels with the focal length of 19 mm, and ±5°C accuracy manufactured by FLIR Systems, Inc. (Wilsonville, OR, USA). The camera has three image formats as an output; RJPG (radiometric JPG, images with embedded radiometric data), TIFF (no radiometric data), and JPG (Colored for visual presentation only). In this study, the RJPEG option was used to define the emissivity of the objects under investigation. For the Pine trees, emissivity was set at 0.97. The collected raw thermal image pixel value was converted from the DN value to non-contact temperature using the provided equation by FLIR Systems Inc (2022).

$$\text{Temperature (Celcius)} = 0.04 * (\text{counts}) - 273 \qquad \text{Eqn.1}$$

Figure 13: FLIR Vue Pro R, 19mm camera (Source: ITC Geoscience-laboratory).

2.3. Structure from motion

Structure from motion (SfM) is a photogrammetric technique that helps produce 3D products from 2D images using the overlap between sequential images (Fonstad et al., 2013); stitching the collected individual images helps to eliminate the y-parallax that occurs as a result of oblique imaging view. Based on the SfM technique collected sequence of images for the sample study area has been processed using Pix4Dmapper. Pix4Dmapper is a photogrammetry software used to produce a point cloud, digital terrain model (DTM), digital surface model (DSM), reflectance, and indices values from the sequenced 2D Images collected using Phantom 4 UAV. The RGB, MS, and TIR images were processed in the SfM separately.

The collected GCPs were imported for block bundle adjustment in each SfM process that later produced a georeferenced and close-to-ground reality output. Some of the field-collected GCPs were not identifiable in the UAV images, mainly in the multispectral and TIR images as a result of the lower resolution and confusion with other nearby features. To overcome the GCP identification problem, additional control points were marked manually from the RGB output (Mosaic and DSM) and further used in the processing of MS and TIR projects; RGB from Phantom 4 UAV has a high spatial resolution compared to the two. The GCP was used to georeference the three datasets (i.e., RGB, MS, and TIR) and made them comparable.

2.4. Vegetation indices

The spectral characteristics of vegetation at different wavelengths can be used for forest health assessment. The wideband range limitation makes it difficult to follow in detail the spectral signature of given vegetation at different wavelengths. In this respect, vegetation indices were developed to overcome this limitation (Gupta and Pandey, 2021). The indices use specific band reflectance/observation responses of vegetation to distinguish the healthy and unhealthy vegetation. In this regard, vegetation indices were calculated and used to analyze health/infestation status. Six vegetation indices were calculated for the study area using Pix4dmapper. Three vegetation indices were used in the classification process, namely Normalized Difference Vegetation Index (NDVI), Soil-adjusted Vegetation Index (SAVI), and Normalized Difference Red-edge Index (NDRE). In addition, the other three vegetation indices were included in the analysis (i.e., Green Chlorophyll Index (GCI), Two-band Enhanced Vegetation Index (EVI2), and Green Normalized Difference Vegetation Index (GNDVI)).

Normalized Difference Vegetation Index

NDVI is implemented in vegetation health assessment by using greenness as an indicator; NIR and Red bands are used to calculate this index (Bhandari et al., 2012). NDVI is seen to be used widely for various applications.

$$NDVI = \frac{NIR - RED}{NIR + RED} \qquad \text{Eqn.2}$$

Soil-Adjusted Vegetation Index

SAVI is a type of vegetation index presented to minimize the effect of soil brightness (Huete, 1988). It uses the NDVI as a base and upgrades the prediction result from the indices by adding a correction factor to soil brightness.

$$SAVI = \frac{(1+L)(NIR - RED)}{(NIR + RED + L)} \qquad \text{Eqn.3}$$

Where L stands as the vegetation coverage of a given area. Depending on the nature of the study area, the value for L can change between 0 (Highly vegetated), 0.5 (Sparsely vegetated area), and 1(no vegetation coverage). Therefore, for this research, a 0.5 correction factor is used as the nature of the study area is sparsely vegetated.

Normalized Difference Red Edge Index

Like most of the other vegetation indices, the NDRE shows the amount of chlorophyll also greenness based on the two bands (NIR and Red edge) (Tucker, 1979).

$$NDRE = \frac{NIR - RE}{NIR + RE} \qquad \text{Eqn.4}$$

Green Chlorophyll Index

GCI estimates the chlorophyll content based on green and near-infrared bands where the sensitivity of chlorophyll is high (Gitelson et al., 2003).

$$GCI = \left(\frac{NIR}{GREEN}\right) - 1 \qquad \text{Eqn.5}$$

Two-band Enhanced vegetation index

EVI2 is derived from the previous existing enhanced vegetation index (use three bands) to compromise for sensors that do not have the third band (Blue). EVI2 shows the greenness of vegetation with additional atmospheric and noise correction (Jiang et al., 2008).

$$EVI2 = 2.5 * \frac{(NIR-RED)}{(NIR+2.4*RED+1.0)} \qquad \text{Eqn.6}$$

Green Normalized Difference Vegetation Index

GNDVI uses green and NIR bands to determine the concentration in the chlorophyll as well as to estimate the vegetation photosynthesis rate (Gitelson et al., 1996).

$$GNDVI = \frac{NIR-GREEN}{NIR+GREEN} \qquad \text{Eqn.7}$$

2.5. Object-based image analysis

Image objects are created by clustering neighbouring pixels based on their similarity in character and having a meaningful spatial object (Chen et al., 2018). Object-based image analysis (OBIA) can produce a sound output when color and texture are considered (Chouhan et al., 2019). Since the aim of this study is to assess the tree health status at the tree level, object-based segmentation was selected to delineate individual trees.

2.5.1. Segmentation

A region-based multi-resolution segmentation algorithm was chosen to segment the data and create an image object. For the purpose of segmentation, the canopy height model (CHM) was calculated by subtracting DTM from DSM derived from SfM processing of RGB data. The RGB-CHM was further used because of its fine resolution; the CHM can easily illustrate the tree crown. The crowns of the 105 trees with field observations were digitized in ArcMap and used as a thematic layer in the segmentation procedure. The scale parameter was set to 18, where shape and compactness were 0.1 and 0.5, respectively. The large-scale parameter allows heterogeneity with large segment objects.

After the segmentation, to differentiate between the tree and the non-tree objects, a threshold condition was set. The segmented object where CHM values were greater than 2 m was defined as tree class, whereas segment objects less than or equal to 2 m were categorized as non-tree. However, some trees were classified as non-tree while using the upper condition. To correct this omission, additional threshold conditions were determined using non-tree as a class filter to solve this issue. The new threshold condition includes SAVI and LST mosaic data. Among the considered vegetation indices (i.e., NDVI, NDRE, and SAVI), SAVI could distinguish between the tree and non-tree objects better. From the non-tree class, based on a try segment, objects with a SAVI value greater than 0.2 and an LST less than 45°C were able to differentiate the trees that are under the non-tree class and used to reclassify. Finally, the non-tree segmented objects were merged into one.

The tree class was refined after the separation of trees and non-trees classes. Refinement is required to have a segment object as an individual tree and minimize the over- or under- segmentation. Two threshold algorithms were applied, watershed transformation for separating individual trees with a length factor of 16 and morphology for smoothening segment objects with close image object operation. Canopy temperature is sensitive to the delineation between tree crown and background objects resulting in additional manual editing of the segmented object.

2.5.2. Classification

Image classification is used for grouping pixels based on the radiance similarity value in continuous image bands; in addition different statistical learning methods are introduced to extract the information from the images (Manthira Moorthi et al., 2011). Supervised classification is a more accurate approach compared to unsupervised methods (Wang et al., 2010). However, supervised classification is highly dependent on training samples. For the present study, of the total collected sample trees, 70% were used for training classification of the segmented trees. The training samples were categorized into four classes. It should be highlighted that the dead class is not included in this study for assessing health status and infestation level. The healthy and slightly unhealthy as well as non-infested and slightly infested were merged as no significant difference was found to distinguish between data from these two classes; also, the number of samples collected for these classes was not statistically enough. The Health and infestation status of the study area was classified based on the 74 observation samples (i.e., individual trees) recorded to train and apply to the whole area.

In total, four classification scenario was performed, using vegetation indices and canopy temperature layer to classify the health status and also using the same layers to classify the infestation status. For the training samples of LST data, each segmented tree's mean and standard deviation features, were used. In addition, in the case of MS data, the mean and standard deviation feature of NDVI, SAVI, and NDRE was also used for each segmented tree.

To observe the classification of in-hand data using an intelligent and efficient classification algorithm is recommended (i.e., machine learning as a classifier algorithm). According to the application and data, there are different machine learning techniques; among them, Random Forest (RF) has gained popularity over the last years. It is a method developed by Leo Breiman in 2001, which generates classification criteria through a voting process (Patel and Jokhakar, 2017). This classifier is one of the statistical learning methods used in image classification by extracting the information from the image. RF classifiers have remarkable potential in forest health classification (Lausch et al., 2017). RF uses training sample-based decision trees.

In the present research, the segmented MS and canopy temperature data for the entire site are classified based on the training data. In this thesis, the mean reflectance value for the 105 sample trees in each band (i.e., green, red, red-edge, and NIR) was extracted using eCognition software and linked to the field observations (i.e., Health and infestation classes). The spectral signature of each class was extracted to understand if there is any relationship between the three health/infestation status and their reflectance value.

2.5.3. Accuracy assessment

A quantified output accuracy helps in analysis and decision-making. It also makes it easier to make comparisons between outputs rather than using only visual observation for quality checking. In order to evaluate the performance of the RF classifier, a confusion matrix was used. A confusion matrix is a way of assessing the accuracy of the classifier based on validation samples. An independent validation sample data was used to evaluate the output accuracy of supervised tree health/infestation classification produced using canopy temperature and MS data. The matrix shows the relationship between the classified and reference. The reference is an independent sample that is not used for training simultaneously. Of the total collected in situ data, 30% were used to validate the classification. The matrix includes user, producer, and overall accuracy.

2.6. Comparison between class

After classifying every delineated tree polygon using the RF classifier, the mean and standard deviation for vegetation indices and canopy temperature of each class were extracted using eCognition software.

Additional to the three vegetation indices (i.e., NDVI, SAVI, and NDRE), which were used in classification, the mean and the standard deviation of three other vegetation indices (i.e., GCI, EVI2, and GNDVI) were extracted using the crown delineated polygons.

An analysis of variance (ANOVA) with a confidence interval of 95% was used to investigate if there is a statistically significant difference among the classes (i.e., Health classes and Infestation classes) for the field observed samples as well as for the classes from classification result. ANOVA shows the difference between the three independent classes using the mean value of vegetation indices and canopy temperature for the classified objects. To understand where the significant difference occurred among the classes Tukey post hoc test was used.
Furthermore, separability analysis was applied. This analysis includes the standard deviation and mean values and quantifies the value difference between the classes. The mean and standard deviation was from the vegetation indices and canopy temperature map. It not only shows the difference between the mean of the class in addition, it includes how low/high is the standard deviation.

$$S = \frac{(\mu 1 - \mu 2)}{(\sigma 1 + \sigma 2)} \qquad \text{Eqn.8}$$

Where S denotes separability and μ is the mean, and σ is the standard deviation.

Canopy temperature and vegetation indices mean value for tree health/infestation classes were assessed to see if there was a defined trend or relation between consecutive classes. The delineated and classified individual trees' mean value was extracted and used for further analysis. In addition, bivariate linear regression was used to show the type of relationship that exists between the canopy temperature and vegetation indices, where the canopy temperature was defined as the independent and vegetation indices as a dependent variable. In addition, the result from regression also shows how much variation percentage the relation accounts for. The relationship between the infestation caused by *Marchalina hellenica* and tree health was investigated.

3. RESULT

3.1. Field observation

In percentile, defoliation and discoloration status for the 105 collected samples was recorded and grouped into four classes, where the number of observations was high for both moderately and severely unhealthy/infested classes. For healthy and slightly unhealthy classes, the collected number of observation (defoliation) samples were nine and 21, respectively, whereas for the none infested and slightly infested classes in assessing infestation using discoloration, five and ten number of the samples were recorded. In this study area, the severely unhealthy and severely infested class has the largest number of sample observations comparing the other classes, where the number of observations was 43 and 49, respectively. The moderately unhealthy and moderately infested class also had a large number of samples, with 32 and 41 number of observation, respectively. The 105 total number of field observed data and their distribution within the defined classes were plotted (Figure 14).

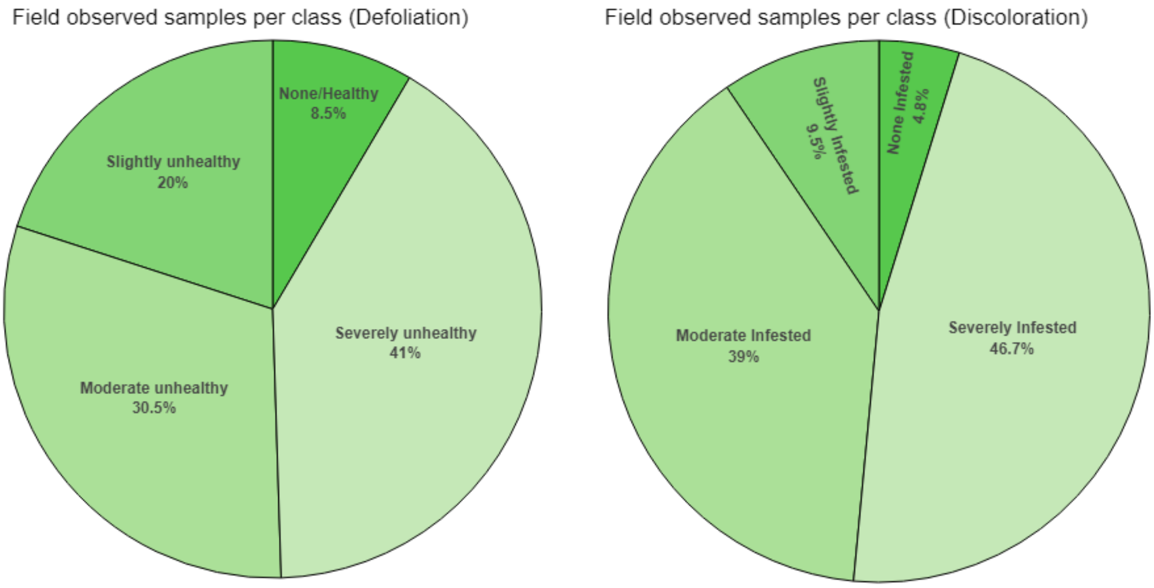

(a) (b)

Figure 14: Number of fields observed samples per each Health(a) and Infestation (b) class.

3.2. Ground control point

As can be seen from Figure 15, most of the field-collected GCPs are found in the south part of the study area, and there were no GCPs in the north and west parts of the study because of accessibility problems.

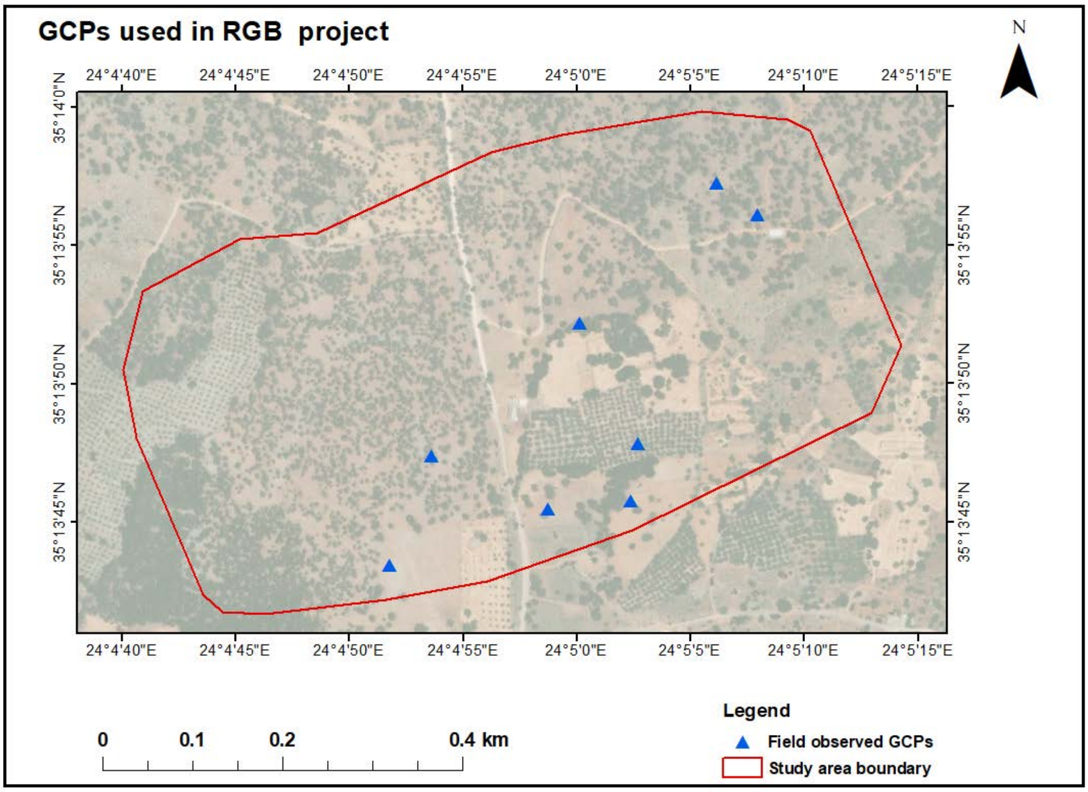

Figure 15: The ground control points location used in the RGB project

As can be seen from Figure 16, the additional 12 control points (CP) were collected and field-collected GCPs used in the process of the MS project. Also, the six identified GCPs in the TIR project and the manually collected 22 CPs were visualized in Figure 17.

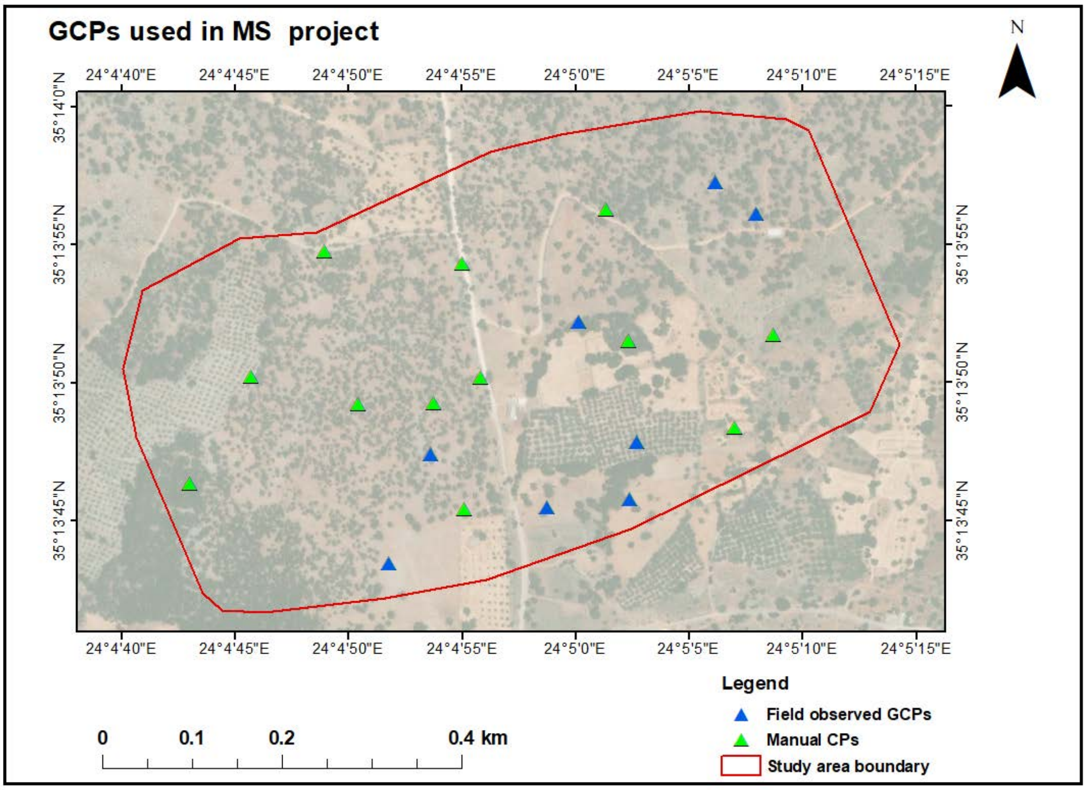

Figure 16: Ground control points (GCPs) and control points (CPs) used in the multispectral (MS) project.

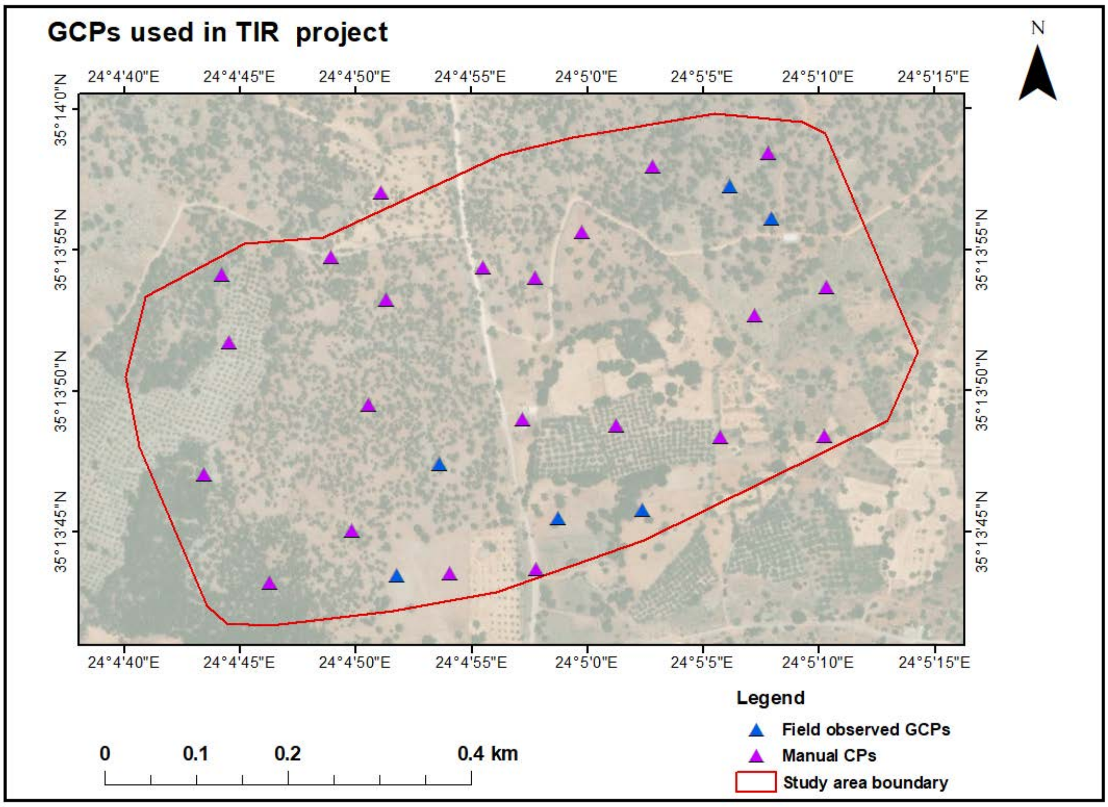

Figure 17: Ground control points (GCPs) and control points (CPs) used thermal infrared (TIR) project.

3.3. Structure from motion

The primary outputs from SfM processing are the RGB orthomosaic, reflectance orthomosaics in the four dedicated spectral bands, an orthomosaic of the LST, and Six calculated vegetation indices.

3.3.1. RGB mosaic

The mosaic for RGB sequenced images, including reflectance value, has an area coverage of 0.446 km^2 and 2.25 cm GSD generated in Pix4Dmapper with RMSE of 0.03, 0.05, and 0.05m for X, Y, and Z, respectively. Figure 18 shows the RGB mosaic output of the study area.

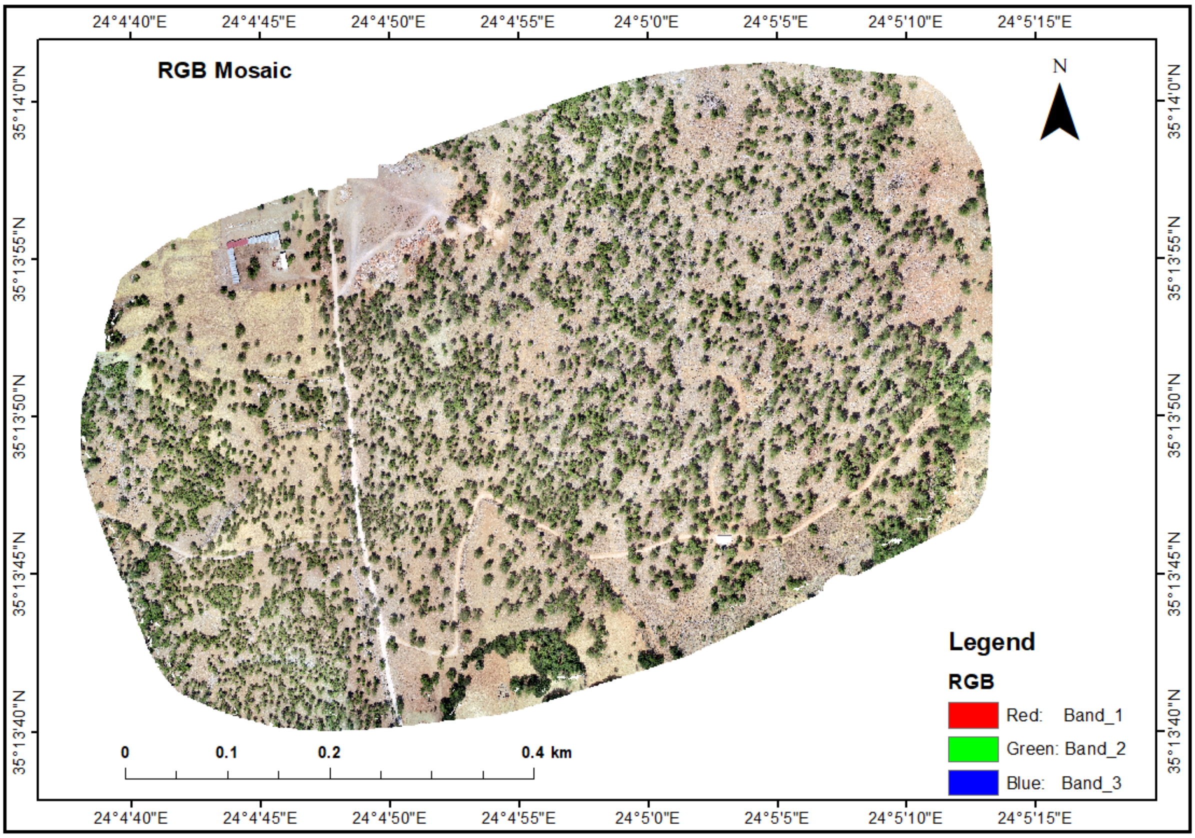

Figure 18: RGB mosaic of the study area.

3.3.2. Multispectral mosaics

The Pix4Dmapper gave reflectance orthomosaics for the four MS bands (i.e., green, red, red-edge, and NIR). Figure 19 shows the composite of the four-band mosaic processed in ArcMap. The total area coverage for the MS project was 0.49 km^2 and 8.46 cm GSD with RMSE of 0.1, 0.16, and 0.39 in X, Y, and Z, respectively.

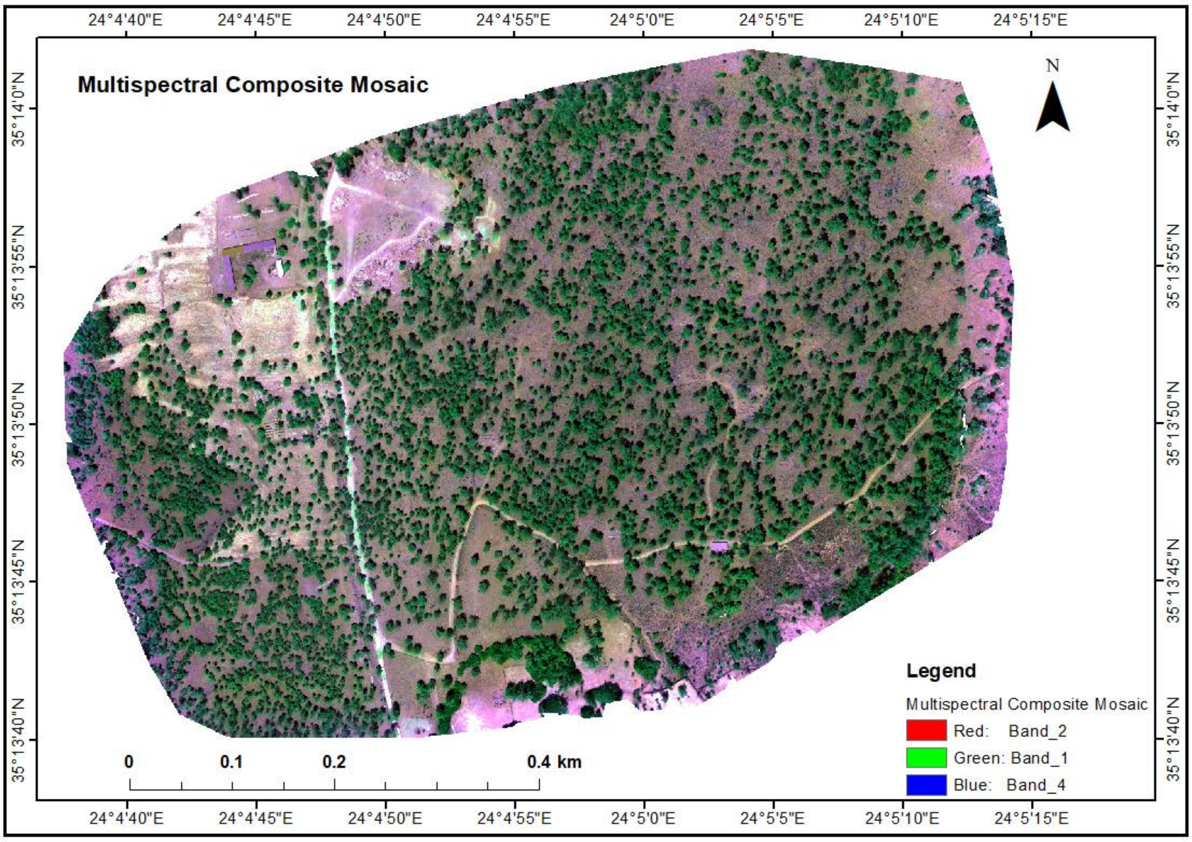

Figure 19: Multispectral composite mosaic of the study area.

3.3.3. Land surface temperature mosaic

An LST mosaic map obtained from the TIR camera was generated by passing through the photogrammetry process (Figure 20). The mosaic map covers an area of 0.455 km^2 with a GSD of 11.37 cm, having 0.19, 0.17, and 0.76 m RMSE in X, Y, and Z, respectively in relation to 22 control points collected from the RGB orthomosaic. In this study area, the temperature of the canopy tree has a lower value compared to the bare soil. The maximum temperature extracted from the canopy of the *in situ* data was approximately 45°C, and the minimum was 31.5°C. LST value for the soil in the west part of the study area was higher than in the east part. The LST at the edge of the study area has an extreme low or high value as a result of the low accuracy in the photogrammetry project at the edge. Also in the LST mosaic, the structure of the trees canopy in the eastern part of the study area is stretched compared with the western part.

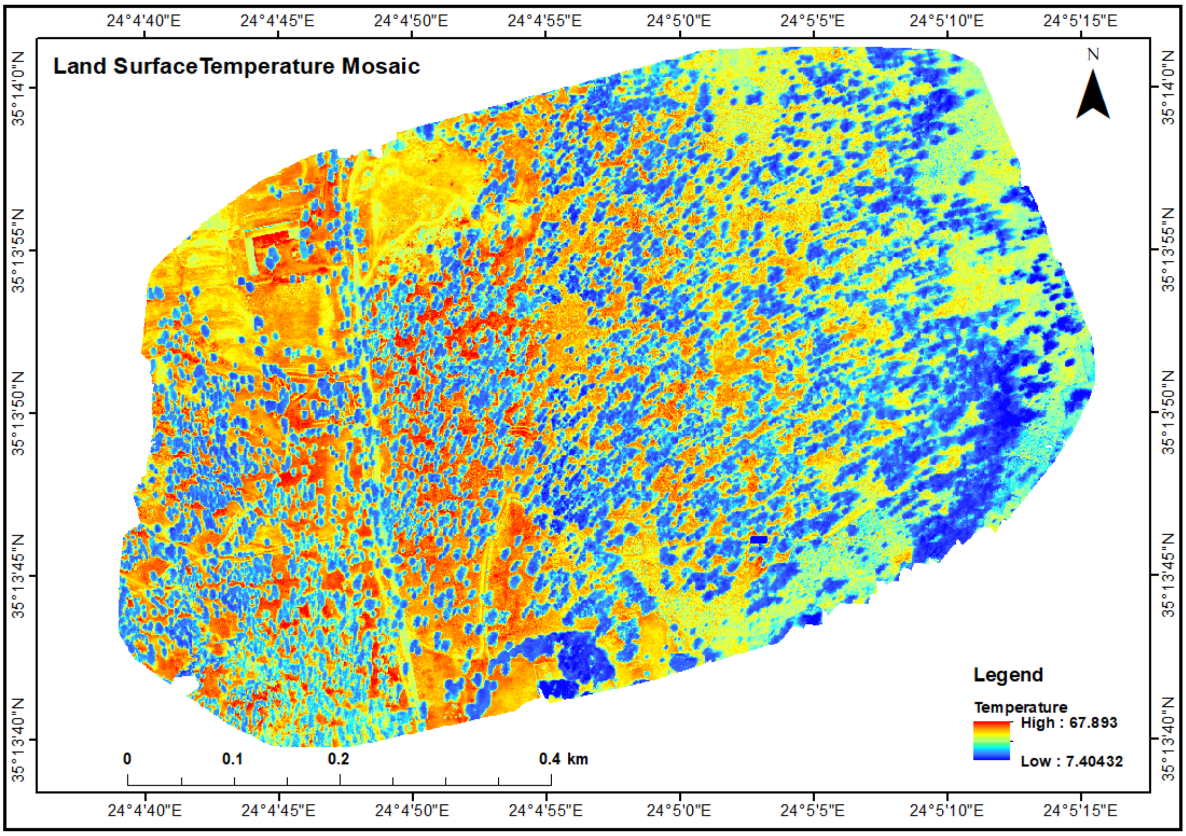

Figure 20: Land surface temperature (LST) map of the study area.

3.3.4. Vegetation indices

The vegetation indices generated in Pix4DMapper have different range values (Table 5). All the vegetation indices in Table 5 except for GCI, are in the range of -1 and 1 where the minimum values are near 0 or -1, and the maximum values are near 1. The average value for SAVI, NDVI, and EVI2 was close; also, NDVI and GNDVI have a close average value. The lower average value from the calculated vegetation index was in NDRE (0.15) and the highest of 1.36 from GCI. The vegetation indices value at the edge of the study area has extremely low or high values as a result of the low photogrammetry MS project accuracy on the edge of the study area.

Table 5: Descriptive statistics of vegetation indices

Vegetation Indices	Minimum	Maximum	Average
NDVI	-0.2	0.92	0.34
SAVI	-0.09	0.68	0.19
NDRE	-0.68	0.82	0.15
EVI2	-0.08	0.74	0.18
GCI	-0.57	18.67	1.36
GNDVI	-0.4	0.9	0.39

The NDVI values of the study area ranged from -0.195 to 0.918. The building and bare soil of the study area were in the lowest value range (Figure 21). In addition, the study area with the open forest has an average NDVI value of 0.34.

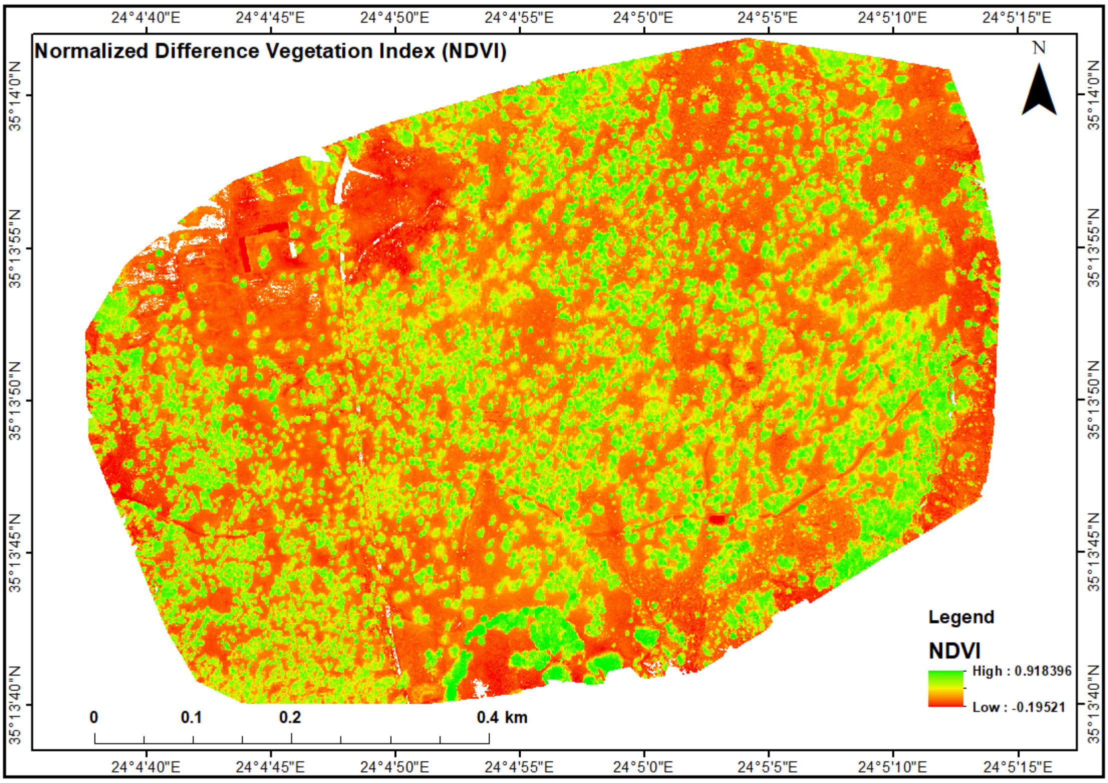

Figure 21: Normalized Difference Vegetation Index (NDVI) map of the study area.

The SAVI values of the study area ranged between -0.092 and 0.678 with an average of 0.19, where most of the trees in the area have approximately above 0.4 values. Similar to the NDVI, the building and bare soil are the ones with low value (Figure 22).

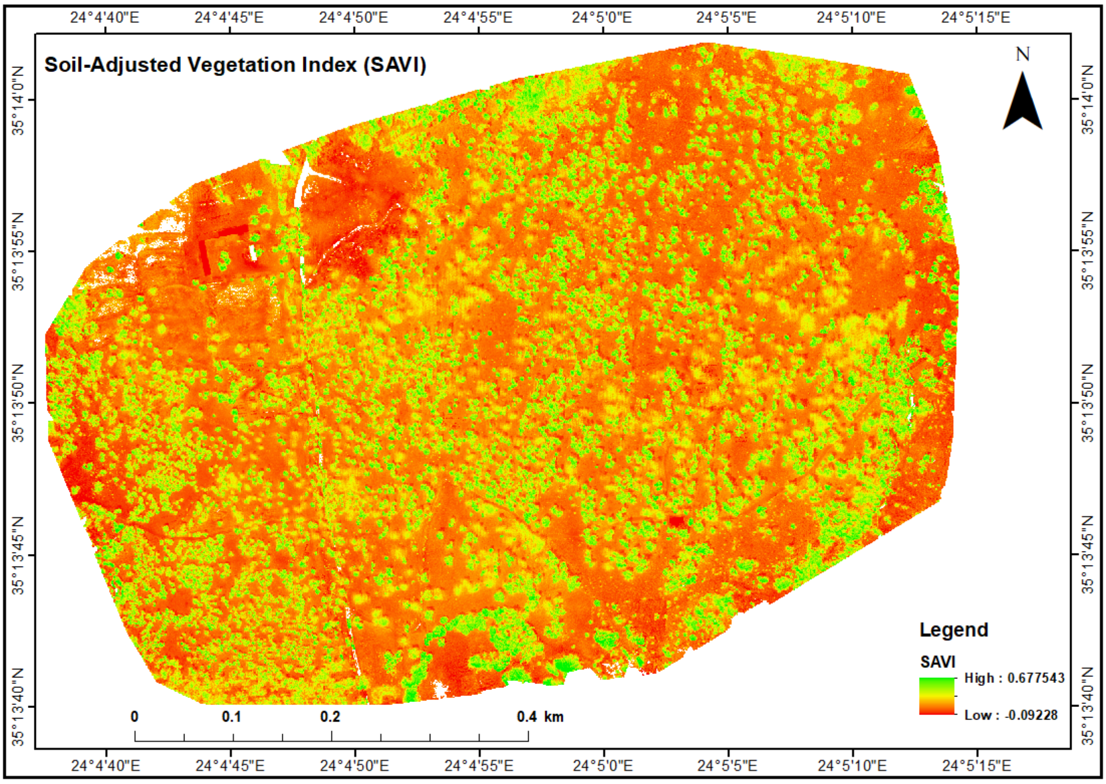

Figure 22: Soil-Adjusted Vegetation Index (SAVI) map of the study area.

A clear difference can be seen using NDRE between areas on edge and the other parts of the study area (Figure 23). The value for this index ranges from -0.676 to 0.816 with a 0.15 average value, where most parts of the study area lay around 0.2.

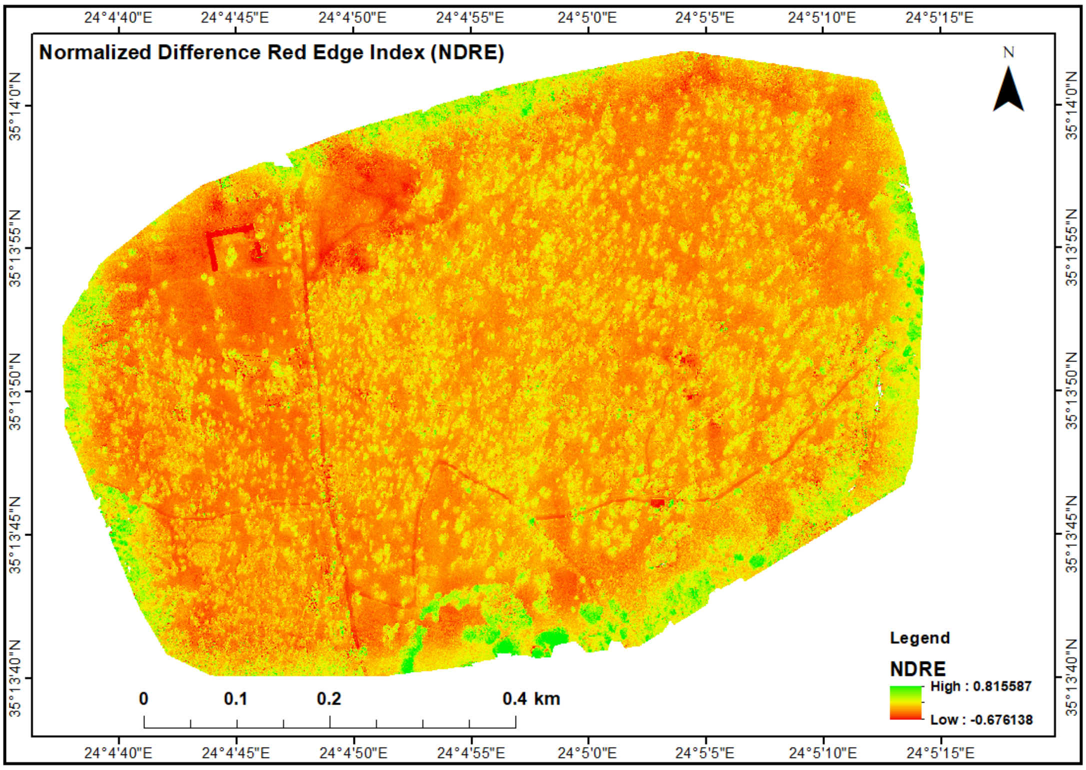

Figure 23: Normalized Difference Red Edge Index (NDRE) map of the study area.

The range of EVI2 values for the research area is -0.079 to 0.744, with an average of 0.18. The majority of trees along the boundary of the research area have a value close to 0.5. Figure 24 depicts the generated EVI2 index map with the research area's value range.

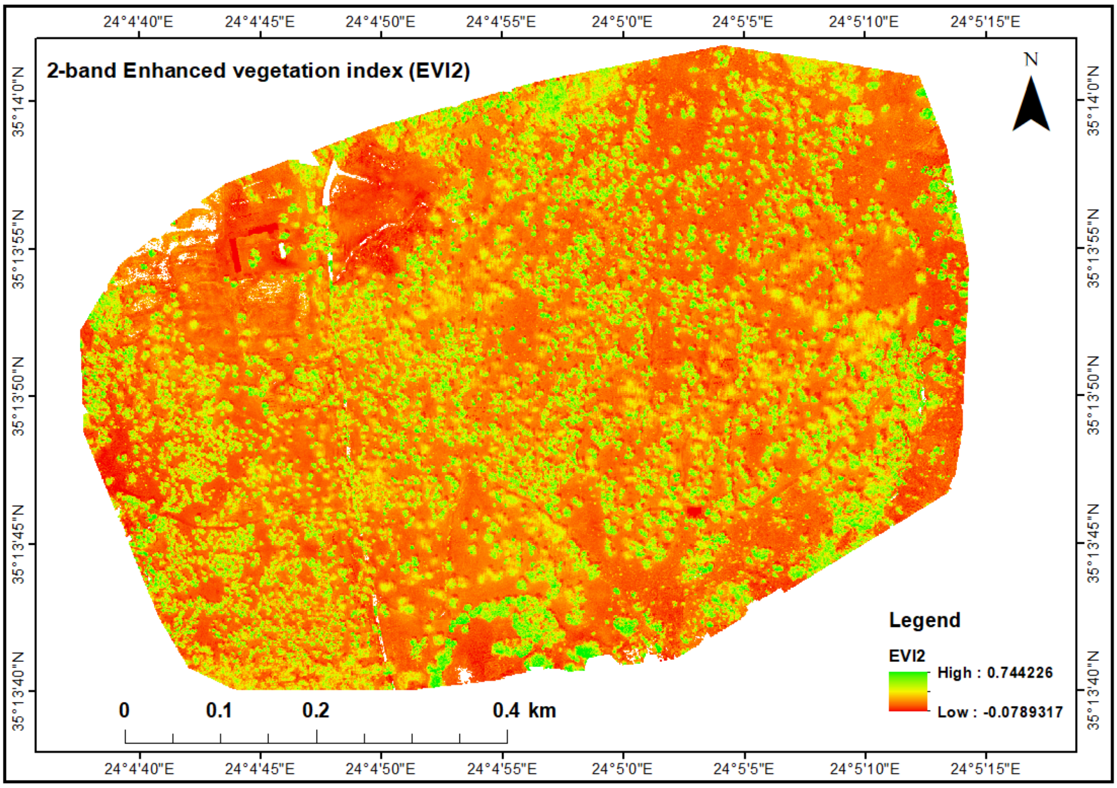

Figure 24: 2-band Enhanced Vegetation Index (EVI2) map of the study area.

The GCI is a non-normalized vegetation index. It can be seen from Figure 25 that the range of GCI for this study area was from -0.572 to 18.67, but only small area coverage has above 0.4 value, where the average value is 1.36.

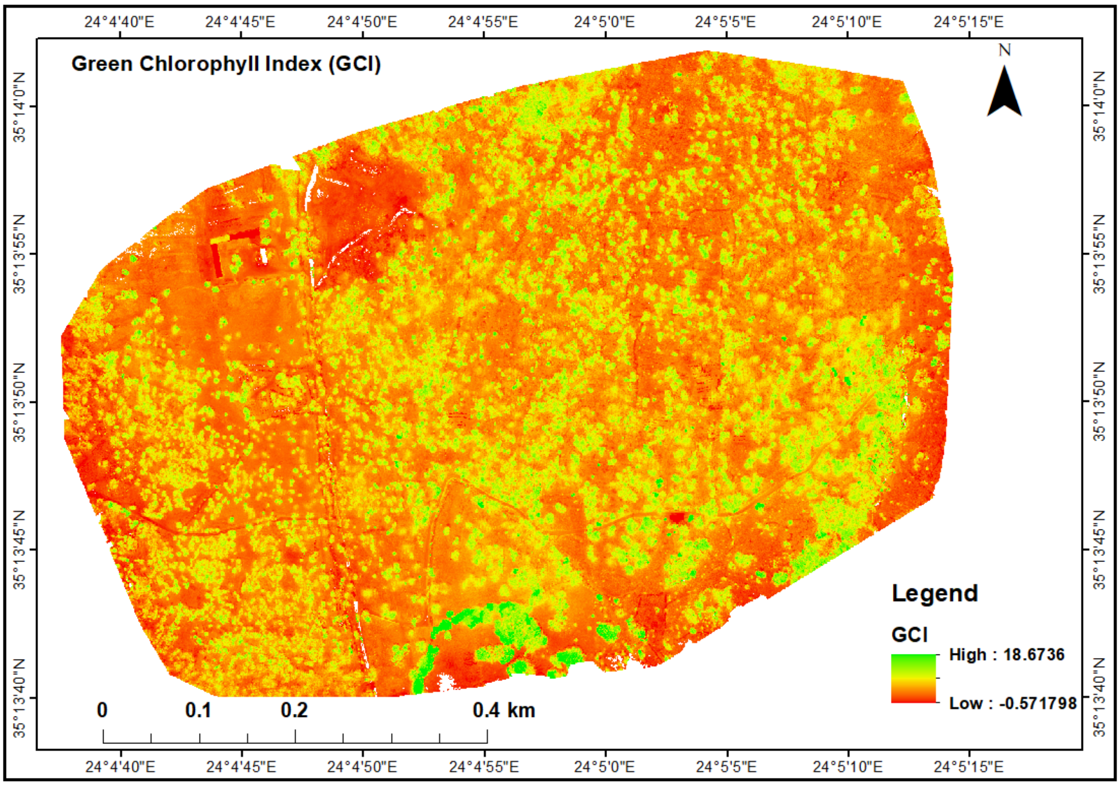

Figure 25: Green Chlorophyll Index (GCI) map of the study area.

Concerning GNDVI, most of the study areas obtained a GNDVI value above 0.5 (Figure 26). This GNDVI value ranges from – 0.4 to 0.9 and has a 0.39 average value. In all the vegetation indices, the building area had a low value.

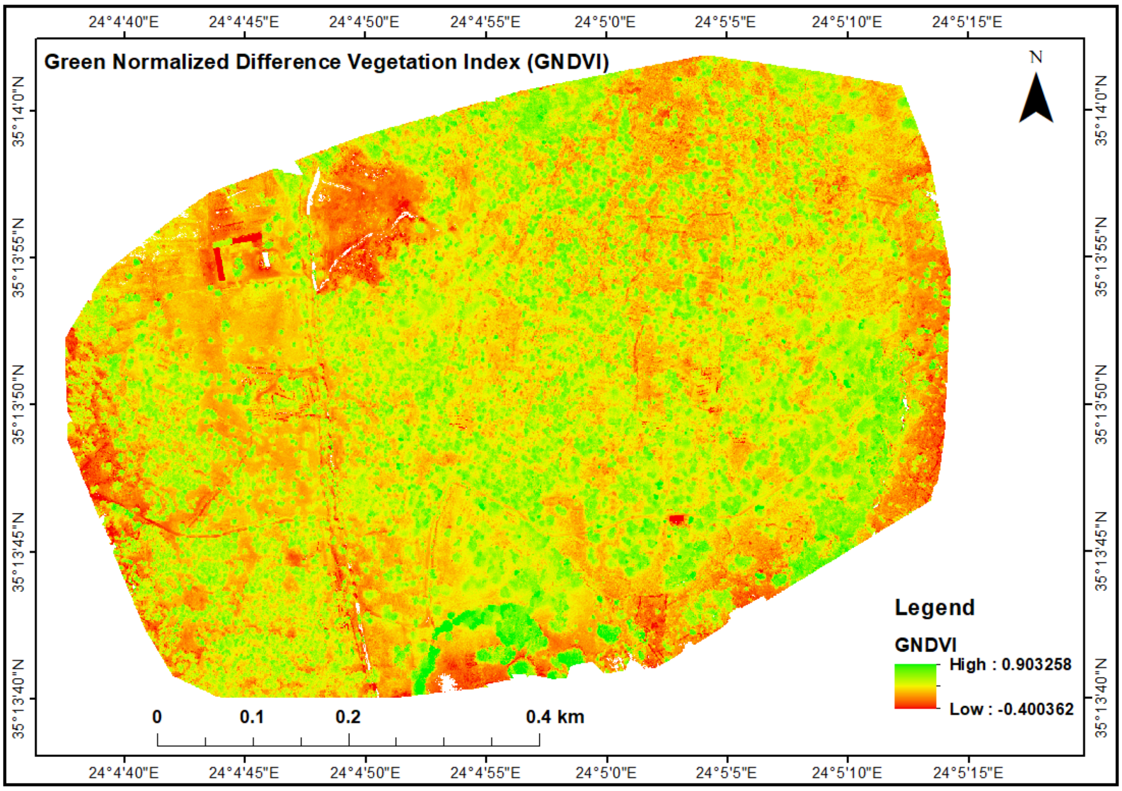

Figure 26: Green Normalized Difference Vegetation Index (GNDVI) map of the study area.

3.4. Classification

From the two performed classification scenarios in classifying the health status Figure 27 shows the first scenario with a classification map of the health status for the study area using information obtained from vegetation indices as an input. More than half of the delineated trees in the study area were classified as severely unhealthy, followed by approximately 30% slightly unhealthy and 15% moderately unhealthy.

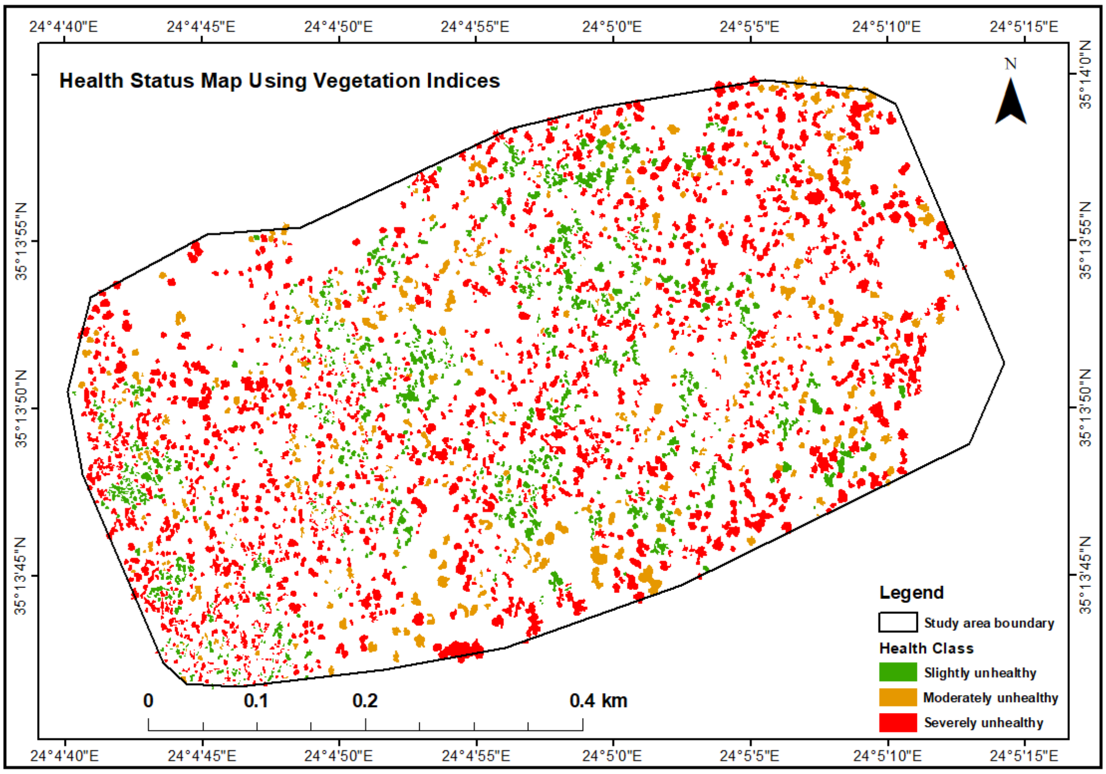

Figure 27: Health status map of the study area using vegetation indices.

The second scenario was canopy temperature-based classification, and the obtained result demonstrated that more than 60% of the study area was classified as severely unhealthy, with approximately 33% and 4% of slightly unhealthy and moderately unhealthy classes, respectively (Figure 28).

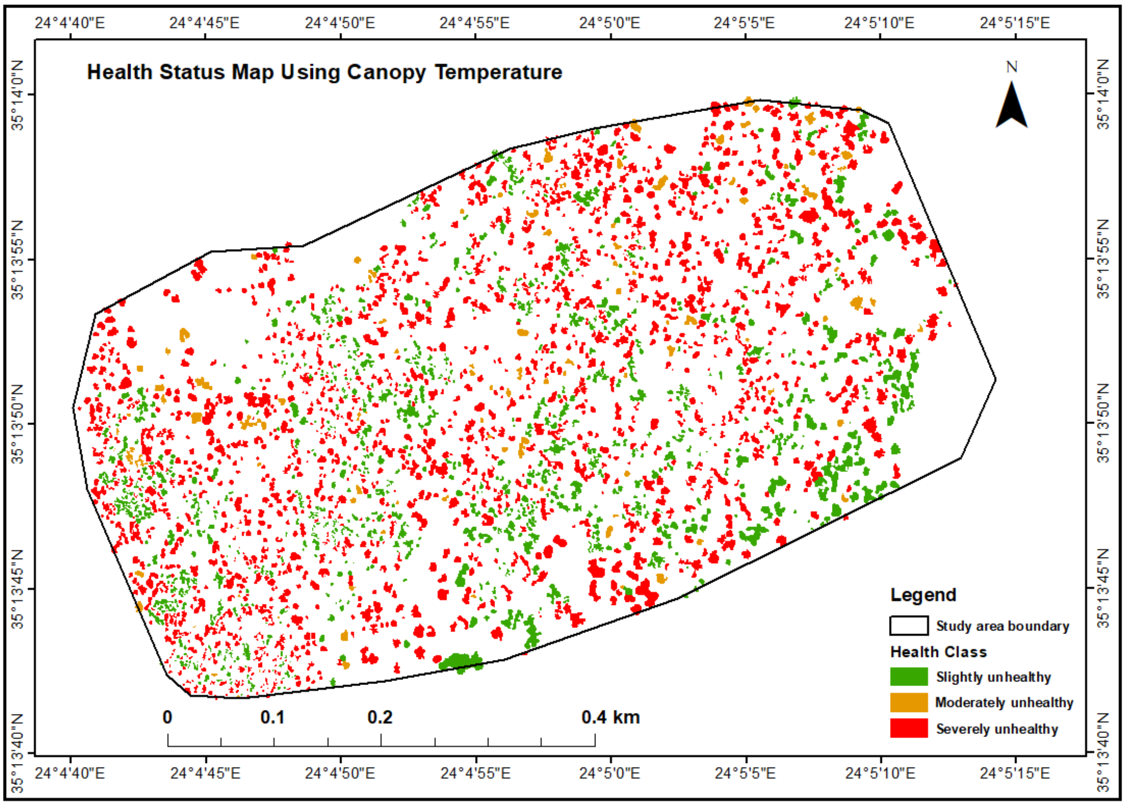

Figure 28: Health status map of the study area using canopy temperature.

As shown in Figure 29, slightly infested trees were rarely found in the study area, covering less than 4% of the classified study area using vegetation indices concerning the discoloration scenario. However, around 34% and 62% were classified as moderately and severely infested.

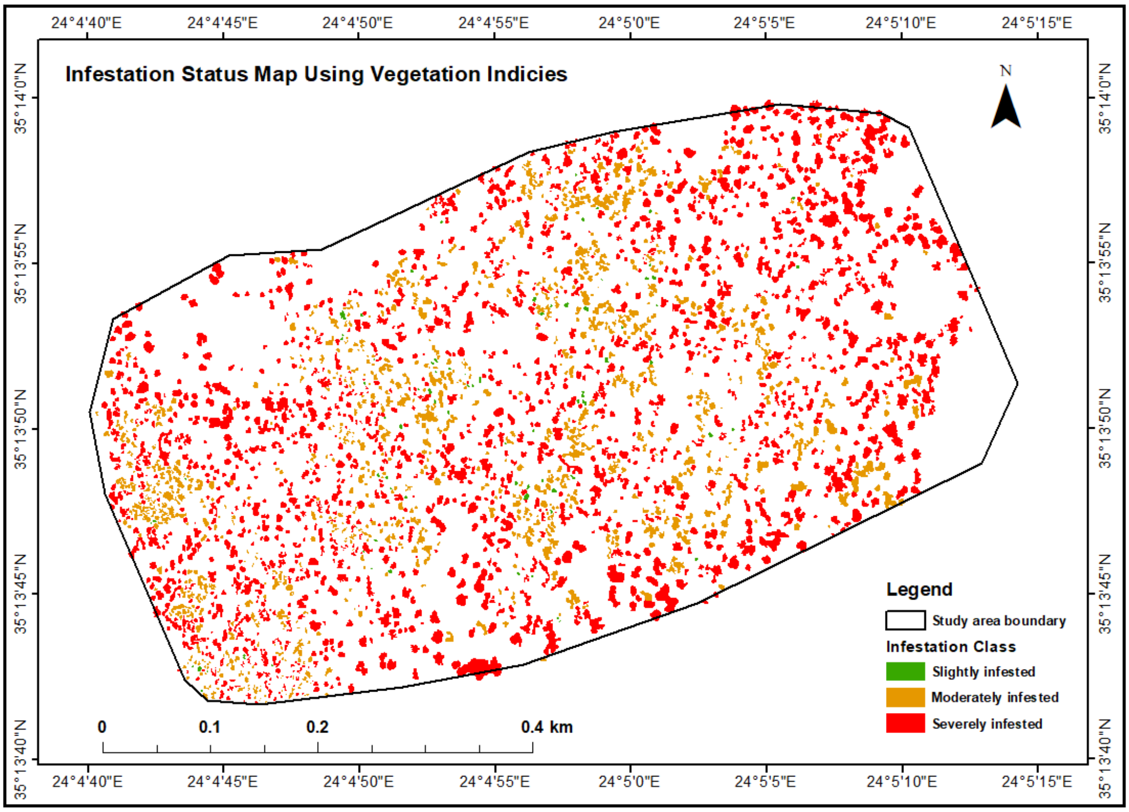

Figure 29: Infestation status map of the study area using canopy temperature.

Figure 30 shows the classification for infestation status using a canopy temperature scenario. The result indicates that 6%, 40%, and 54% of the study area were classified as slightly infested, moderate infested, and severe infested, respectively.

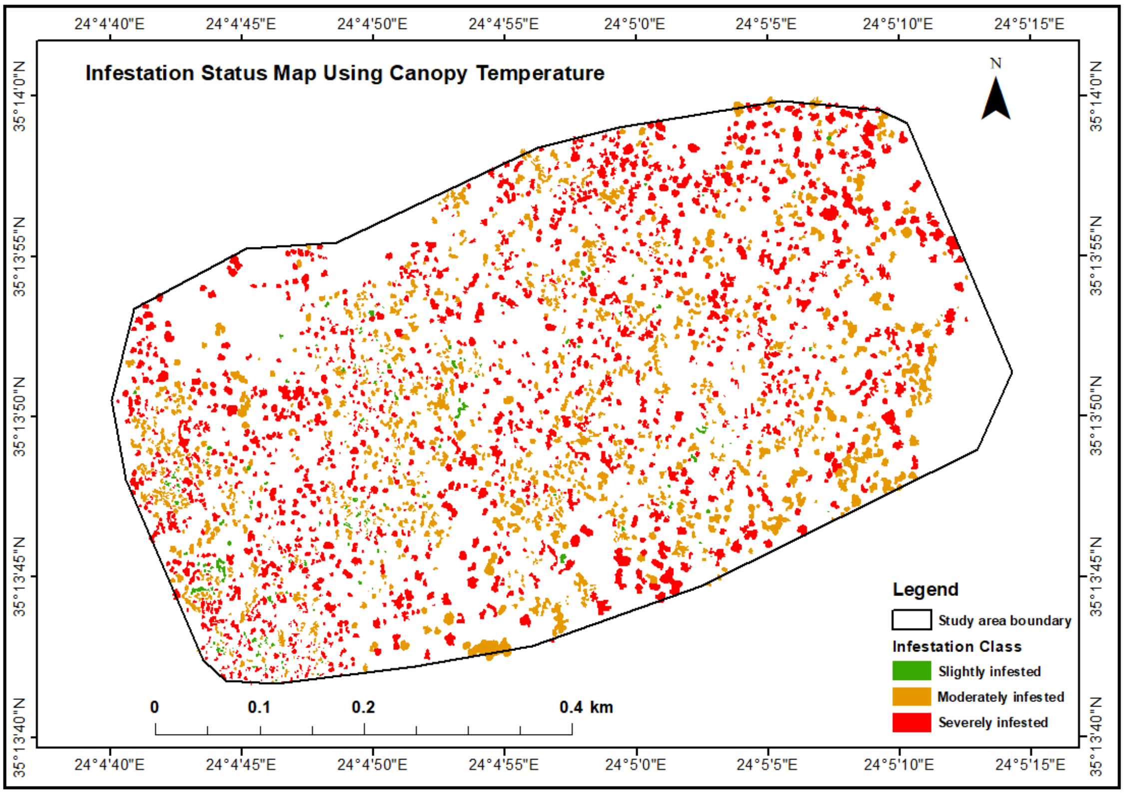

Figure 30: Infestation status map of the study area using canopy temperature.

Table 6 shows the classification accuracy for the four scenarios as mentioned above. The vegetation indices layer had a higher producer, user, and overall accuracy than the canopy temperature in classifying trees using defoliation with 52% and 45% overall accuracy, respectively. In discoloration-based classification, both layers had the same 42% producer accuracy. However, the overall accuracy was higher when classified using vegetation indices (55%) than canopy temperature (48%).

Table 6: Classification accuracy assessment in the four different scenarios.

Scenarios		Accuracy		
Indicators	**Layers**	**Producer**	**User**	**Overall**
Defoliation	Vegetation Indices	80%	47%	52%
	Canopy temperature	70%	41%	45%
Discoloration	Vegetation Indices	42%	57%	55%
	Canopy temperature	42%	42%	48%

3.5. Spectral signature of individual class

The relation between the mean spectral reflectance value of delineated tree crowns (i.e., defoliation-based health classes) and MS bands is shown in Figure 31. As shown in Figure 31, slightly unhealthy classified trees showed higher reflectance value in NIR and higher absorption in red bands compared to the other two classes (i.e., moderately and severely unhealthy). Whereas unexpectedly, the reflectance for severely defoliated trees had a higher reflectance value than the moderate defoliated trees in red-edge and NIR bands.

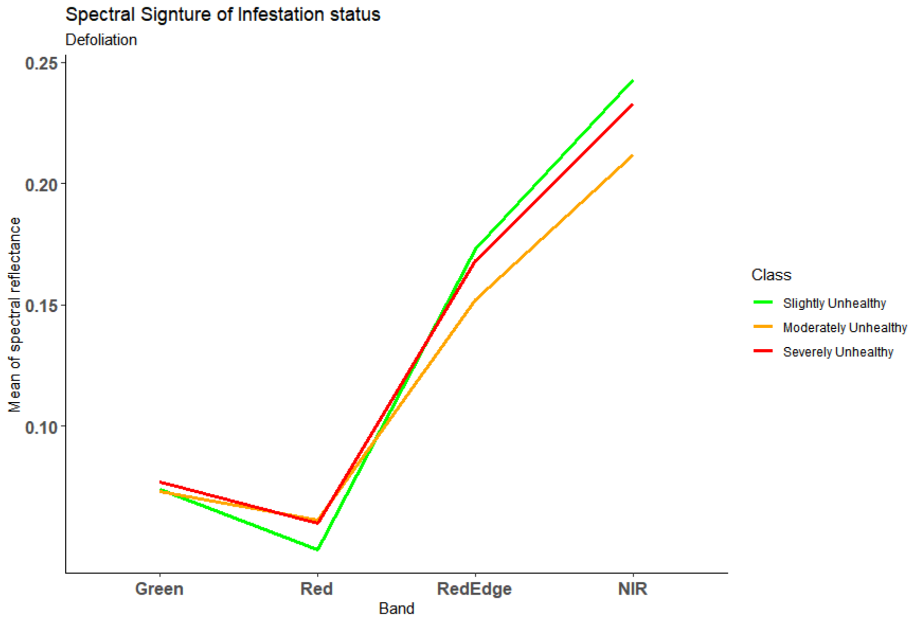

Figure 31: Spectral signature of trees according to their health status.

Figure 32 shows the reflectance value in the four bands for delineated trees grouped in three discoloration-based infestation classes. The slightly infested class has a higher reflectance value in red-edge and NIR bands. The reflectance value for the moderately infested class was lower than the severely infested class in the red band and vice versa in the NIR bands. Figure 32 also illustrates a trend where the reflectance values decrease in the NIR band when infestation levels increase.

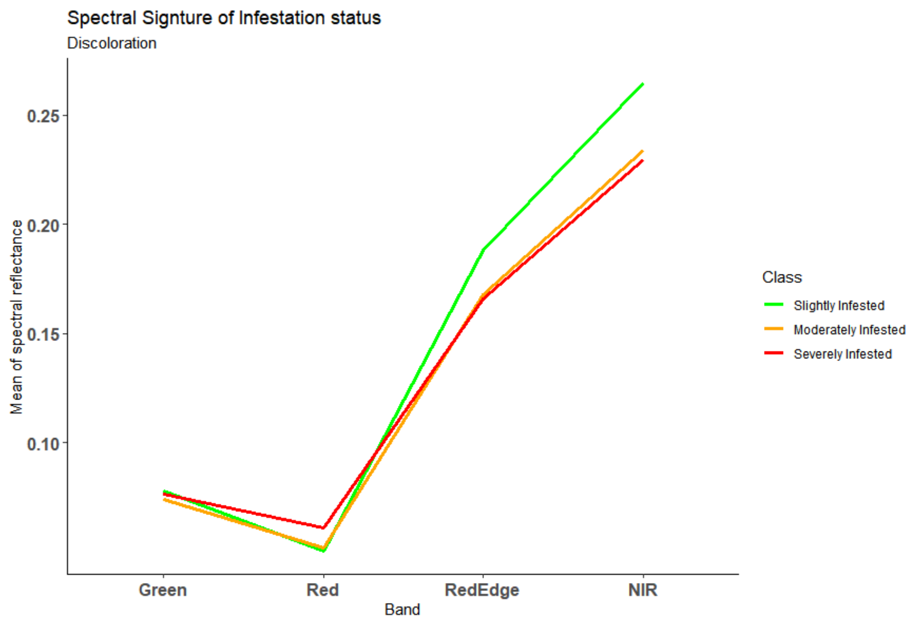

Figure 32: Spectral signature of trees according to their infestation status.

3.6. Statistical comparison

For the 105 field observed sample trees, *P*-Values from Post hoc Tukey's HSD show that there is no statistically significant difference between moderately and severely unhealthy classes in all the layers used to assess health status, compared to the other used layers canopy temperature and NDRE seems to be close to the 0.05 where mean difference is expected to be significant. In addition, there is no significant difference between slightly and moderately infested classes while using canopy temperature and NDRE mean values to assess the infestation status (Table 7).

The result from ANOVA and Post hoc Tukey's HSD test with a confidence interval of 95% after classification shows a statistically significant difference between the classes in both assessment types (i.e., health and infestation status assessment). For most layers, the class difference shares the same *P*-value in Tukey's HSD test for multiple comparisons (Table 8).

Table 7: Post hoc analysis result for 105 sample trees in health and infestation assessment.

Layer	*P*-Values					
	Health status assessment			Infestation status assessment		
	Slightly-Moderately	Slightly-Severely	Moderately-Severely	Slightly - Moderately	Slightly - Severe	Moderately-Severely
Canopy temperature	$1.53x10^{-2}$	$1.0x10^{-5}$	$1.34x10^{-1}$	$7.82*10^{-1}$	$1.05*10^{-3}$	$1.76x10^{-4}$
NDVI	$9.37*10^{-4}$	$1.2*10^{-5}$	$6.29*10^{-1}$	$6.3*10^{-2}$	$2.19*10^{-4}$	$3.65*10^{-2}$
SAVI	$5.2*10^{-5}$	$5.2*10^{-5}$	$7.38*10^{-1}$	$7.62*10^{-3}$	$5.0*10^{-6}$	$2.12*10^{-2}$
EVI2	$4.9*10^{-5}$	$8.33*10^{-7}$	$7.71*10^{-1}$	$6.84*10^{-3}$	$5.0*10^{-6}$	$2.49*10^{-2}$
GCI	Not used	Not used	Not used	$1.42*10^{-2}$	$1.8*10^{-5}$	$3.06*10^{-2}$
GNDVI	$6.7*10^{-5}$	$2.68*10^{-7}$	$5.53*10^{-1}$	Not used	Not used	Not used
NDRE	$5.55*10^{-2}$	$6.0*10^{-5}$	$1.14*10^{-1}$	$7.70*10^{-1}$	$2.6*10^{-2}$	$2.2*10^{-2}$

Table 8: Post hoc analysis results in health and infestation status assessment after classification.

Layer	*P*-Values					
	Health status assessment			Infestation status assessment		
	Slightly-Moderately	Slightly-Severely	Moderately-Severely	Slightly - Moderately	Slightly - Severely	Moderately-Severely
Canopy temperature	$9.7*10^{-9}$	$5.1*10^{-9}$	$3.5*10^{-5}$	$5.1*10^{-9}$	$5.4*10^{-7}$	$5.1*10^{-9}$
NDVI	$5.1*10^{-9}$	$5.1*10^{-9}$	$5.1*10^{-9}$	$5.1*10^{-9}$	$5.1*10^{-9}$	$5.1*10^{-9}$
SAVI	$5.1*10^{-9}$	$5.1*10^{-9}$	$5.1*10^{-9}$	$5.1*10^{-9}$	$5.1*10^{-9}$	$5.1*10^{-9}$
EVI2	$5.1*10^{-9}$	$5.1*10^{-9}$	$5.1*10^{-9}$	$5.1*10^{-9}$	$5.1*10^{-9}$	$5.1*10^{-9}$
GCI	Not used	Not used	Not used	$5.1*10^{-9}$	$5.1*10^{-9}$	$5.1*10^{-9}$
GNDVI	$5.1*10^{-9}$	$5.1*10^{-9}$	$5.1*10^{-9}$	Not used	Not used	Not used
NDRE	$1.43*10^{-2}$	$5.1*10^{-9}$	$1.43*10^{-4}$	$2.28*10^{-4}$	$3.84*10^{-4}$	$1.33*10^{-3}$

The result of separability analysis between classes in order to assess the health status is shown in Table 9. The separability analysis between health classes defined based on the defoliation indicates that slightly unhealthy class is higher than moderately unhealthy class; however, moderately unhealthy class is less than severely unhealthy class, while using the vegetation indices except in NDRE. However, using canopy temperature, the separability between slightly and moderately unhealthy classes was -0.417. The separability between moderately and severely unhealthy status was -0.250, meaning the difference was negative.

Table 9: Separability analysis between defoliation-based classes.

		Separability					
Indicator	**Class**	**NDRE**	**NDVI**	**SAVI**	**EVI2**	**GNDVI**	**Canopy temperature**
Defoliation	Slightly unhealthy – Moderately unhealthy	0.017	0.254	1.215	1.187	0.151	-0.417
	Moderately unhealthy - Severely unhealthy	0.122	-0.300	-0.508	-0.521	-0.059	-0.250
	Slightly unhealthy - Severely unhealthy	0.037	0.158	0.485	0.453	0.405	-0.559

In assessing the difference among the infestation classes separability method was used, where the classes were discoloration based. The result from separability analysis for the infestation classes shows that vegetation indices enable to show the difference between the classes (Table 10). For instance, SAVI was able to show separability well compared to the other vegetation indices and the highest separability was found between slightly infested and severely infested status (1.014), as well as between slightly infested and moderately infested classes (0.716). On the other hand, canopy temperature obtained from TIR data did not follow the same trend among the classes, where the separability between slightly infested and moderately infested classes was found between 0.462 and -0.567 for moderately and severely infested classes.

Table 10: Separability analysis between discoloration-based classes.

		Separability					
Indicator	**Class**	**NDRE**	**NDVI**	**SAVI**	**EVI2**	**GCI**	**Canopy temperature**
Discoloration	Slightly infested - Moderately infested	0.15	0.527	0.716	0.708	0.41	0.462
	Moderate infested - Severely infested	0.061	0.387	0.297	0.281	0.18	-0.567
	Slightly infested – Severely infested	0.216	0.952	1.014	0.986	0.59	-0.254

3.7. Canopy temperature and vegetation indices versus health class

The results revealed that the mean canopy temperature value increased with rising defoliation in health classes (Figure 33). The severely unhealthy class had many outliers, and approximately 75% of the trees had a temperature greater than 35°C. For the moderately class, the canopy temperature of many trees was found to be approximately between 35°C and 35.5°C temperatures and very close to each other.

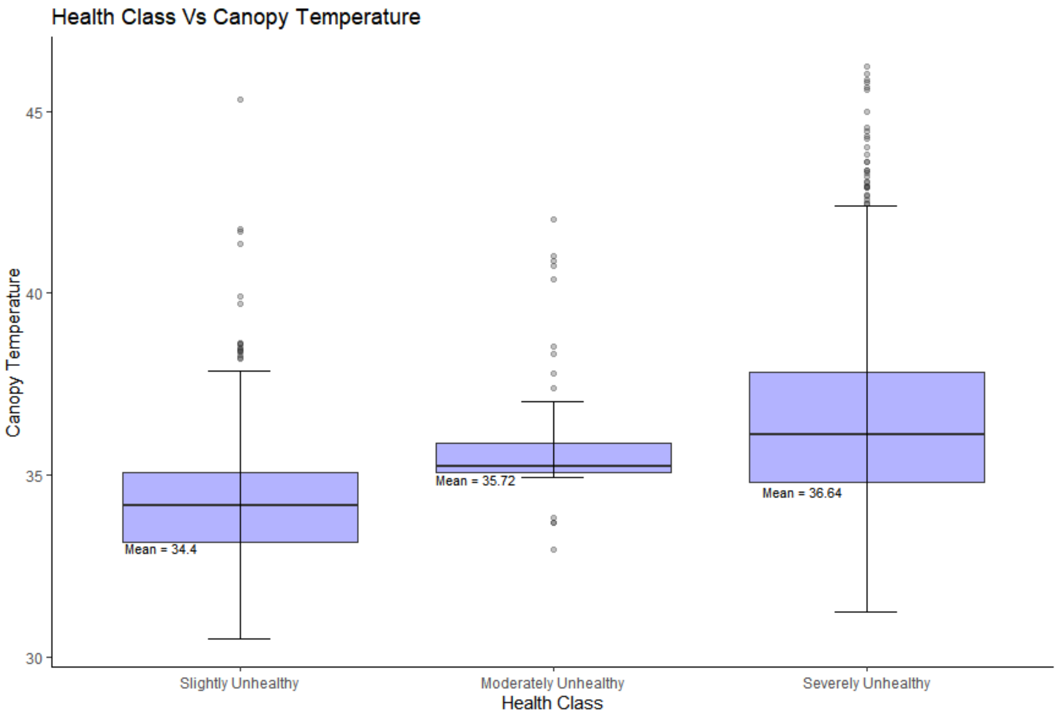

Figure 33: Relation between Canopy temperature and health class.

Figures 34 to 38 show the relationship between different vegetation indices and defoliation-based health classes. For NDVI, the slightly unhealthy class was normally distributed, whereas, for moderately and severely unhealthy classes, the skewness of outliers started around 0.4 with a mean value of 0.66, 0.55, and 0.59 for slightly, moderately, and severely unhealthy classes, respectively. As can be noticed from Figure 34, the mean value change between moderately and severely unhealthy classes did not follow the same downward direction as the change between slightly and moderately unhealthy classes using NDVI; also, the result showed that there no relationship can be found between the health class and the NDVI values.

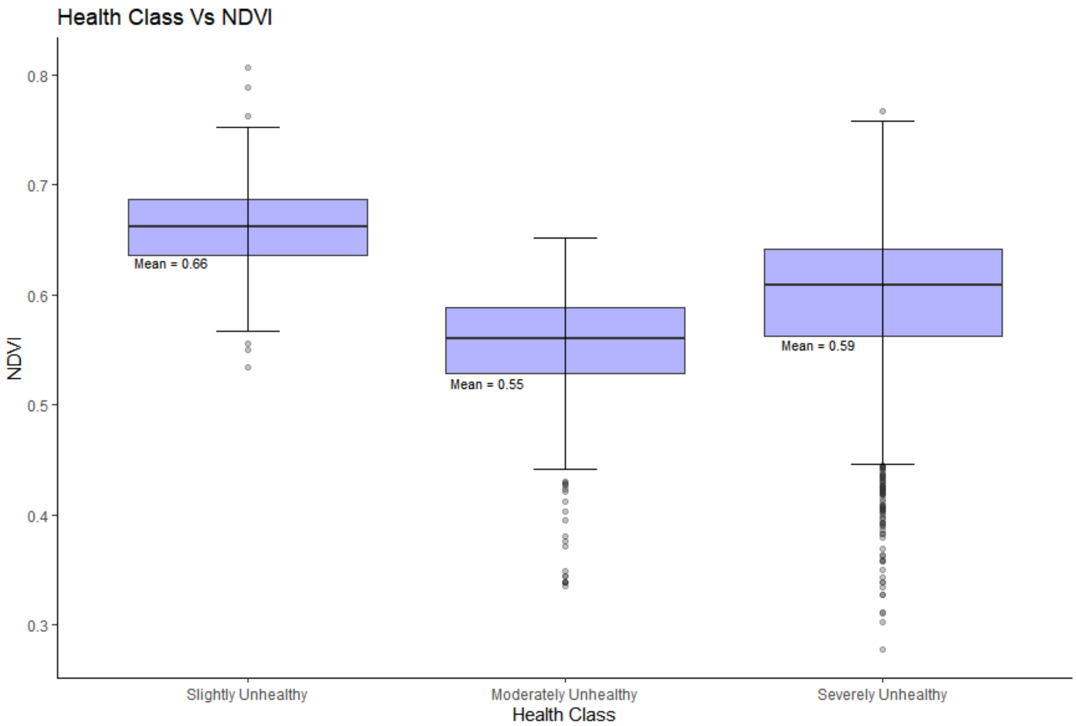

Figure 34: Relation between NDVI and health class.

Similar to NDVI, a defined positive or negative relation can not be seen between the SAVI and health classes. As can be seen from Figure 35, the mean value for the severely unhealthy class increased to 0.32 value unexpectedly from the moderately unhealthy class of 0.29 value. The moderately unhealthy class mean value was lower than the slightly unhealthy class, where the slightly unhealthy class mean value was 0.36. The change between consecutive classes did not follow a consistence order and did not show a defined positive or negative relationship between the SAVI and the health class.

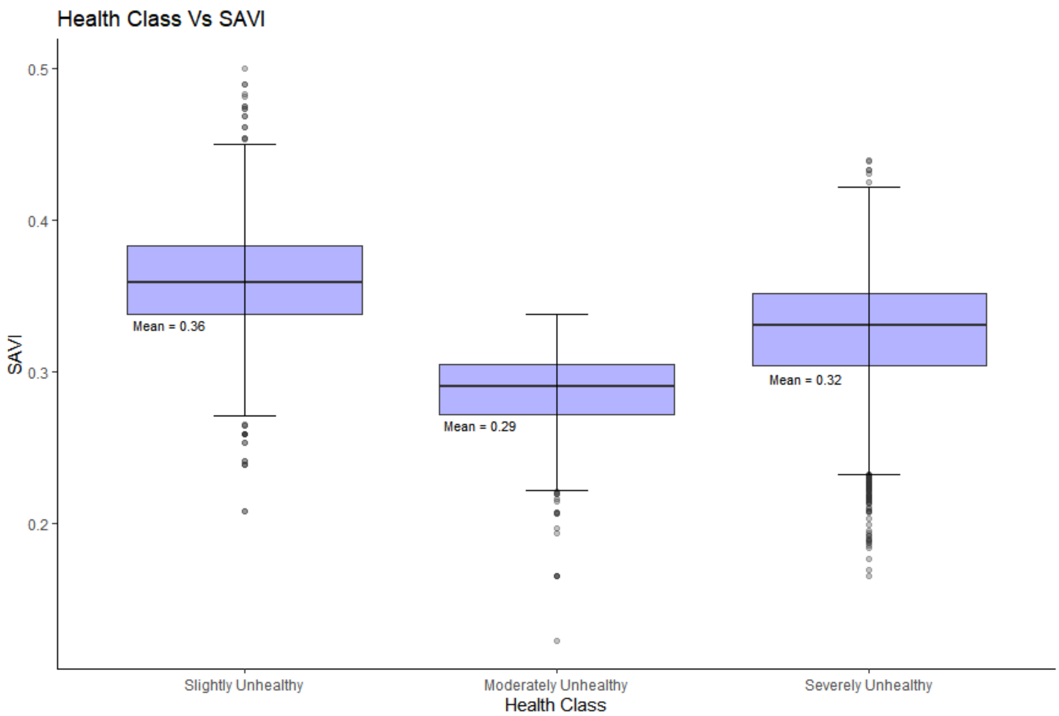

Figure 35: Relation between SAVI and health class.

The other relation analysis was performed between EVI2 and health classes. The mean values for the three classes were the same as SAVI. The relationship with the increment in defoliation was not able to be fully described by the EVI2 values (Figure 36).

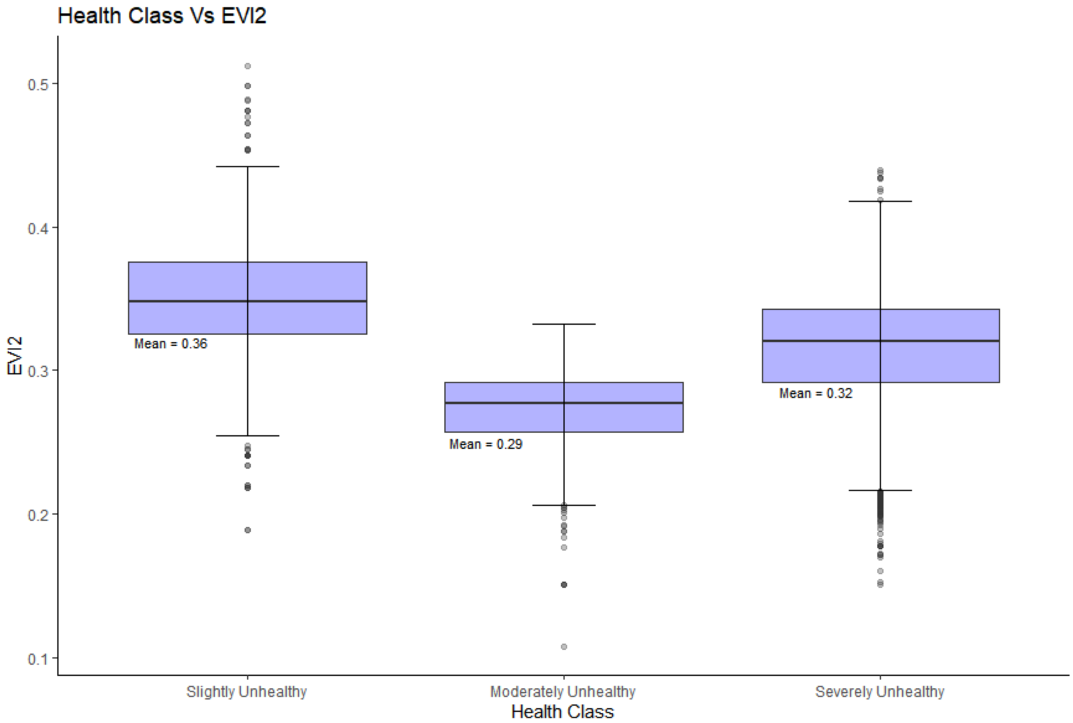

Figure 36: Relation between EVI2 and health class.

Figure 37 shows the relationship between health class and GNDVI. From all the vegetation indices used to indicate a relationship with the defoliation-based health class, the GNDVI value of the three classes had more or less a normal distribution type; even if it was normally distributed, a clear relationship could not be seen. The 0.53 GNDVI mean value of the slightly unhealthy class was closer to the severely unhealthy class (0.5) than the moderately unhealthy class (0.48).

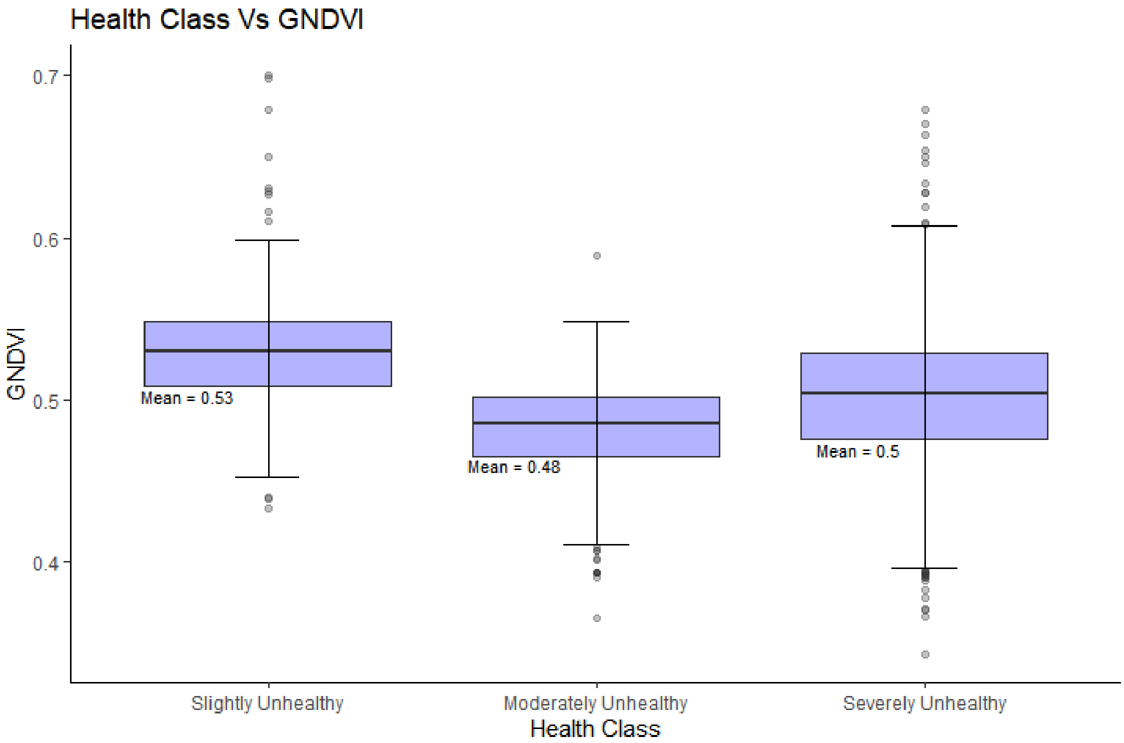

Figure 37: Relation between GNDVI and health class.

The mean difference between the two classes (i.e., Slightly and moderately unhealthy classes) in NDRE was minor. The mean value for the slightly, moderately, and severely unhealthy was approximately 0.17, 0.17, and 0.16, respectively. For the three classes, the skewness as a result of outliers started at approx. 0.20 (Figure 38).

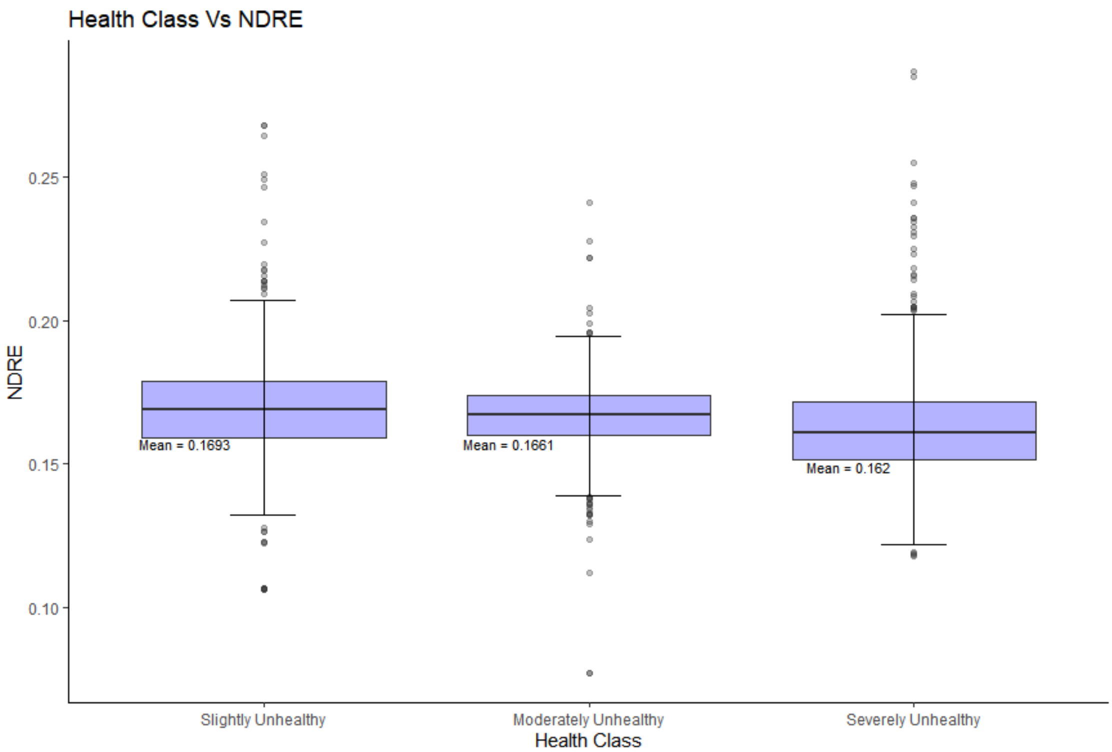

Figure 38: Relation between NDRE and health class.

3.8. Canopy temperature and vegetation indices versus infestation class

The result indicates that canopy temperature and discoloration-based infestation classes did not have a defined relation (Figure 39). Most trees in the slightly infested class had 35°C canopy temperature values. The moderately infested tree class had a lower mean canopy temperature value (34.42°C) than the slightly infested unexpectedly, whereas the severely infested class showed a 37°C average canopy temperature. Considering the canopy temperature mean value, three infestation classes did not follow the same upward trend when discoloration increased.

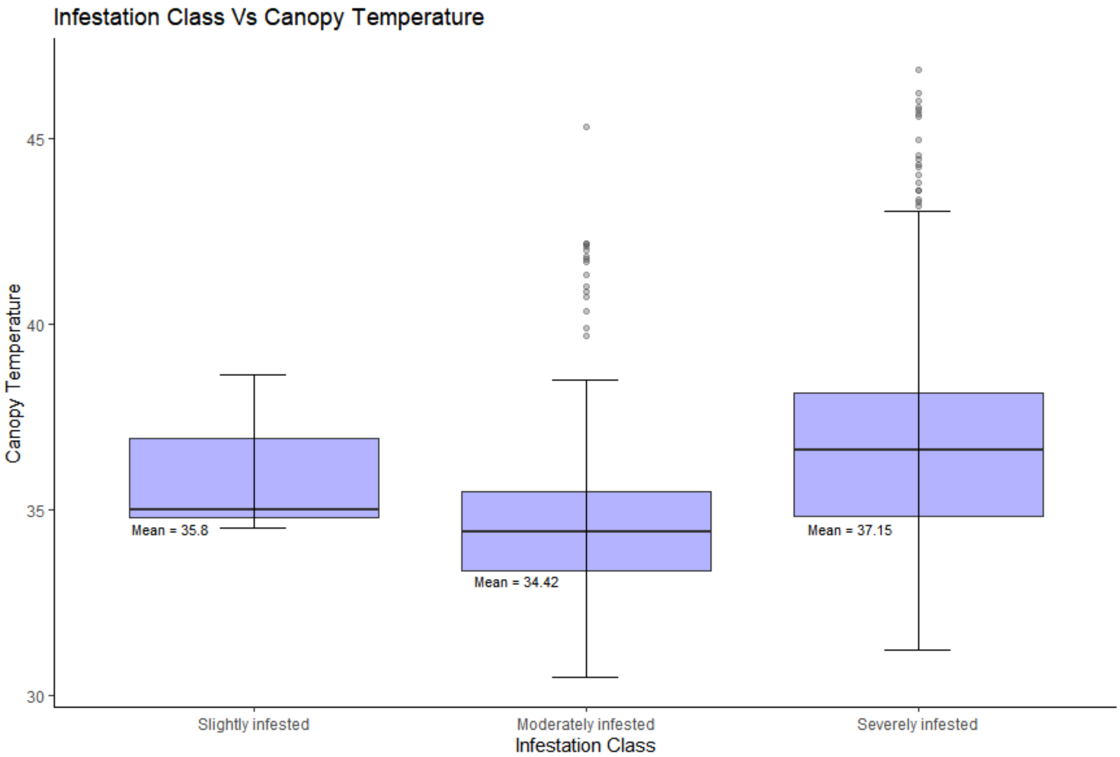

Figure 39: Relation between Canopy temperature and Infestation class.

The Figures below (Figure 40 - 44) show the relationship between infestation classes and vegetation indices; The infestation class had the same downward trend in all vegetation indices. An inverse relationship can be seen between NDVI and the infestation class (Figure 40). Moderately and severely infested classes had mean values of 0.63 and 0.58, respectively, while the slightly infested class had a higher NDVI mean value of 0.68.

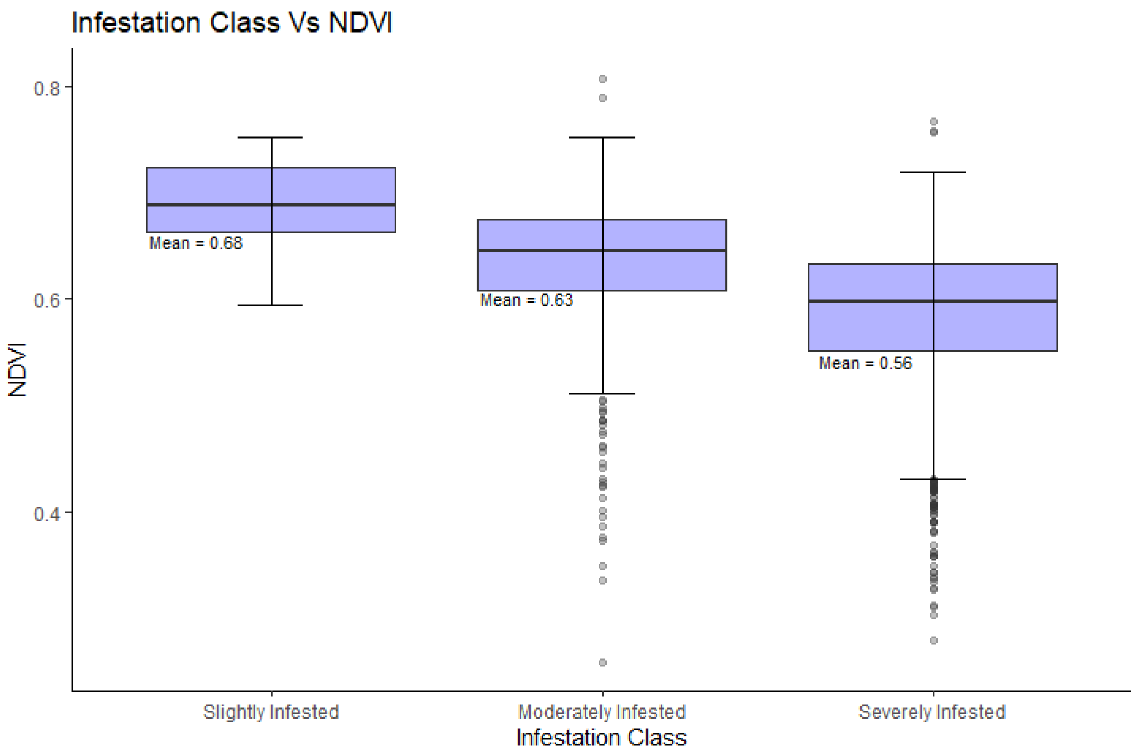

Figure 40: Relation between NDVI and Infestation class.

The SAVI and infestation class relationship shown in Figure 41 implies there was a negative relationship. Unlike the NDVI, SAVI values were not normally distributed for the slightly infested class. The SAVI mean value decreased from slightly to severely infested class, where the mean value for the classes was 0.4, 0.34, and 0.32 for slightly, moderately, and severely infested, respectively.

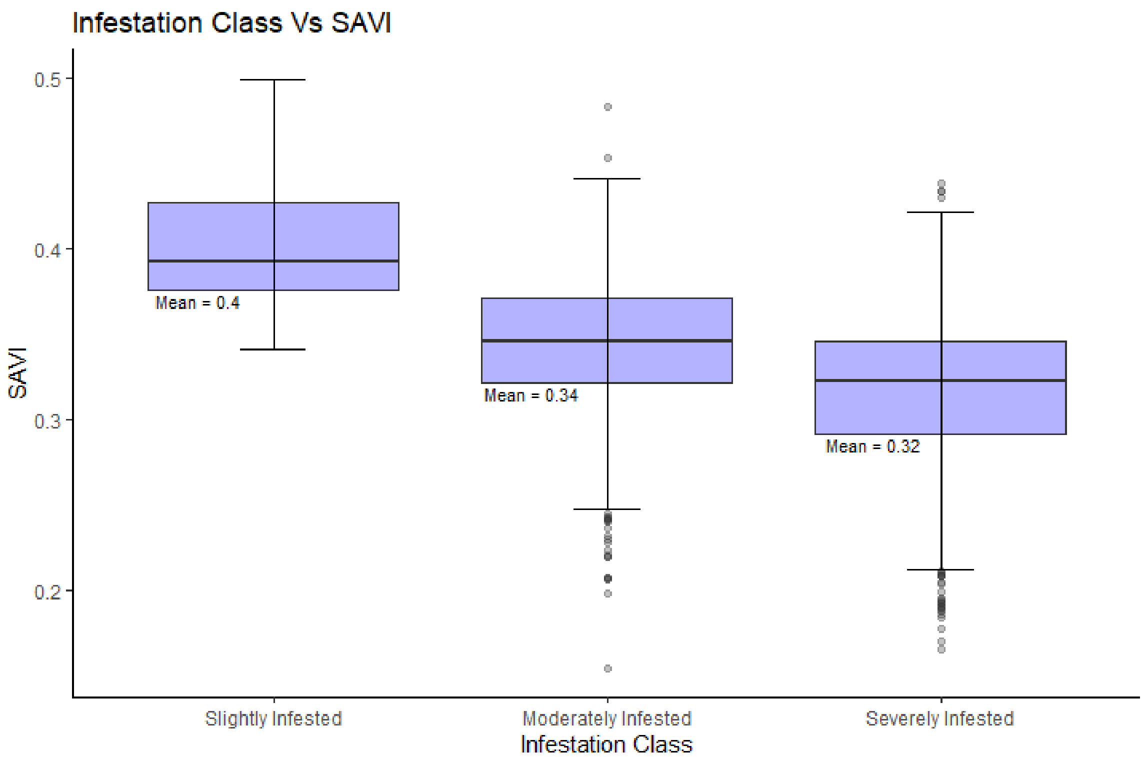

Figure 41: Relation between SAVI and Infestation class.

Figure 42 shows the EVI2 mean values decreased when the discoloration in trees increased for the infestation class. With this inverse relationship, the mean values decreased from 0.39 (slightly infested) to 0.33 (moderately infested) and 0.31(severely infested).

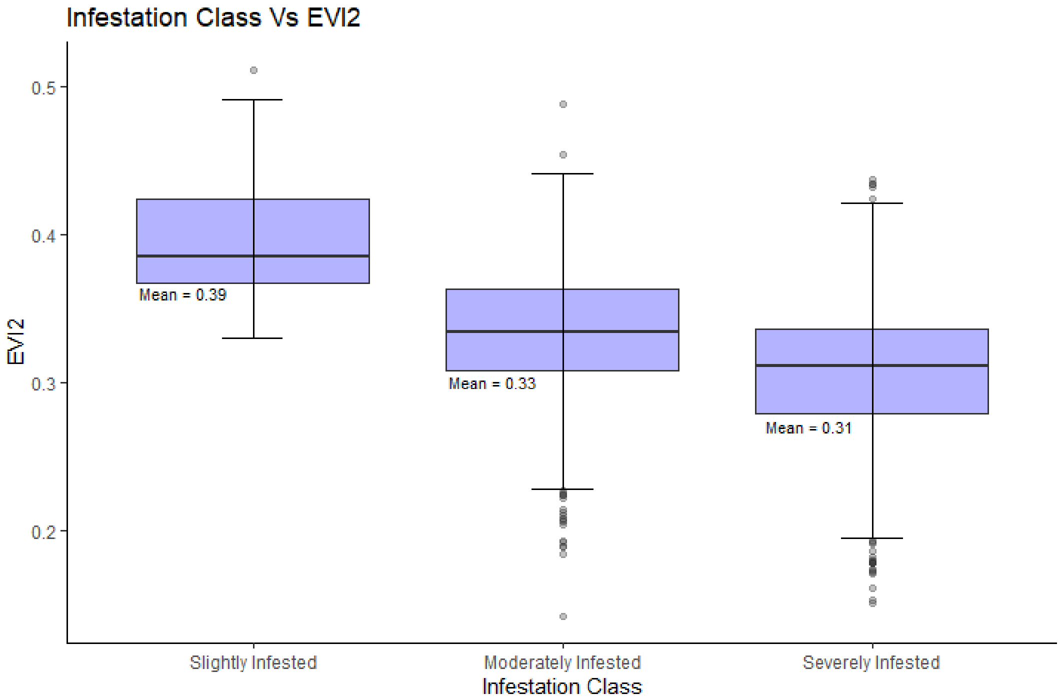

Figure 42: Relation between EVI2 and Infestation class.

There was a defined relationship between GCI and infestation class, as shown in Figure 43. Moderately and severely infested classes had a skewed distribution than the slightly infested class. The mean values give a picture of how the GCI decreased from slightly to severely infested status, where the mean values of the classes are 2.45, 2.17, and 2.04 for slightly infested, moderately infested, and severely infested, respectively.

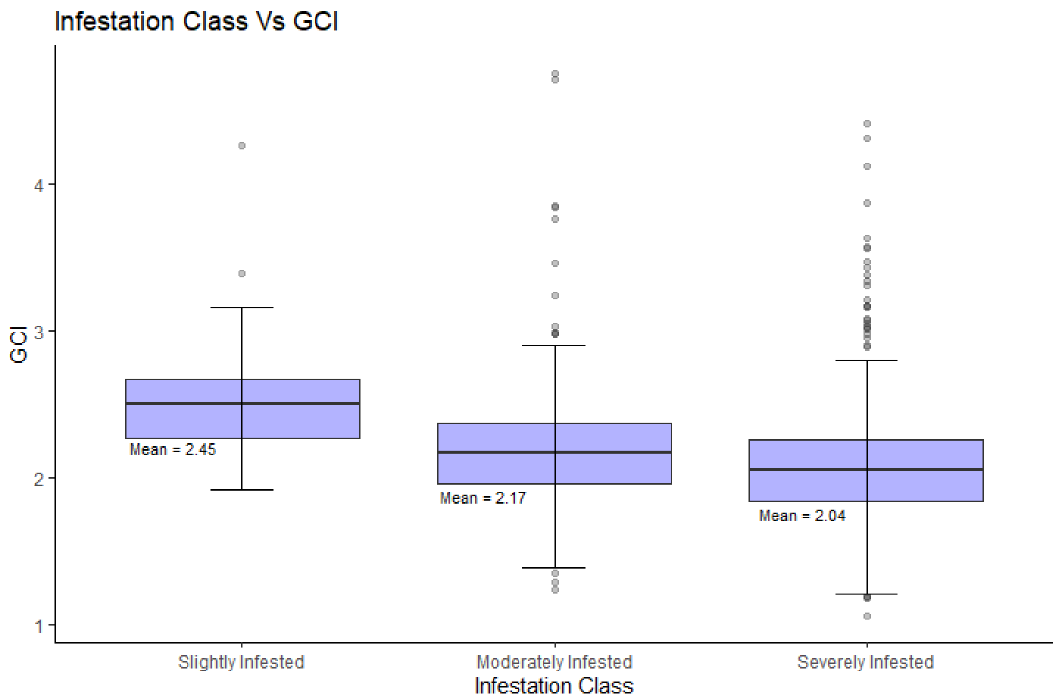

Figure 43: Relation between GCI and Infestation class.

The same as the above-explained relations NDRE and infestation class followed the same trend between slightly infested and moderately infested as well as between moderately infested and severely infested. However, the mean value difference between successive classes was slightly different (Figure 44). The mean values of the classes were close and were 0.171, 0.168, and 0.164 for the slightly, moderately, and severely infested classes, respectively.

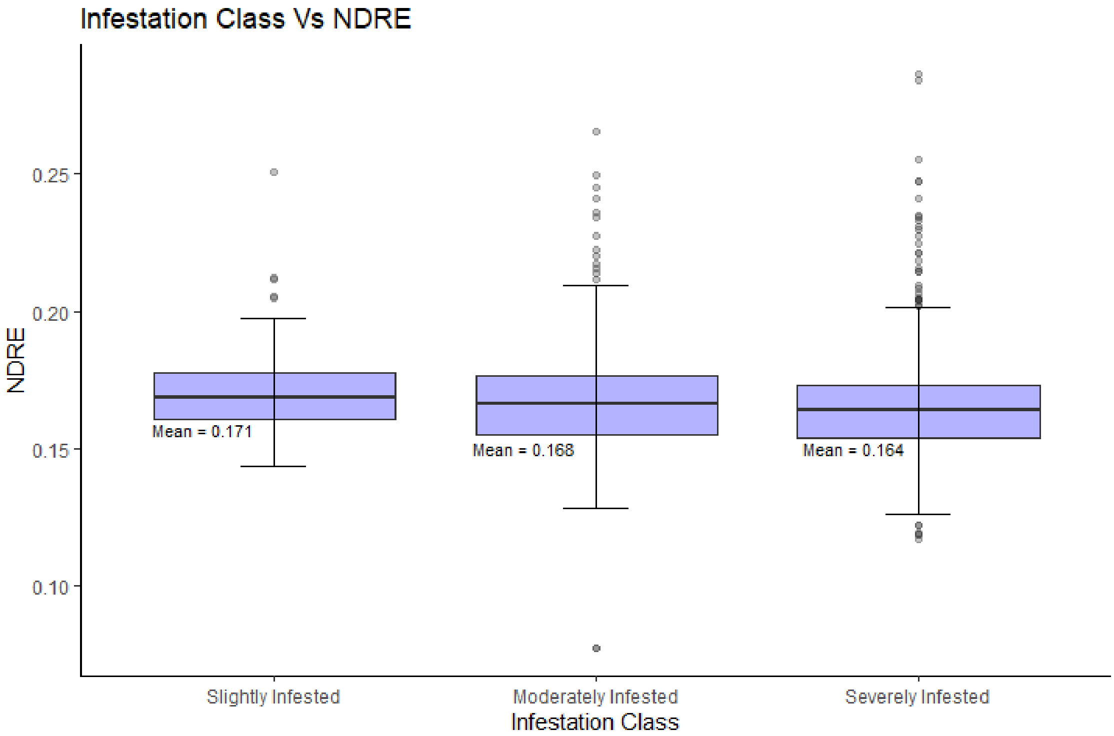

Figure 44: Relation between NDRE and Infestation class.

3.9. Relationship between canopy temperature and vegetation indices

As can be seen in Figure 45, there is a negative relationship between all vegetation indices and canopy temperature. Among the applied vegetation indices, NDVI had a better relationship with canopy temperature (Figure 45(a)). For example, NDVI showed a very weak relationship with canopy temperature (R^2=0.2) despite it was performed better in comparison with other considered vegetation indices in this study. In addition, NDRE showed the weakest relation (R^2=0.013) with canopy temperature.

In addition, an overestimation can be found between canopy temperature and NDVI, SAVI, and EVI2. In general, in this study area, the relationship between canopy temperature and vegetation indices was found weak.

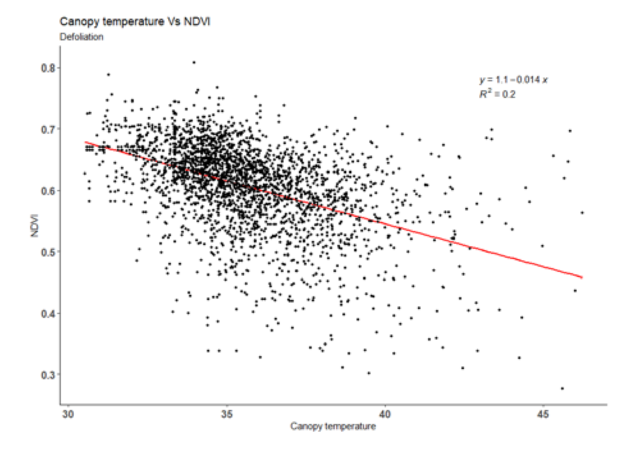

(a)

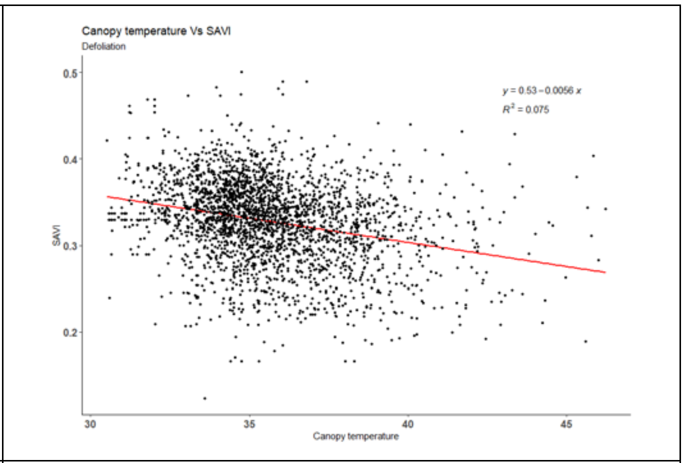

(b)

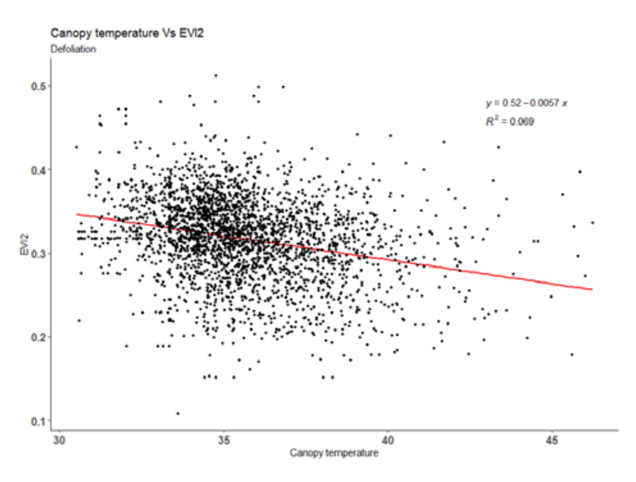

(c)

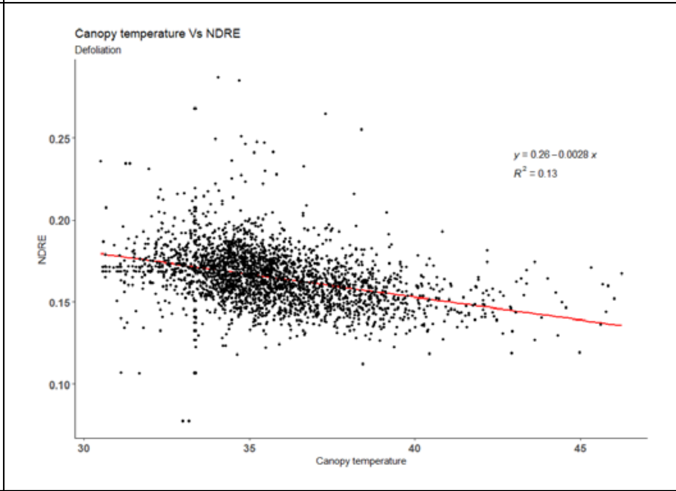

(d)

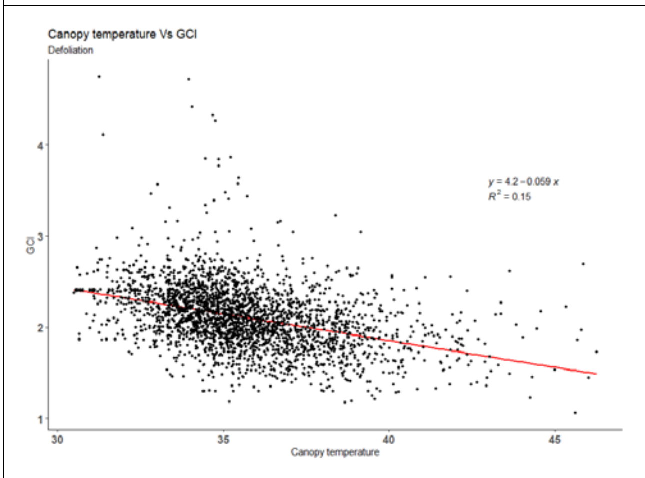

(e)

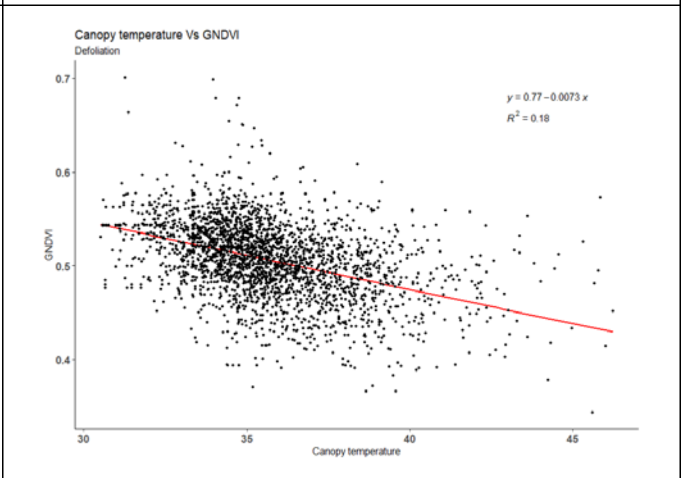

(f)

Figure 45: The relationship between canopy temperature and vegetation indices NDVI (a), SAVI (b), EVI2(c), NDRE (d), GCI (e), and GNDVI (f) concerning health status assessment.

3.10. Relationship between tree Infestation and health

The relationship plot in Figure 46 shows a high positive correlation between discoloration from *Marchalina hellenica* infestation and defoliation (R^2=0.69) using the average percentile for each class (Table 11). Many of the observations overlapped in health and infestation classes (n=105); all field observed trees that were classified as slightly infested for infestation class are also slightly unhealthy for the health class. Mostly the difference between the indicators (i.e., discoloration and defoliation) was in the moderately and severely infested/unhealthy observed tee classes.

Table 11: Average discoloration and defoliation percentile for each class in infestation/health class.

Infestation class	Healthy class	Average percentile(%)
Slightly infested	Slightly unhealthy	12.5
Moderately infested	Moderately unhealthy	42.5
Severely infested	Severely unhealthy	80

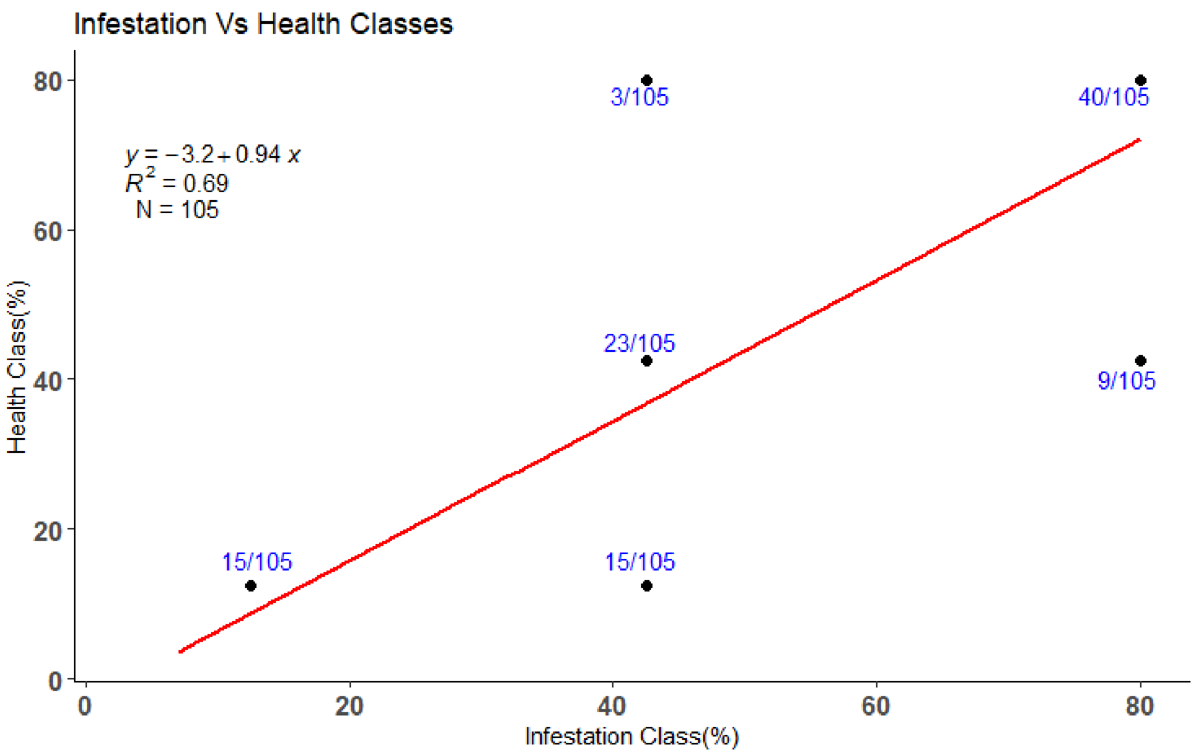

Figure 46: Relationship between tree infestation and health.

4. DISCUSSION

4.1. Classification and accuracy assessment

In this study, four scenarios were used to assess the health and infestation status, where vegetation indices and canopy temperature data were used as the input layers. Concerning tree health status manifested as defoliation, the vegetation indices-based classification obtained a low overall accuracy (52%). In addition, the canopy temperature was also used to classify defoliation status with a low overall classification accuracy (45%). However, the classification accuracy obtained using canopy temperature was less compared with vegetation indices. These results are not in agreement with previous research by Marx and Kleinschmit (2017), who applied NDRE and NDVI using a decision tree-based classification of *Pinus sylvestris* defoliation classes as they classified defoliation classes with higher overall accuracy compared to the results obtained in this research. Their visual observation of tree samples was less subjective compared to our study, and they used the percent remaining foliage to estimate the defoliation by considering various factors (e.g. crown shade). In another study done by Cardil et al. (2019) that assessed the impact of the Pine processionary moth in a Pine-oak mixed forest using UAS technology with multispectral data, the results showed high overall accuracy in classifying the non-defoliated, partially defoliated and completely defoliated trees using a combination of NDVI and Excess green index with an overall accuracy of 81%. Implementing the individual tree identification and delineation (ITDe) algorithm for automatic individual canopy delineation can be the reason for this study to have higher overall accuracy compared to our study.

Additionally, vegetation indices (e.g., NDVI and moisture stress index) derived from Landsat imagery that was calibrated using UAV showed high overall accuracy in classifying the degree of defoliation from the *Thaumetopea pityocampa* attack on the Mediterranean pine forest (Otsu et al., 2018). In line with Otsu et al., (2018), implementing a moisture stress index using NIR and shortwave infrared bands in this study can give a good indication of tree stress and moisture content.

The classification accuracy for vegetation indices and canopy temperature in classifying the intermediate stage of defoliation demonstrated misclassification problems with other classes (i.e.., slightly and severely unhealthy). This can be attributed to the inconsistency of tree structure within the field-collected moderately unhealthy trees. Most of the trees in this class had an open canopy by nature in addition to the defoliation effect, making it difficult to use those trees' information for training a classifier. The trees characterised as severely unhealthy in the field often appeared heavily defoliated in the lower parts but with a restricted but dense green canopy at the top. Although this could be a sign of recovery, it led to confusion with the other classes (i.e., slightly unhealthy and moderate unhealthy). As it can be seen in Table 7, the Post Hoc test performed in the classes of the 105 collected samples shows that there is no significant difference between moderately and severely unhealthy classes concerning health status assessment. This no significant difference between the classes can contribute to the misclassification.

The vegetation indices-based classification in discoloration showed a low overall accuracy. As mentioned above, the vegetation indices obtained slightly higher overall classification accuracy considering discoloration than the canopy temperature-based classification. In assessing infestation status, there was mostly misclassification between moderately and severely infested classes. The number of sample observations for the slightly infested class counts for only 14.3% of the total observation, this can be the reason to have lowest classification accuracy for the slightly infested class in using layers (i.e., canopy temperature, and vegetation indices).

In this study area, tree health degradation could also be caused by drought and three pests factors (Ogeda Oliech, 2019; Tsiaras et al.. 2016). As shown in Figure 46, from the total field observed sample trees, nine were severely discolored by *Marchalina hellenica* and moderately defoliated, while some of the sample trees (18) that were moderately infested are considered as slightly or severely unhealthy based on defoliation. Discoloration of the bark and branches was not directly observed by the sensor and, therefore an indirect indicator, also defoliation has a contribution in assessing discoloration.

Dash et al. (2017) applied an RF classifier using a UAV-based vegetation index (NDVI) and were able to classify the discoloration level in *Pinus radiata.* Classification had good accuracy (82.3%), and discoloration level was shown to be promising using UAV-based NDVI ($R^2 = 0.84$) followed by satellite-based NDRE ($R^2 = 0.73$) compared to GNDVI. In another study, TIR remote sensing data acquired together with visible and NIR bands were used in the classification of an infested Citrus tree using a support vector machine classifier, which resulted in a promising accuracy (Overall accuracy of 87%) (Sankaran et al., 2013).

The results showed that the vegetation indices as a layer obtained higher overall accuracy compared to the canopy temperature layer in assessing health and infestation status. This can be due to the fact that the canopy temperature is sensitive to defoliation (Junttila et al., 2016). The vegetation indices that were used in classification include SAVI, which helps the training process in addition to NDVI and NDRE; unlike thermal-based canopy temperature, which has a single information layer, the vegetation indices used different multispectral bands and have different responses to the health status of vegetation. Additionally, the vegetation indices such as SAVI minimize the uncertainty that occurs caused by the soil as a background. In other words, the uncertainty in classification will minimize if more information is provided to a classifier.

This study also observed the reflectance spectra of the health and infestation classes for the Pine trees. In assessing the health status, the reflectance spectra showed a higher value for the slightly unhealthy class in the NIR band compared to the two other classes (i.e., moderately and severely unhealthy). However, unexpectedly, the severely unhealthy class showed a higher reflectance value in the NIR band than the moderate unhealthy class. In green wavelength, the reflectance difference between the classes was minor, and the reflectance value of the severe unhealthy class was higher than the healthy class, which can be due to the dense canopy on top of the highly defoliated trees. This is in line with Fletcher et al. (2001) finding that revealed the green reflectance value was higher for infected Citrus trees (Phytophthora foot rot) than the non-infected trees; however, infected trees have lower NIR reflectance than healthy trees. When moderate and severe unhealthy classes were merged into one class, the present study's results agree with the previous study done by Baynes (2007), which found a negative relationship between red bands and Pine needles' health. However, our results are in disagreement with Radeloff et al. (1999) study, which did not show the expected negative relation between reflectance in NIR and defoliation for Jack pine stands. Recently, Yu et al. (2021) observed that the UAV-based spectral signature for Pine wilt disease-infected trees has a lower reflectance in green, red-edge, and NIR bands and is absorbed less in red band compared to non-infected trees in the early stage of infestation.

The spectral reflectance value of green and red bands was not able to show a clear difference among the infestation classes, whereas by seeing the NIR, a negative relationship between reflectance value and infestation status can be defined. The effect on distinguishing the classes in the green band was weak. It should be highlighted that the recorded discoloration status as an indicator of infestation could not be observed at the needle or canopy level by the observer, whereas it could be only observed in the bark and branches. In normal circumstances, healthy vegetation has leaf pigments that lead to high absorption in the visible part of the spectrum and high reflectance in the NIR band (e.g., absorption is low or non). Near-infrared reflectance, declines compared to the visible reflectance due to a drop in the near-infrared enhancement resulting from fewer overlapping leaf layers, an increase in understory and soil exposure as a background (Sankaran et al., 2013).

Minařík and Langhammer (2016) and Sankaran et al. (2013) findings showed that infested trees have a higher reflectance value in the visible wavelength compared to a healthy tree and vice versa for red-edge and NIR wavelengths using UAV data. This is in line with our study that showed the reflectance difference in NIR and red-edge wavelength for non-infested and infested Pine trees were easily distinguishable where the slightly infested class has a higher reflectance value compared to moderately and severely infested classes in both wavelengths (i.e., NIR and red-edge). However, the difference between moderately and severely infested classes was minor.

4.2. Separability of health/infestation classes using canopy temperature and vegetation indices

Concerning defoliation, the health classes' separability did not show a consistence result while using the four vegetation indices (i.e., NDVI, SAVI, EVI2, and GNDVI). The separability value between slightly and moderately unhealthy classes was positive, while among moderately unhealthy and severely unhealthy classes was negative. Unexpectedly, the severely unhealthy class has a higher average vegetation index value compared to the moderately unhealthy class. Unlike the other vegetation indices, NDRE calculated separability result shows the average vegetation indices value decrease with defoliation status by considering the standard deviation where the separability between moderately and severely unhealthy was high compared to slightly and moderately unhealthy. However, the calculated separability values between classes were low. This can be related to NDRE being the only vegetation index that used red-edge reflectance in its equation, which can differentiate well between the healthy and defoliated Pine trees.

Canopy temperature was able to show the separability between health classes. Slightly and moderately unhealthy classes can be distinguished moderately; however, the difference between moderately and severely unhealthy classes was low; this can be because the trees that are classified as moderately unhealthy were low in the amount of number compared to the two other classes (i.e., slightly and severe unhealthy). Additionally, the detected canopy temperature values for moderately and severely unhealthy were also close to each other.

Regarding discoloration, all used vegetation indices were able to show the separability between the infestation classes (i.e., NDRE, NDVI, SAVI, EVI2, and GCI). All vegetation indices perform well in distinguishing the infestation stages in Pine trees; slightly infested trees were differentiated from moderately and severely infested trees. Also, our results successfully showed the variation between moderately and severely infested classes. Among applied vegetation indices, SAVI performed well in differentiating the slightly infested from the moderately infested classes, followed by EVI2. The ability of SAVI to minimize the effect of soil as a background for the open forest ecosystem like this study area can be the reason for performing better. Also, EVI2 includes background correction (i.e., Atmospheric and noise), which helps minimize the effect of other external factors in assessing tree health. A study by Sankaran et al. (2013) showed a maximum separability between healthy and huanglongbing infected trees using NDVI among different vegetation indices.

However, the canopy temperature was not able to perform a descriptive separability between the infestation classes. The average canopy temperature of the severely infested class was higher than the non-infested class; however, the moderately infested class was lower than both other classes. The low performance of the canopy temperature in separating the classes can be from the inconsistency in the structure of the trees resulting in uncertainties while training the classifier.

Overall, canopy temperature exhibited a good separability between the health classes concerning defoliation, whereas the vegetation indices performed well for infestation classes in discoloration.

4.3. Relationship between health/infestation class and canopy temperature

Although there was low overall accuracy and misclassification of the health classes while using canopy temperature, our results revealed a positive relationship between defoliation and canopy temperature. As stated previously, the defoliation in this study area starts from the trees' lower part, resulting in some highly defoliated Pine trees having a similar or lower temperature than slightly unhealthy trees due to the dense green canopy on top. This result is in agreement with Smigaj et al. (2015) finding, who found a positive relation between the infected Pine trees (*Pinus sylvestris* and *Pinus contorta*) and canopy temperature using UAV-based thermal data.

Considering discoloration, canopy temperature was a weak indicator to show infestation degrees. The mean value of canopy temperature for the slightly infested class was greater than the moderately infested class and less than the severely infested class. Unexpectedly, as mentioned a large number of trees in the slightly infested class had canopy temperatures greater than the mean value in the moderately infested class. Our interpretation from the field observation was that the canopy size of healthy trees was small, making it difficult to perform the CHM-based segmentation and might result in uncertainty in the canopy temperature estimation. However, it needs further investigation to understand the effect of the canopy size or other related variables on canopy temperature. Previous findings stated that infested canopy trees have a higher temperature than healthy trees in the TIR wavelength due to changes in water content, stomatal opening, and transpiration (Sankaran et al., 2013; Oerke et al., 2006).

The canopy temperature was highly affected by defoliation rather than discoloration of the bark and branches by *M. Hellenica*. In addition, the canopy temperature seems more sensitive to the openness of the canopy. The openness in the canopy (canopy fraction) can be resulted from defoliation or the tree's canopy structure, which leads to an increase the soil's effect as a background on the canopy temperature. In addition to pests and drought, which can affect canopy temperature, other factors can also contribute to canopy temperatures, such as air temperature and soil properties (Junttila et al., 2016; Leinonen et al., 2006; Pineda et al., 2020). The LST of soil in this study area was overestimated which can be from different additive factors such as soil type and time of acquisition; this might have a high effect on calculating the mean value of canopy temperature.

4.4. Relationship between health/infestation class and vegetation indices

Regarding defoliation, a negative relationship was observed between NDRE value and discolorated classes. In this regard, the differences between the classes are slight while using the NDRE vegetation index. However, the other used vegetation indices for assessing the defoliation were not able to show any defined relationship among health classes. In fact, in this study, two-band indices could not define the separability among defoliation-based health classes. It should be highlighted that this result might be associated with the bands which were used in calculating vegetation indices. For instance, NDVI, SAVI, EVI2, and GNDVI use a green or red band with a combination of NIR bands in their equation, while NDRE applies red-edge and NIR bands. The red-edge reflectance occurs at the abrupt transition between lower red and higher NIR reflectance values. Due to its sensitivity to the change of chlorophyll content, red-edge reflectance can easily manifest the spectral features of vegetation and various indicators of tree health status (Boiarskii, 2019; Hallik et al., 2019). The reflectance in NIR is commonly used in assessing tree health because of the distinguishable highest reflectance value compared to the visible part of the spectrum (Lillesaeter, 1982).

Moreover, the severely unhealthy trees had a higher reflectance value than moderately unhealthy in red-edge and NIR bands. In spite, both bands (i.e., Red-edge and NIR) were able to determine the slightly unhealthy class and had higher reflectance than the other classes. However, our findings disagree with Marx and Kleinschmit (2017), who found a highly negative correlation between the vegetation indices (i.e., NDRE and NDVI) and defoliation. Our results also are in disagreement with Chávez and Clevers (2012) findings, who used NIR/Red-edge ratio, NDRE, and NDVI and showed a significant correlation between considered vegetation indices and green canopy percentage (defoliation). In this study, NDVI, SAVI, EVI2, and GNDVI mean value for the healthy class was greater than the severely defoliated class.

In this study, trees in slightly and severely defoliated classes with a close vegetation indices mean value can be explained by having a dense canopy in some severely defoliated Pine trees which affects the spectral reflectance of the bands used to calculate the index. It should be highlighted that the literature review revealed the background of the vegetation canopy could affect the reflectance spectral and vegetation indices (Dash et al., 2017). However, the moderately defoliated class had a lower mean value in the four vegetation indices compared to the severely defoliated ones. In common with other studies (Dash et al., 2017; Marx and Kleinschmit, 2017), vegetation indices find it challenging to classify the middle defoliated class. There is no defined reason why this difficulty occurs, but there are various factors that can contribute including the structure of the tree, canopy fraction, soil properties, type of defoliation, and ecological effect.

Concerning infestation, the decrease in the mean value of the vegetation indices has been observed in moderately and severely infested trees more than in the slightly infested classes; this showed that there was a positive relationship between vegetation indices (i.e., NDVI, SAVI, EVI2, GCI, and NDRE) and non infested Pine trees. In this study, SAVI and EVI2 showed well the difference between slightly and moderately infested classes, whereas the NDVI showed a bigger difference between moderately and severely infested classes. However, in this study, NDRE was the least performer to establish the relationship between the infestation classes. In agreement with the finding by Minařík and Langhammer (2016), the UAV-based NDVI and NDRE were able to show that infested trees have a lower value compared to the healthy class, although anthocyanin reflectance index and red-edge GNDVI were not able to show the difference between infested and healthy classes. In disagreement with Donchenko et al. (1997), who observed that the discoloration percentage in trees related to losing chlorophyll content has unexpectedly a positive relationship with the NDVI value. On the other hand (Sankaran et al., 2013) stated that NDVI and NDRE values in the infested trees have a lower value compared to healthy classes.

4.5. Relationship between canopy temperature and vegetation indices

Previous studies showed a negative relationship between vegetation indices and canopy temperature (Lin and Lv, 2010). In this research study, all used vegetation indices also showed a negative relationship with the canopy temperature; however, the correlation between canopy temperature and vegetation indices was found to be weak.

Outlier values are observed for the relationship between canopy temperature and vegetation indices; however, unexpectedly, the Pine trees with higher canopy temperature have higher vegetation indices values at the same time (Figures 45). The tree canopy's size and structure can cause this uncertainty (Nisio et al., 2020; Pineda et al., 2020; Junttila et al., 2016). It is also possible that a weak correlation between vegetation indices and canopy temperature might be due to the high sensitivity of canopy temperature to defoliation compared to discoloration caused by *Marchalina hellenica,* as well as the low performance of vegetation indices in assessing the defoliation.

In wilted or infested trees, decreasing chlorophyll content, stomatal closure, and water stress lead to a reduction in the photosynthesis process (Boiarskii, 2019 Marx and Kleinschmit, 2017; Smigaj et al., 2015). The discoloration (needle) and defoliation in wilted or infested trees have an influence on spectral reflectance, vegetation indices, and canopy temperature (Donchenko et al., 1997; Marx and Kleinschmit, 2017). In addition, it was revealed that healthy trees have high vegetation indices value and low canopy temperature compared to wilted or infested trees (Marx and Kleinschmit 2017, Smigaj et al. 2015).

5. CONCLUSION AND RECOMMENDATION

5.1. Conclusion

This study investigated the capability of TIR and MS ultra-high-resolution UAV remote sensing in assessing the health and infestation status of an open Mediterranean pine forest. Defoliation and discoloration of the bark and branches were considered as the indicators of the health and infestation status, respectively. In line with the previous studies, this study showed that canopy defoliation in Pine trees reflects their canopy temperature. Also, the vegetation indices performed well in describing the different degrees of infestation by *Marchalina hellenica*. The highest separability was found using SAVI to differentiate infestation classes. The canopy temperature has a weak negative relationship with all the vegetation indices used in defoliation and discoloration-based assessments.

This study suggests that UAV-based multispectral-derived vegetation indices and TIR remote sensing data can be used in the assessment of tree health status at the individual canopy level despite the possible uncertainties that occur from various factors (e.g., unreliable field observation, miss classification, scarcity of thermal multispectral, and random errors). Below are the answers to the research question.

Can UAV-based TIR temperature data map the health status of Mediterranean pine trees?

The canopy temperature was increasing with an increase in the defoliation. However, at the individual tree level, a miss classification of trees was observed, especially between slightly and severely unhealthy trees, when using the canopy temperature as a layer.

What is the difference in classification accuracy of the MS and TIR UAV images for detecting the health status of Mediterranean Pine trees?

NDVI, SAVI, and NDRE obtained slightly higher overall accuracy compared to the canopy temperature for detecting the health status using the RF as a classifier.

Can TIR UAV data detect the variability in infestation by *Marchalina hellenica* in Pine trees?

The overall accuracy for the RF classifier-based classification using canopy temperature derived from TIR UAV data was low (48%) in line with that, this study indicates a weak relation between the discoloration and canopy temperature.

5.2. Recommendation

The field observation data were not fairly distributed over the study area, and there was an inconsistency in the number of sample trees within the defined health/infestation class. Well-planned field observation is necessary, including additional information recording (e.g., structure of the canopy) for a better description of trees' health and infestation status. In this study, the acquired LST mosaic using the FLIR Vue Pro R camera includes a shadow, removing the shadow while delineating the tree crown. However, a more advanced approach needs to be considered to increase the quality of the TIR images and minimize the overestimated LST value resulting from the soil as a background. Increasing acquisition accuracy through forwarding motion compensation can help reduce or remove the blurred/stretch seen in TIR images. Also, introducing hyperspectral and multispectral thermal data seems necessary for better accuracy in the separability of defoliated or discolored trees. Since the study area is an open forest, applying approaches that minimize soil as background more efficiently can be introduced.

LIST OF REFERENCES

Ahmed, A., Ibrahim, A., Hussein, S., 2019. Detection of Palm Tree Pests Using Thermal Imaging: A Review. Stud. Comput. Intell. 801, 253–270. https://doi.org/10.1007/978-3-030-02357-7_12

Al-doski, J., Mansor, S., Shafri, H., 2016. Thermal imaging for pests detecting-a review. Int. J. Agric. For. Plant 2, 10-30 https://www.ijafp.com/wp-content/uploads/201.

Baynes, J., 2007. The Reflectance Signature of Canopy Components : Implications for the Interpretation of Remotely Sensed Images. Ann. Trop. Res. 29, 21–31.

Bhandari, A.K., Kumar, A., Singh, G.K., 2012. Feature Extraction using Normalized Difference Vegetation Index (NDVI): A Case Study of Jabalpur City. Procedia Technol. 6, 612–621. https://doi.org/10.1016/J.PROTCY.2012.10.074

Boiarskii, B., 2019. Comparison of NDVI and NDRE Indices to Detect Differences in Vegetation and Chlorophyll Content. J. Mech. Contin. Math. Sci. spl1. https://doi.org/10.26782/JMCMS.SPL.4/2019.11.00003

Boydak, M., 2004. Silvicultural characteristics and natural regeneration of Pinus brutia Ten. A review. Plant Ecol. 171, 153–163. https://doi.org/10.1023/B:VEGE.0000029373.54545.D2

Cardil, A., Otsu, K., Pla, M., Silva, C.A., Brotons, L., 2019. Quantifying pine processionary moth defoliation in a pine-oak mixed forest using unmanned aerial systems and multispectral imagery. PLoS One 14, e0213027. https://doi.org/10.1371/JOURNAL.PONE.0213027

Catsadorakis, G., 1994. The vertebrate animals of Samaria National Park (Crete, Greece). Biol. Gall. 22, 9–22.

Chávez, R.O., Clevers, J.G.P.W., 2012. Object-based analysis of 8-bands Worldview2 imagery for assessing health condition of desert trees.

Chen, G., Weng, Q., Hay, G.J., He, Y., 2018. Geographic object-based image analysis (GEOBIA): emerging trends and future opportunities. GIScience Remote Sens. 55, 159–182. https://doi.org/10.1080/15481603.2018.1426092

Chouhan, A., S, S., Chutia, D., Raju, P., 2019. Comparison of tree canopy extraction using Object Based Image Analysis and Deep Learning Technique in UAV images, in: 2019 International Conference on Intelligent Computing and Remote Sensing (ICICRS). Institute of Electrical and Electronics Engineers (IEEE), pp. 1–5. https://doi.org/10.1109/ICICRS46726.2019.9555767

Dash, J.P., Pearse, G.D., Watt, M.S., 2018. UAV multispectral imagery can complement satellite data for monitoring forest health. Remote Sens. 10, 1216. https://doi.org/10.3390/rs10081216

Dash, J.P., Watt, M.S., Pearse, G.D., Heaphy, M., Dungey, H.S., 2017. Assessing very high resolution UAV imagery for monitoring forest health during a simulated disease outbreak. ISPRS J. Photogramm. Remote Sens. 131, 1–14. https://doi.org/10.1016/J.ISPRSJPRS.2017.07.007

Degerickx, J., Roberts, D.A., McFadden, J.P., Hermy, M., Somers, B., 2018. Urban tree health assessment using airborne hyperspectral and LiDAR imagery. Int. J. Appl. Earth Obs. Geoinf. 73, 26–38. https://doi.org/10.1016/j.jag.2018.05.021

Donchenko, V. V., Goltsova, N.I., Bobylev, L.P., Johannessen, O.M., Kritsuk, S.G., Pitulko, V.M., 1997. Synergistic use of ERS-1/SAR and other satellite data for the polluted areas identification for boreal forests of St. Petersburg region. Eur. Sp. Agency, (Special Publ. ESA SP 369–375.

Eriksson, E., Gillespie, A.R., Gustavsson, L., Langvall, O., Olsson, M., Sathre, R., Stendahl, J., 2007. Integrated carbon analysis of forest management practices and wood substitution. Can. J. For. Res. 37, 671–681. https://doi.org/10.1139/X06-257

Ferreira, L.S., Duarte, D.H.S., 2019. Exploring the relationship between urban form, land surface temperature and vegetation indices in a subtropical megacity. Urban Clim. 27, 105–123. https://doi.org/10.1016/J.UCLIM.2018.11.002

Fletcher, R.S., Skaria, M., Escobar, D.E., Everitt, J.H., 2001. Field Spectra and Airborne Digital Imagery for Detecting Phytophthora Foot Rot Infections in Citrus Trees. HortScience 36, 94–97. https://doi.org/10.21273/HORTSCI.36.1.94

FLIR Systems Inc, 2022. FLIR sUAS cameras Radiometric Information [WWW Document], 2022. URL https://flir.custhelp.com/app/answers/detail/a_id/3108/~/flir-suas-cameras-radiometric-information (accessed 7.2.22).

Fonstad, M.A., Dietrich, J.T., Courville, B.C., Jensen, J.L., Carbonneau, P.E., 2013. Topographic structure from motion: a new development in photogrammetric measurement. Earth Surf. Process. Landforms 38, 421–430. https://doi.org/10.1002/ESP.3366

Gallis, A.T., 2007. Evaluation of the damage by insect Marchalina Hellenica (GENN.) in Eastern Attica, Greece. Conclusions for Sustainable Management of Forests Ecosystems. Technol. Kos Isl. 191–196.
Giménez-Gallego, J., González-Teruel, J.D., Soto-Valles, F., Jiménez-Buendía, M., Navarro-Hellín, H., Torres-Sánchez, R., 2021. Intelligent thermal image-based sensor for affordable measurement of crop canopy temperature. Comput. Electron. Agric. 188, 106319. https://doi.org/10.1016/J.COMPAG.2021.106319
Gitelson, A.A., Kaufman, Y.J., Merzlyak, M.N., 1996. Use of a green channel in remote sensing of global vegetation from EOS- MODIS. Remote Sens. Environ. 58, 289–298. https://doi.org/10.1016/S0034-4257(96)00072-7
Gitelson, A.A., Vina, A., Arkebauer, T.J., Rundquist, D.C., Keydan, G., Leavitt, B., 2003. Remote estimation of leaf area index and green leaf biomass in maize canopies. Geophys. Res. Lett. 30, 1248. https://doi.org/10.1029/2002GL016450
Gupta, R.K., Prasad, S., Sesha Sai, M.V.R., Viswanadham, T.S., 1997. The estimation of surface temperature over an agricultural area in the state of haryana and panjab, india, and its relationship with the normalized difference vegetation index (NDVI), using NOAA-AVHRR data. Int. J. Remote Sens. 18, 3729–3741. https://doi.org/10.1080/014311697216586
Gupta, S.K., Pandey, A.C., 2021. Spectral aspects for monitoring forest health in extreme season using multispectral imagery. Egypt. J. Remote Sens. Sp. Sci. 24, 579–586. https://doi.org/10.1016/J.EJRS.2021.07.001
Hall, J.P., 2002. Sustainable production of forest biomass for energy. For. Chron. 78, 391-396 https://pubs.cif-ifc.org/doi/pdf/10.5558/t.
Hallik, L., Kuusk, A., Lang, M., Kuusk, J., 2019. Reflectance Properties of Hemiboreal Mixed Forest Canopies with Focus on Red Edge and Near Infrared Spectral Regions. Remote Sens. 11, 1717. https://doi.org/10.3390/RS11141717
Huete, A.., 1988. A soil-adjusted vegetation index (SAVI). Remote Sens. Environ. 25, 295–309. https://doi.org/10.1016/0034-4257(88)90106-X
Huete, A.R., 2012. Vegetation Indices, Remote Sensing and Forest Monitoring. Geogr. Compass 6, 513–532. https://doi.org/10.1111/j.1749-8198.2012.00507.x
Hulley, G.C., Ghent, D., Göttsche, F.M., Guillevic, P.C., Mildrexler, D.J., Coll, C., 2019. Land Surface Temperature, Taking the Temperature of the Earth. https://doi.org/10.1016/b978-0-12-814458-9.00003-4
Iizuka, K., Itoh, M., Shiodera, S., Matsubara, T., Dohar, M., Watanabe, K., 2018. Advantages of unmanned aerial vehicle (UAV) photogrammetry for landscape analysis compared with satellite data: A case study of postmining sites in Indonesia. Cogent Geosci. 4, 1498180. https://doi.org/10.1080/23312041.2018.1498180
Jiang, Z., Huete, A.R., Didan, K., Miura, T., 2008. Development of a two-band enhanced vegetation index without a blue band. Remote Sens. Environ. 112, 3833–3845. https://doi.org/10.1016/J.RSE.2008.06.006
Junttila, S., Vastaranta, M., Hämäläinen, J., Latva-käyrä, P., Holopainen, M., Hernández Clemente, R., Hyyppä, H., Navarro-Cerrillo, R.M., 2016. Effect of forest structure and health on the relative surface temperature captured by airborne thermal imagery – Case study in Norway Spruce-dominated stands in Southern Finland. Scand. J. For. Res. 32, 154–165. https://doi.org/10.1080/02827581.2016.1207800
Kafy, A. Al, Al Rakib, A., Akter, K.S., Rahaman, Z.A., Faisal, A. Al, Mallik, S., Nasher, N.M.R., Hossain, M.I., Ali, M.Y., 2021. Monitoring the effects of vegetation cover losses on land surface temperature dynamics using geospatial approach in Rajshahi City, Bangladesh. Environ. Challenges 4. https://doi.org/10.1016/J.ENVC.2021.100187
Kaukoranta, T., Murto, J., Takala, J., Tahvonen, R., 2005. Detection of water deficit in greenhouse cucumber by infrared thermography and reference surfaces. Sci. Hortic. (Amsterdam). 106, 447–463. https://doi.org/10.1016/j.scienta.2005.02.026
Kukarskih, V. V., Devi, N.M., Surkov, A.Y., Bubnov, M.O., Gorlanova, L.A., Ekba, Y.A., Hantemirov, R.M., 2020. Climatic responses of Pinus brutia along the Black Sea coast of Crimea and the Caucasus. Dendrochronologia 64, 125763. https://doi.org/10.1016/J.DENDRO.2020.125763
Lakatos, F., Mirtchev, S., Mehmeti, A., Shabanaj, H., 2014. Manual for visual assessment of forest crown condition Editorial Staff 1–23.
Lambin, E.F., Ehrlich, D., 1995. Combining vegetation indices and surface temperature for land-cover

mapping at broad spatial scales. Int. J. Remote Sens. 16, 573–579. https://doi.org/10.1080/01431169508954423
Lange, H., Solberg, S., 2008. Leaf area index estimation using lidar and forest reflectance modelling of airborne hyperspectral data. Int. Geosci. Remote Sens. Symp. 3, III–475. https://doi.org/10.1109/IGARSS.2008.4779387
Lausch, A., Erasmi, S., King, D.J., Magdon, P., Heurich, M., Waser, L.T., Atzberger, C., Gloaguen, R., Thenkabail, P.S., 2017. Understanding Forest Health with Remote Sensing-Part II—A Review of Approaches and Data Models. Remote Sens. 9, 129. https://doi.org/10.3390/RS9020129
Leinonen, I., Grant, O.M., Tagliavia, C.P.P., Chaves, M.M., Jones, H.G., 2006. Estimating stomatal conductance with thermal imagery. Plant. Cell Environ. 29, 1508–1518. https://doi.org/10.1111/J.1365-3040.2006.01528.X
Lenk, S., Chaerle, L., Pfündel, E.E., Langsdorf, G., Hagenbeek, D., Lichtenthaler, H.K., Van Der Straeten, D., Buschmann, C., 2007. Multispectral fluorescence and reflectance imaging at the leaf level and its possible applications. J. Exp. Bot. 58, 807–814. https://doi.org/10.1093/jxb/erl207
Liew, L.H., Wang, Y.C., Cheah, W.S., 2012. Evaluation of control points' distribution on distortions and geometric transformations for aerial images rectification. Procedia Eng. 41, 1002–1008. https://doi.org/10.1016/J.PROENG.2012.07.275
Lillesaeter, O., 1982. Spectral reflectance of partly transmitting leaves: Laboratory measurements and mathematical modeling. Remote Sens. Environ. 12, 247–254. https://doi.org/10.1016/0034-4257(82)90057-8
Lin, H.R., Lv, X., 2010. Monitoring frost disaster of cotton based on difference of vegetation index and canopy temperature by remote sensing, in: 2010 2nd Conference on Environmental Science and Information Application Technology, ESIAT 2010. pp. 552–557. https://doi.org/10.1109/ESIAT.2010.5568971
Lindenthal, M., Steiner, U., Dehne, H., Oerke, E., 2005. Effect of downy mildew development on transpiration of cucumber leaves visualized by digital infrared thermography. Phytopathology 95, 233–240. https://doi.org/10.1094/PHYTO-95-0233
Manthira Moorthi, S., Misra, I., Kaur, R., Darji, N.P., Ramakrishnan, R., 2011. Kernel based learning approach for satellite image classification using support vector machine. IEEE Recent Adv. Intell. Comput. Syst. 107–110. https://doi.org/10.1109/RAICS.2011.6069282
Marx, A., Kleinschmit, B., 2017. Sensitivity analysis of RapidEye spectral bands and derived vegetation indices for insect defoliation detection in pure Scots pine stands. iForest - Biogeosciences For. 10, 659. https://doi.org/10.3832/IFOR1727-010
Masaitis, G., Mozgeris, G., Augustaitis, A., 2013. Spectral reflectance properties of healthy and stressed coniferous trees. iForest - Biogeosciences For. 6, 30. https://doi.org/10.3832/IFOR0709-006
Meola, C., Carlomagno, G.M., 2004. Recent advances in the use of infrared thermography. Meas. Sci. Technol. 15, R27. https://doi.org/10.1088/0957-0233/15/9/R01
Minařík, R., Langhammer, J., 2016. Use of a multispectral UAV photogrammetry for detection and tracking of forest disturbance dynamics. Int. Arch. Photogramm. Remote Sens. Spat. Inf. Sci. - ISPRS Arch. 41, 711–718. https://doi.org/10.5194/isprsarchives-XLI-B8-711-2016
Mita, E., Tsitsimpikou, C., Tsiveleka, L., Petrakis, P. V., Ortiz, A., Vagias, C., Roussis, V., 2002. Seasonal variation of oleoresin terpenoids from Pinus halepensis and Pinus pinea and host selection of the scale insect Marchalina hellenica (homoptera, coccoidea, margarodidae, coelostonidiinae). Holzforschung 56, 572–578. https://doi.org/10.1515/HF.2002.087
Moore, D.J.P., Trahan, N.A., Wilkes, P., Quaife, T., Stephens, B.B., Elder, K., Desai, A.R., Negron, J., Monson, R.K., 2013. Persistent reduced ecosystem respiration after insect disturbance in high elevation forests. Ecol. Lett. 16, 731–737. https://doi.org/10.1111/ele.12097
Neary, D.G., Ice, G.G., Jackson, C.R., 2009. Linkages between forest soils and water quality and quantity. For. Ecol. Manage. 258, 2269–2281. https://doi.org/10.1016/j.foreco.2009.05.027
Neinavaz, E., 2017. Sensing vegetation canopies in the thermal domain. University of Twente, Enschede, The Netherlands. https://doi.org/10.3990/1.9789036543514
Nisio, A. Di, Adamo, F., Acciani, G., Attivissimo, F., 2020. Fast detection of olive trees affected by xylella fastidiosa from uavs using multispectral imaging. Sensors 20, 1–23. https://doi.org/10.3390/s20174915
Oerke, E.C., Steiner, U., Dehne, H.W., Lindenthal, M., 2006. Thermal imaging of cucumber leaves affected by downy mildew and environmental conditions. J. Exp. Bot. 57, 2121–2132. https://doi.org/10.1093/JXB/ERJ170

Ogeda Oliech, I., 2019. Geo-spatial assessment of forest health status using UAS technology in Anopoli, Crete. University of Twente http://purl.utwente.nl/essays/83735.
Oğuzoğlu, Ş., Avcı, M., İpekdal, K., 2021. Predators of the giant pine scale, Marchalina hellenica (Gennadius 1883; Hemiptera: Marchalinidae), out of its natural range in Turkey. Open Life Sci. 16, 682. https://doi.org/10.1515/BIOL-2021-0066
Otsu, K., Pla, M., Vayreda, J., Brotons, L., 2018. Calibrating the Severity of Forest Defoliation by Pine Processionary Moth with Landsat and UAV Imagery. Sensors 2018, Vol. 18, Page 3278 18, 3278. https://doi.org/10.3390/S18103278
Patel, S. V., Jokhakar, V.N., 2017. A random forest based machine learning approach for mild steel defect diagnosis, in: IEEE International Conference on Computational Intelligence and Computing Research, ICCIC 2016. Institute of Electrical and Electronics Engineers Inc., pp. 1–8. https://doi.org/10.1109/ICCIC.2016.7919549
Pediaditi, K., Gadanakis, Y., Belean, C., Nyktas, P., Meramveliotakis, Y., Dermanakis, N., 2008. The Greek pilot project: Lefka Ori National Park, Crete.
Pineda, M., Barón, M., Pérez-Bueno, M.-L., 2020. Thermal Imaging for Plant Stress Detection and Phenotyping. Remote Sens. 13, 68. https://doi.org/10.3390/RS13010068
Prakash, A., 2000. Thermal remote sensing: concepts, issues and applications, in: International Archives of Photogrammetry and Remote Sensing. pp. 239–243.
Radeloff, V.C., Mladenoff, D.J., Boyce, M.S., 1999. Detecting jack pine budworm defoliation using spectral mixture analysis: Separating effects from determinants. Remote Sens. Environ. 69, 156–169. https://doi.org/10.1016/S0034-4257(99)00008-5
Ramakrishna, R.N., 1989. Estimation of regional surface resistance to evapotranspiration from NDVI and Thermal-IR AVHRR data. J. Appl. Meteorol. Climatol. 276–284.
Rowland, D., Ickowitz, A., Powell, B., Nasi, R., Sunderland, T., 2017. Forest foods and healthy diets: Quantifying the contributions. Environ. Conserv. 44, 102–114. https://doi.org/10.1017/S0376892916000151
Sankaran, S., Maja, J.M., Buchanon, S., Ehsani, R., 2013. Huanglongbing (Citrus Greening) Detection Using Visible, Near Infrared and Thermal Imaging Techniques. Sensors 13, 2117–2130. https://doi.org/10.3390/s130202117
Santas, L.A., 1983. Insects producing honeydew exploited by bees in Greece. Apidologie 14, 93–103. https://doi.org/10.1051/APIDO:19830204
Sebald, J., Senf, C., Seidl, R., 2021. Human or natural? Landscape context improves the attribution of forest disturbances mapped from Landsat in Central Europe. Remote Sens. Environ. 262, 112502. https://doi.org/10.1016/J.RSE.2021.112502
Smigaj, M., Gaulton, R., Barr, S.L., Suárez, J.C., 2015. UAV-Borne thermal imaging for forest health monitoring: Detection Of disease-induced canopy temperature increase, in: International Archives of the Photogrammetry, Remote Sensing and Spatial Information Sciences - ISPRS Archives. International Society for Photogrammetry and Remote Sensing, pp. 349–354. https://doi.org/10.5194/isprsarchives-XL-3-W3-349-2015
Spanos, K.A., Skouteri, A., Gaitanis, D., Petrakis, P. V., Meliadis, I., Michopoulos, P., Solomou, A., Koulelis, P., Avramidou, E. V., 2021. Forests of Greece, Their Multiple Functions and Uses, Sustainable Management and Biodiversity Conservation in the Face of Climate Change. Open J. Ecol. 11, 374–406. https://doi.org/10.4236/OJE.2021.114026
Syifa, M., Park, S.J., Lee, C.W., 2020. Detection of the Pine Wilt Disease Tree Candidates for Drone Remote Sensing Using Artificial Intelligence Techniques. Engineering 6, 919–926. https://doi.org/10.1016/J.ENG.2020.07.001
Trumbore, S., Brando, P., Hartmann, H., 2015. Forest health and global change. Science. 349, 814-818. https://doi.org/10.1126/science.aac6759
Tsagkarakis, A.E., Emmanouel, N.G., Tsagkarakis, A.E., Emmanouel, N.G., 2016. A Note on the Natural Relocation of Marchalina hellenica (Gennadius) from Pine to Fir Trees. Adv. Entomol. 4, 163–166. https://doi.org/10.4236/AE.2016.43017
Tsiaras, D., Palaskas, A., Zahariadis, A., 2016. Evaluation and assessment of Pine infestations and expansion in Lefka Ori (white Mountains) with management suggestions. Consultancy deliverable to Samaria National Park Management body. (Μελέτη εκτίμησης και αξιολόγησης των ασθενειών του πεύκου και της επεκτασιμότητάς του στα Λευκά Όρη, με επακόλουθες διαχειριστικές προτάσεις).
Tubby, K. V., Webber, J.F., 2010. Pests and diseases threatening urban trees under a changing climate. Forestry 83, 451–459. https://doi.org/10.1093/forestry/cpq027

Tucker, C.J., 1979. Red and photographic infrared linear combinations for monitoring vegetation. Remote Sens. Environ. 8, 127–150. https://doi.org/10.1016/0034-4257(79)90013-0
Turhan, I., Tetik, N., Karhan, M., Gurel, F., Reyhan Tavukcuoglu, H., 2008. Quality of honeys influenced by thermal treatment. LWT - Food Sci. Technol. 41, 1396–1399. https://doi.org/10.1016/J.LWT.2007.09.008
Vidal, D., Pitarma, R., 2019. Infrared Thermography Applied to Tree Health Assessment: A Review. Agriculture 9, 156. https://doi.org/10.3390/AGRICULTURE9070156
Wang, J., Sammis, T.W., Gutschick, V.P., Gebremichael, M., Dennis, S.O., Harrison, R.E., 2010. Review of Satellite Remote Sensing Use in Forest Health Studies. Open Geogr. J. 3, 28–42. https://doi.org/10.2174/1874923201003010028
Wulder, M.A., Franklin, S.E., 2003. Remote sensing of forest environments : concepts and case studies. Kluwer Academic Publishers.
Yesil, A., Gurkan, B., Saracoglu, O., Zengin, H., 2005. Effect of the pest Marchalina hellenica Gennadius (Homoptera, Margarodidae) on the growth parameters of Pinus brutia Ten. in Mugla Region (Turkey). Polish J. Ecol. 53, 451–458.
Yu, R., Luo, Y., Zhou, Q., Zhang, X., Wu, D., Ren, L., 2021. Early detection of pine wilt disease using deep learning algorithms and UAV-based multispectral imagery. For. Ecol. Manage. 497, 119493. https://doi.org/10.1016/J.FORECO.2021.119493

APPENDICES

Appendix 1: Field observations recording form

Observation ID	Coordinate			Class type		Characteristic of the infested tree	Remarks
	X	Y	Z	Discoloration (%)	Defoliation (%)		

Appendix 2: Quality check for RGB photogrammetry project of the study area

Images	median of 65572 keypoints per image	✔
Dataset	829 out of 829 images calibrated (100%), all images enabled	✔
Camera Optimization	3.28% relative difference between initial and optimized internal camera parameters	✔
Matching	median of 12784.5 matches per calibrated image	✔
Georeferencing	yes, 7 GCPs (7 3D), mean RMS error = 0.042 m	✔

Appendix 3: Quality check for MS photogrammetry project of the study area

Images	median of 22474 keypoints per image	✔
Dataset	3404 out of 3404 images calibrated (100%), 8 images disabled	✔
Camera Optimization	0.01% relative difference between initial and optimized internal camera parameters	✔
Matching	median of 2556.25 matches per calibrated image	✔
Georeferencing	yes, 20 GCPs (20 3D), mean RMS error = 0.193 m	⚠

Appendix 4: Quality check for TIR photogrammetry project of the study area

Images	median of 8479 keypoints per image	⚠
Dataset	5960 out of 6086 images calibrated (97%), all images enabled, 7 blocks	⚠
Camera Optimization	194.6% relative difference between initial and optimized internal camera parameters	⚠
Matching	median of 2772.75 matches per calibrated image	✔
Georeferencing	yes, 28 GCPs (28 3D), mean RMS error = 0.364 m	⚠

Appendix 5: ANOVA and Post hoc test within vegetation indices and canopy temperature using defoliation as an indicator

ANOVA					
NDRE					
	Sum of Squares	df	Mean Square	F	Sig.
Between Groups	.025	2	.013	42.112	0.00
Within Groups	.723	2417	.000		
Total	.748	2419			

Multiple Comparisons						
Dependent Variable: NDRE						
Tukey HSD						
(I) Class_Numeric	(J) Class_Numeric	Mean Difference (I-J)	Std. Error	Sig.	95% Confidence Interval Lower Bound	95% Confidence Interval Upper Bound
1	2	.00314*	.00112	.014	.0005	.0058
	3	.00729*	.00081	5.1001E-9	.0054	.0092
2	1	-.00314*	.00112	.014	-.0058	-.0005
	3	.00415*	.00102	0.000143	.0018	.0065
3	1	-.00729*	.00081	5.1001E-9	-.0092	-.0054
	2	-.00415*	.00102	0.000143	-.0065	-.0018
*. The mean difference is significant at the 0.05 level.						

ANOVA					
NDVI					
	Sum of Squares	df	Mean Square	F	Sig.
Between Groups	3.353	2	1.677	442.161	0.00
Within Groups	9.165	2417	.004		
Total	12.518	2419			

Multiple Comparisons						
Dependent Variable: NDVI						
Tukey HSD						
(I) Class_Numeric	(J) Class_Numeric	Mean Difference (I-J)	Std. Error	Sig.	95% Confidence Interval Lower Bound	95% Confidence Interval Upper Bound
1	2	.10730*	.00399	5.1001E-9	.0979	.1167
	3	.06937*	.00288	5.1001E-9	.0626	.0761
2	1	-.10730*	.00399	5.1001E-9	-.1167	-.0979
	3	-.03793*	.00363	5.1001E-9	-.0464	-.0294
3	1	-.06937*	.00288	5.1001E-9	-.0761	-.0626
	2	.03793*	.00363	5.1001E-9	.0294	.0464
*. The mean difference is significant at the 0.05 level.						

ANOVA					
SAVI					
	Sum of Squares	df	Mean Square	F	Sig.
Between Groups	1.498	2	.749	452.034	0.00
Within Groups	4.005	2417	.002		
Total	5.503	2419			

Multiple Comparisons

Dependent Variable: SAVI

Tukey HSD

(I) Class_Numeric	(J) Class_Numeric	Mean Difference (I-J)	Std. Error	Sig.	95% Confidence Interval	
					Lower Bound	Upper Bound
1	2	.07682*	.00264	5.1001E-9	.0706	.0830
	3	.03926*	.00190	5.1001E-9	.0348	.0437
2	1	-.07682*	.00264	5.1001E-9	-.0830	-.0706
	3	-.03756*	.00240	5.1001E-9	-.0432	-.0319
3	1	-.03926*	.00190	5.1001E-9	-.0437	-.0348
	2	.03756*	.00240	5.1001E-9	.0319	.0432

*. The mean difference is significant at the 0.05 level.

ANOVA					
GNDVI					
	Sum of Squares	df	Mean Square	F	Sig.
Between Groups	.603	2	.301	213.769	0.00
Within Groups	3.408	2417	.001		
Total	4.011	2419			

Multiple Comparisons

Dependent Variable: GNDVI

Tukey HSD

(I) ClassNumeric	(J) ClassNumeric	Mean Difference (I-J)	Std. Error	Sig.	95% Confidence Interval	
					Lower Bound	Upper Bound
1	2	.04593*	.00243	5.1001E-9	.0402	.0516
	3	.02896*	.00176	5.1001E-9	.0248	.0331
2	1	-.04593*	.00243	5.1001E-9	-.0516	-.0402
	3	-.01697*	.00221	5.1001E-9	-.0222	-.0118
3	1	-.02896*	.00176	5.1001E-9	-.0331	-.0248
	2	.01697*	.00221	5.1001E-9	.0118	.0222

*. The mean difference is significant at the 0.05 level.

ANOVA					
EVI2					
	Sum of Squares	df	Mean Square	F	Sig.
Between Groups	1.640	2	.820	436.895	0.00
Within Groups	4.536	2417	.002		
Total	6.176	2419			

Multiple Comparisons						
Dependent Variable: EVI2						
Tukey HSD						
(I) Class_Numeric	(J) Class_Numeric	Mean Difference (I-J)	Std. Error	Sig.	95% Confidence Interval	
					Lower Bound	Upper Bound
1	2	.08072*	.00281	5.1001E-9	.0741	.0873
	3	.04032*	.00203	5.1001E-9	.0356	.0451
2	1	-.08072*	.00281	5.1001E-9	-.0873	-.0741
	3	-.04040*	.00255	5.1001E-9	-.0464	-.0344
3	1	-.04032*	.00203	5.1001E-9	-.0451	-.0356
	2	.04040*	.00255	5.1001E-9	.0344	.0464
*. The mean difference is significant at the 0.05 level.						

ANOVA					
Canopy temperature					
	Sum of Squares	df	Mean Square	F	Sig.
Between Groups	2601.696	2	1300.848	302.302	0.00
Within Groups	10310.317	2396	4.303		
Total	12912.013	2398			

Multiple Comparisons						
Dependent Variable: Canopy temperature						
Tukey HSD						
(I) Class_Numeric	(J) Class_Numeric	Mean Difference (I-J)	Std. Error	Sig.	95% Confidence Interval	
					Lower Bound	Upper Bound
1	2	-1.31098*	.21626	9.6936E-9	-1.8182	-.8038
	3	-2.23475*	.09092	5.0989E-9	-2.4480	-2.0215
2	1	1.31098*	.21626	9.6936E-9	.8038	1.8182
	3	-.92376*	.21036	0.000035	-1.4171	-.4304
3	1	2.23475*	.09092	5.0989E-9	2.0215	2.4480
	2	.92376*	.21036	0.000035	.4304	1.4171
*. The mean difference is significant at the 0.05 level.						

Appendix 6: ANOVA and Post hoc test within vegetation indices and canopy temperature using discoloration as an indicator

ANOVA					
NDRE					
	Sum of Squares	df	Mean Square	F	Sig.
Between Groups	.006	2	.003	9.995	<.001
Within Groups	.691	2377	.000		
Total	.697	2379			

Multiple Comparisons						
Dependent Variable: NDRE						
Tukey HSD						
(I) Class_Numeric	(J) Class_Numeric	Mean Difference (I-J)	Std. Error	Sig.	95% Confidence Interval	
					Lower Bound	Upper Bound
1	2	.00502*	.00190	.023	.0006	.0095
	3	.00713*	.00186	0.000384	.0028	.0115
2	1	-.00502*	.00190	.023	-.0095	-.0006
	3	.00210*	.00075	.013	.0004	.0039
3	1	-.00713*	.00186	0.000384	-.0115	-.0028
	2	-.00210*	.00075	.013	-.0039	-.0004
*. The mean difference is significant at the 0.05 level.						

ANOVA					
NDVI					
	Sum of Squares	df	Mean Square	F	Sig.
Between Groups	1.908	2	.954	221.182	0.00
Within Groups	10.254	2377	.004		
Total	12.163	2379			

Multiple Comparisons						
Dependent Variable: NDVI						
Tukey HSD						
(I) Class_Numeric	(J) Class_Numeric	Mean Difference (I-J)	Std. Error	Sig.	95% Confidence Interval	
					Lower Bound	Upper Bound
1	2	.05033*	.00734	5.124E-9	.0331	.0675
	3	.10058*	.00717	5.1E-9	.0838	.1174
2	1	-.05033*	.00734	5.124E-9	-.0675	-.0331
	3	.05025*	.00287	5.1E-9	.0435	.0570
3	1	-.10058*	.00717	5.1E-9	-.1174	-.0838
	2	-.05025*	.00287	5.1E-9	-.0570	-.0435
*. The mean difference is significant at the 0.05 level.						

ANOVA					
SAVI					
	Sum of Squares	df	Mean Square	F	Sig.
Between Groups	.796	2	.398	207.397	0.00
Within Groups	4.563	2377	.002		
Total	5.359	2379			

Multiple Comparisons						
Dependent Variable: SAVI						
Tukey HSD						
(I) Class_Numeric	(J) Class_Numeric	Mean Difference (I-J)	Std. Error	Sig.	95% Confidence Interval	
					Lower Bound	Upper Bound
1	2	.05523*	.00489	5.1E-9	.0438	.0667
	3	.08117*	.00478	5.1E-9	.0700	.0924
2	1	-.05523*	.00489	5.1E-9	-.0667	-.0438

	3	.02594*	.00192	5.1E-9	.0214	.0304
3	1	-.08117*	.00478	5.1E-9	-.0924	-.0700
	2	-.02594*	.00192	5.1E-9	-.0304	-.0214
*. The mean difference is significant at the 0.05 level.						

ANOVA					
GCI					
	Sum of Squares	df	Mean Square	F	Sig.
Between Groups	19.613	2	9.806	82.696	0.00
Within Groups	281.877	2377	.119		
Total	301.490	2379			

Multiple Comparisons						
Dependent Variable: GCI						
Tukey HSD						
(I) Class_Numeric	(J) Class_Numeric	Mean Difference (I-J)	Std. Error	Sig.	95% Confidence Interval	
					Lower Bound	Upper Bound
1	2	.28790*	.03846	5.1003E-9	.1977	.3781
	3	.41166*	.03758	5.1E-9	.3235	.4998
2	1	-.28790*	.03846	5.1003E-9	-.3781	-.1977
	3	.12376*	.01506	5.1E-9	.0884	.1591
3	1	-.41166*	.03758	5.1E-9	-.4998	-.3235
	2	-.12376*	.01506	5.1E-9	-.1591	-.0884
*. The mean difference is significant at the 0.05 level.						

ANOVA					
EVI2					
	Sum of Squares	df	Mean Square	F	Sig.
Between Groups	.865	2	.433	199.703	0.00
Within Groups	5.150	2377	.002		
Total	6.015	2379			

Multiple Comparisons					
Dependent Variable: ENVI2					
Tukey HSD					
(I) Class_Numeric	(J) Class_Numeric		Std. Error	Sig.	95% Confidence Interval

		Mean Difference (I-J)			Lower Bound	Upper Bound
1	2	.06011*	.00520	5.1E-9	.0479	.0723
	3	.08624*	.00508	5.1E-9	.0743	.0982
2	1	-.06011*	.00520	5.1E-9	-.0723	-.0479
	3	.02613*	.00204	5.1E-9	.0214	.0309
3	1	-.08624*	.00508	5.1E-9	-.0982	-.0743
	2	-.02613*	.00204	5.1E-9	-.0309	-.0214

*. The mean difference is significant at the 0.05 level.

ANOVA

Canopy temperature

	Sum of Squares	df	Mean Square	F	Sig.
Between Groups	3258.907	2	1629.453	384.861	0.00
Within Groups	11054.654	2611	4.234		
Total	14313.560	2613			

Multiple Comparisons

Dependent Variable: Canopy temperature

Tukey HSD

(I) Class_Numeric	(J) Class_Numeric	Mean Difference (I-J)	Std. Error	Sig.	95% Confidence Interval Lower Bound	Upper Bound
1	2	1.39376*	.17809	5.1002E-9	.9761	1.8114
	3	-.92062*	.17594	5.4412E-7	-1.3332	-.5080
2	1	-1.39376*	.17809	5.1002E-9	-1.8114	-.9761
	3	-2.31438*	.08344	5.1002E-9	-2.5101	-2.1187
3	1	.92062*	.17594	5.4412E-7	.5080	1.3332
	2	2.31438*	.08344	5.1002E-9	2.1187	2.5101

*. The mean difference is significant at the 0.05 level.